Doctoral theses at NTNU, 2024:190

Wadi Mawad

Right ventricular energetics using blood speckle tracking in pediatric congenital heart disease

Doctoral thesis

NTNU
Norwegian University of Science and Technology
Thesis for the Degree of
Philosophiae Doctor
Faculty of Medicine and Health Sciences
Department of Circulation and Medical Imaging

NTNU
Norwegian University of
Science and Technology

Wadi Mawad

Right ventricular energetics using blood speckle tracking in pediatric congenital heart disease

Thesis for the Degree of Philosophiae Doctor

Trondheim, May 2024

Norwegian University of Science and Technology
Faculty of Medicine and Health Sciences
Department of Circulation and Medical Imaging

NTNU
Norwegian University of
Science and Technology

NTNU
Norwegian University of Science and Technology

Thesis for the Degree of Philosophiae Doctor

Faculty of Medicine and Health Sciences
Department of Circulation and Medical Imaging

ISBN 190 978-82-326-7972-0 (printed ver.)
ISBN 190 978-82-326-7971-3 (electronic ver.)
ISSN 1503-8181 (printed ver.)
ISSN 2703-8084 (online ver.)

Doctoral theses at NTNU, 2024:190

Printed by NTNU Grafisk senter

Right ventricular energetics using blood speckle tracking in pediatric congenital heart disease

Thesis for the degree of Philosophiae Doctor

Trondheim, May 2024

Department of Circulation and Medical Imaging,

Norwegian University of Science and Technology

Trondheim, Norway

Department of Paediatrics, division of cardiology

Montreal Children's Hospital

Montreal, Canada

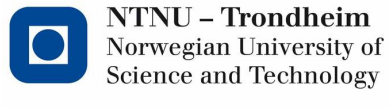

TABLE OF CONTENT

1. Norsk sammendrag

Denne avhandlingen består av tre delstudier hvor vi har studert høyre ventrikkels (RV) blodstrøms og energidynamikk hos pediatriske pasienter med hjertesykdom ved bruk av *blood speckle tracking* (BST). Målene var å beskrive RV blodstrøms- og energidynamikk ved ulike typer

hjertesykdom hos barn som gir ulike trykk- og volumbelastninger av RV. Vi sammenlignet disse pasientgruppene med friske kontroller.

Artikkel 1: I denne pilotstudien brukte vi BST for å avbilde RV strømningsmønstre hos barn med store atrieseptum defekter (ASD) og reparert Fallots tetrade (rTOF) med alvorlig gjenværende pulmonal insuffisiens (PI). Denne studien inkluderte 57 deltakere: 21 med rTOF, 11 med store ASDer og 25 friske individer (CTL). I tillegg ble et strømningsfantom benyttet for å evaluere effekten av avbildningsplan og glattingstilpasninger på parameteren energitap (EL). Vi observerte at RV diastolisk EL i ASD og rTOF var sammenlignbare, men begge var høyere enn i CTL. Områder med høyt EL under systolen var relativt like i alle grupper, og var å se i RV utløpet og nær trikuspidalklaffseilene i tidlig diastole. Spesielt ble et ekstra område med tidlig diastolisk EL ved apex identifisert hos rTOF-pasienter, relatert til samspillet mellom trikuspidal inflow og PI. Strømningsfantomforsøket indikerte at selv om EL varierte med avbildningsplan og glattingsteknikker, forble den generelle EL-trenden stabil hvis disse innstillingene var konsekvente.

Artikkel 2: Denne studien brukte vi BST for å studere blodstrømningsdynamikk og mønstre i høyre ventrikkel og lungepulsåren hos pediatriske pasienter med pulmonal arteriell hypertensjon (PAH) sammenlignet med friske kontroller. Atten barn ble inkludert i hver gruppe. En diastolisk virvel i lungepulsårens hovedstamme ble identifisert hos 16 av PAH-pasientene, men ikke hos kontrollene. Betydelig høyere systolisk og diastolisk EL, samt økt vektor kompleksitet (VC) og diastolisk virveldannelse i lungepulsårens hovedstamme ble observert i PAH sammenlignet med kontroller. Denne studien demonstrerte unormale strømningsmønstre i lungepulsårens

hovedstamme med diastolisk virveldannelse hos de fleste pasienter med PAH. Denne diastoliske virvelen skyldes sannsynligvis reflekterte bølger fra den distale lungekarsengen. Våre data indikerer at diastolisk virveldannelse potensielt kan brukes i diagnostisering av PAH.

Artikkel 3: Denne studien inkluderte pasienter med univentrikulære hjerter (UVH) etter Fontan-palliasjon og sammenlignet deres intrakardiale strømningsmønstre med friske kontroller. UVH-gruppen inkluderte 29 pasienter og 30 CTL. Kvalitativ virveldannelse var lik mellom gruppene i systole og diastole med unntak av undergruppen med dobbelt innløp til venstre ventrikkel som hadde mer komplekse blodstrøms-mønstre bestående av kolliderende virvler. Kvantitativt var UVH kinetisk energi (KE), energitap (EL) og vortisitet(VO) lavere sammenlignet med friske kontroller. Vi demonstrerte også en korrelasjon mellom KE, EL og VO. Vi konkluderte med at selv om lignende virveldannelser som vi ser hos friske er bevart i velfungerende UVH etter Fontan, er sistnevnte en energifattig sirkulasjon hvor alle mekanismer for energibesparelse er viktige.

Kandidat: Wadi Mawad, MD

Institutt: Institutt for sirkulasjon og bildediagnostikk (ISB), Fakultet for medisin og helsevitenskap, Norges teknisk-naturvitenskapelige universitet (NTNU), Trondheim, Norge

Veiledere: Hovedveileder Siri Ann Nyrnes (St. Olavs hospital/ISB, NTNU). Biveiledere Lasse Løvstakken (ISB, NTNU), Institutt for sirkulasjon og bildediagnostikk (ISB), Solveig Fadnes (ISB, NTNU) og Luc Mertens (The Hospital for Sick Children, Toronto, Canada)

Finansiering: CIUS (Centre for Innovative Ultrasound Solutions)

2. English Abstract

This thesis is composed of three studies of right ventricular (RV) energetics in pediatric patients with congenital heart disease (CHD), using blood speckle tracking (BST). The objectives were to describe the RV energetics and flow dynamics in the context of various CHD resulting in adverse loading of the RV. We compared these patient groups with healthy controls.

Paper 1: In this pilot study, we used BST to image RV flow patterns in children with large atrial septal defects (ASD) and those with repaired tetralogy of Fallot (rTOF) with severe residual pulmonary insufficiency (PI). This study included 57 participants: 21 with rTOF, 11 with large ASD, and 25 healthy individuals (CTL). Additionally, a flow phantom was utilized to evaluate the impact of imaging plane and smoothing adjustments on the parameter of energy loss (EL) obtained with BST. We observed that RV diastolic EL in ASD and rTOF was comparable, but both were higher than in CTL. High EL areas during systole were consistent across all groups, appearing in the RV outflow tract and near the tricuspid valve leaflets in early diastole. Notably, an extra area of early diastolic EL at the apex was identified in rTOF patients, related to the interaction of tricuspid inflow and PI. The flow phantom experiment indicated that while EL varied with imaging plane and smoothing settings, the overall EL trend remained stable if these settings were consistent.

Paper 2: This study used BST to study of blood flow dynamics and patterns in the right ventricle and main pulmonary artery in pediatric pulmonary hypertension (PAH) compared to healthy controls. Eighteen subjects were included in each group. A diastolic vortex in the main pulmonary artery (MPA) was identified in 16 of the PAH patients, but not in controls. Significantly

higher MPA systolic and diastolic EL, as well as increased vector complexity (VC) and diastolic vorticity were noted in PAH compared to controls. This study demonstrated abnormal flow patterns in the MPA with diastolic vortex formation in most patients with PAH. This diastolic vortex likely results from reflected waves from the distal pulmonary bed. Our data indicate that diastolic vortex could potentially be used in the diagnosis of PAH.

Paper 3: This study included patients with univentricular hearts (UVH) after Fontan palliation and compared their intracardiac flow patterns to healthy controls. The UVH included 29 patients and 30 CTL. Qualitative vortex formation was similar between groups in systole and diastole except for double inlet left ventricle which had more complex inflow patterns consisting of colliding vortices. Quantitatively, UVH kinetic energy (KE), energy loss (EL) and vorticity (VO) were lower when compared to healthy controls. We also demonstrated a correlation between KE, EL and VO. We concluded that although similar vortex formation is preserved in well-functioning UVH after Fontan, the latter is an energy-deprived circulation where all mechanisms of energy conservation are important.

Candidate: Wadi Mawad, MD

Department: Circulation and medical imaging

Supervisors: Main supervisor Siri Ann Nyrnes (St. Olav's hospital/ISB, NTNU). Co-supervisors: Lasse Løvstakken (ISB, NTNU), Solveig Fadnes (ISB, NTNU) and Luc Mertens (The Hospital for Sick Children, Toronto, Canada)

Funding: CIUS (Centre for Innovative Ultrasound Solutions)

3. Résumé en français:

Cette thèse se compose de trois études sur la dynamique des flux du ventricule droit (VD) chez les patients pédiatriques atteints de cardiopathie congénitale (CHD), en utilisant une nouvelle technologie d'imagerie cardiaque, le « speckle-traking » sanguin (BST). Les objectifs étaient de décrire la dynamique énergétique et les flux du RV dans le contexte de diverses CHD entraînant une charge défavorable sur le VD. Nous avons comparé ces groupes de patients à des témoins sains.

Article 1 : Dans cette étude pilote, nous avons utilisé le BST pour imager les motifs de flux du VD chez les enfants avec d'un large communication inter auriculaire (CIA) et ceux avec une tétralogie de Fallot réparée (rTdF) avec une insuffisance pulmonaire résiduelle sévère (IP). Cette étude comprenait 57 participants : 21 avec rTdF, 11 avec de grands CIA et 25 individus sains (CTL). De plus, un fantôme de flux a été utilisé pour évaluer l'impact du plan d'imagerie et des ajustements de lissage sur le paramètre de perte d'énergie (PE) obtenu avec le BST. Nous avons observé que l'EL diastolique du VD dans l'ASD et le rTdF était comparable, mais tous deux étaient plus élevés que dans le CTL. Les zones de EL élevé pendant la systole étaient constantes dans tous les groupes, apparaissant dans le tractus de sortie du VD et près des feuillets de la valve tricuspide en diastole précoce. Notamment, une zone supplémentaire de PE diastolique précoce à l'apex a été identifiée chez les patients rTdF, liée à l'interaction de l'entrée tricuspide et de l' IP. L'expérience du fantôme

de flux a indiqué que bien que la PE varie avec le plan d'imagerie et les techniques de lissage, la tendance générale de la PE restait stable si ces réglages étaient standard.

Article 2 : Cette étude a utilisé le BST pour l'étude de la dynamique des flux sanguins dans le ventricule droit (VD) et l'artère pulmonaire principale (APP) chez les patients pédiatriques atteints d'hypertension artérielle pulmonaire (HTAP) par rapport à des patients sains. Dix-huit sujets ont été inclus dans chaque groupe. Un vortex diastolique dans l'APP a été identifié chez 16 des patients HTAP, mais pas chez les témoins. Une PE systolique et diastolique de l'APP significativement plus élevée, ainsi qu'une complexité vectorielle (VC) et une vorticité (VO) diastolique accrues ont été notées dans le groupe avec HTAP par rapport aux témoins. Cette étude a démontré des motifs de flux anormaux dans l'APP avec la formation de vortex diastolique chez la plupart des patients atteints de HTAP. Ce vortex diastolique résulte probablement d'ondes réfléchies provenant du lit pulmonaire distal. Nos données indiquent que le vortex diastolique pourrait potentiellement être utilisé dans le diagnostic de la HTAP.

Article 3 : Cette étude comprenait des patients avec des cœurs univentriculaires (CUV) après palliation de Fontan et comparait leurs motifs de flux intracardiaques à des témoins sains (CTL). Le groupe CUV comprenait 29 patients et 30 CTL. La formation qualitative de vortex était similaire entre les groupes en systole et en diastole à l'exception du ventricule gauche à double entrée qui présentait des flux plus complexes comprenant des vortex en collision. Quantitativement, l'énergie cinétique (EC), la perte d'énergie (PE) et la vorticité (VO) dans le groupe CUV étaient inférieures par rapport aux témoins sains. Nous avons également démontré une corrélation

positive entre EC, PE et VO. Nous avons conclu que bien que la formation de vortex soit préservée dans le groupe CUV après une chirurgie de Fontan, cette circulation appauvrie en énergie où tous les mécanismes de conservation de l'énergie sont importants.

Financement: CIUS (Centre for Innovative Ultrasound Solutions)

(In case of acceptance: This thesis has been found worthy of public defense for the degree of PhD in Medicine. The public defense will take place in Trondheim, Norway, May 14th 2024)

4. PREFACE

This thesis is submitted in partial fulfillment of the requirements for the degree of *Philosophiae Doctor* (Ph.D.) at the Faculty of Medicine of the Norwegian University of Science and Technology (NTNU). The research was funded by CIUS (Centre for Innovative Ultrasound Solutions) at the Department of Circulation and Medical Imaging and conducted at the Hospital for Sick Children in Toronto, Canada, St Olavs Hospital, in Trondheim, Norway and Ålesund Hospital, Ålesund, Norway. The main supervisor was associate professor Siri Ann Nyrnes with the co-supervisors professor Lasse Løvstakken, researcher Solveig Fadnes and professor Luc Mertens.

5. ACKOWLEDGEMENTS

The heart has always fascinated me and inspired a great sense of awe in me. An organ so beautiful and loud, orchestrating our lives from within, one beat by beat. It is my experience that the study of such marvels of biology brings us closer to the divine, a thought shared by many

scientists, not the least of which is Charles Darwin who said in *The Correspondence of Charles Darwin, vol. 9*: "One cannot look at this Universe with all living productions & man without believing that all has been intelligently designed". I believe it is a great privilege to study the heart, and with it comes a great responsibility to use our knowledge to improve our patient's lives. My gratitude goes to them first, all the patient and families who generously participated in this work.

In the same way that the heart functions thanks to many brilliant structures and functions, this work was accomplished thanks to brilliant people who gave me encouragement, direction, wisdom and motivation. First, is my supervisor, Siri Ann Nyrnes. Her patience, diligence, knowledge and wisdom were pivotal in making me a better scientist and clinician. The same can be said for Lasse Løvstakken, whose positivity, insightfulness and solution-oriented attitude were a driving force for our group. Solveig Fadnes faced my many questions and request with poise and an always encouraging smile. My teacher, co-supervisor and mentor, Luc Mertens, who gave me this opportunity and supported me throughout with unwavering belief that I could see this through. It was also an immense pleasure and privilege to work with Thomas Grønli, Matthew Henry and Kristian Sørensen towards the latter parts of my PhD. There are many colleagues, who also helped in many ways, including Wei Hui, Cameron Slorach and Guillermo Larios Goldenberg, who helped me with patient recruitment and scanning. I am also very grateful to my colleagues in the division of cardiology at the Montreal Children's Hospital, who have given me time and space to accomplish this work: Adrian Dancea, Tiscar Cavallé-Garrido, Claudia Renaud, Virginie Beauséjour-Ladouceur, Luc Jutras and Charles Rohlicek.

Last but certainly not least, the following people can be considered the most elemental part of "my heart", my family, the whole of it. Firstly, my loving wife Christine, who surrounded me

with love, tenderness and encouragement in the face of challenges. To my mother whose unconditional love has driven me to seize opportunities and to risk failing. To my brother, his wife and children, whose wisdom and support are always precious. My family in-law, who always believed and encouraged me with kind words and great food. Finally, to my late father, to whom this work is dedicated. He is a model of perseverance, integrity and strength.

6. LIST OF PAPERS

Study 1: Mawad, W., Løvstakken, L., Fadnes, S., Grønli, T., Segers, P., Mertens, L., & Nyrnes, S. A. (2021). Right Ventricular Flow Dynamics in Dilated Right Ventricles: Energy Loss Estimation Based on Blood Speckle Tracking Echocardiography—A Pilot Study in Children. *Ultrasound in Medicine and Biology*, *47*(6), 1514–1527. https://doi.org/10.1016/j.ultrasmedbio.2021.02.004

Study 2: Mawad, W., Fadnes, S., Løvstakken, L., Henry, M., Mertens, L., & Nyrnes, S. A. (2022). Pulmonary Hypertension in Children is Associated With Abnormal Flow Patterns in the Main Pulmonary Artery as Demonstrated by Blood Speckle Tracking. *CJC Pediatric and Congenital Heart Disease*, *1*(5), 213–218. https://doi.org/10.1016/j.cjcpc.2022.09.001

Study 3: Mawad, W., Sørensen, K., Fadnes, S., Henry, M., Løvstakken, L., Mertens, L. & Nyrnes, S. A Intracardiac flow dynamics in children with Functionally Univentricular Hearts using blood speckle tracking. Submitted for publication in the Journal of the American Society of Echocardiography (Dec 31, 2023)

7. RELATED PAPERS PUBLISHED DURING PhD

1. Schäfer M, Mawad W. Advanced Imaging Technologies for Assessing Tetralogy of Fallot: Insights Into Flow Dynamics. *CJC Pediatr Congenit Hear Dis*. December 2023. doi:10.1016/j.cjcpc.2023.09.011
2. Dallaire F, Grewal J, Mawad W, Wald RM. Challenges and Opportunities for Patients With Tetralogy of Fallot Across the Lifespan. *CJC Pediatr Congenit Hear Dis*. December 2023. doi:10.1016/j.cjcpc.2023.11.001
3. Henry M, Fadnes S, Lovstakken L, Mawad W, Mertens L, Nyrnes SA. Flow Dynamics in Children With Bicuspid Aortic Valve: A Blood Speckle Tracking Study. *Ultrasound Med Biol*. 2023;49(11):2354-2360. doi:10.1016/j.ultrasmedbio.2023.07.012
4. Asaadi M, Mawad W, Djebbari A, Keshavardz-Motamed Z, Dahdah N, Kadem L. On Left Ventricle Stroke Work Efficiency in Children with Moderate Aortic Valve Regurgitation or Moderate Aortic Valve Stenosis. *Pediatr Cardiol*. 2021;(0123456789). doi:10.1007/s00246-021-02690-2
5. Mawad W, Mertens L, Pagano JJ, et al. Effect of anthracycline therapy on myocardial function and markers of fibrotic remodelling in childhood cancer survivors. *Eur Heart J Cardiovasc Imaging*. June 2020. doi:10.1093/ehjci/jeaa093
6. Mawad W, Mertens LL. Recent Advances and Trends in Pediatric Cardiac Imaging. *Curr Treat Options Cardiovasc Med*. 2018;20(1):9. doi:10.1007/s11936-018-0599-x

7. Mawad W, Friedberg MK. The continuing challenge of evaluating diastolic function by echocardiography in children: developing concepts and newer modalities. *Curr Opin Cardiol*. 2017;32(1):93-100. doi:10.1097/HCO.0000000000000346

8. ABBREVIATIONS

ASD: Atrial septal defect

BFI: Blood flow imaging

B-mode: Brightness mode

BST: blood speckle tracking

CDI: Color Doppler imaging

CFD: computational fluid dynamics

CHD: Congenital heart disease

CMR: cardiac magnetic resonance imaging

CW: continuous wave

DILV: Double inlet left ventricle

EL: Energy loss

FPS: Frames per second

HFRUS: High frame rate ultrasound imaging

KE: Kinetic energy

LV: left ventricle

MI : mechanical index

M-mode: motion-mode

MPA: Main pulmonary artery

PAH: Pulmonary arterial hypertension

PI: pulmonary insufficiency

PIV: particle imaging velocimetry

PRB: Parallel receive beam

PRF: Pulse repetition frequency

PW: pulsed wave

rTOF: repaired tetralogy of Fallot

RV: right ventricle

RV3C: apical right ventricular three chamber view

RV4C: apical right ventricular four chamber view

RVEDD: Right ventricular end-diastolic diameter

SLV: single left ventricle

SRV: single right ventricle

STE: Speckle tracking echocardiography

UVH: univentricular hearts

TOF: Tetralogy of Fallot

TI: thermal index

V4C: apical ventricular four chamber view

VC: Vector complexity

VFM: vector flow mapping

VO: vorticity

CTL: control

BSA: body surface area

RPA: right pulmonary artery

9. INTRODUCTION

Congenital heart disease (CHD) is one of the most prevalent congenital malformations, affecting around 1% of neonates and standing out as the primary cause of mortality from any congenital malformations[1]. The advancement of surgical and interventional treatments has resulted in significantly increased survival of CHD patients and has led to a rapidly growing population of both children and adults, living with congenital heart disease[2]. For the diagnosis and management of CHD patients, echocardiography has become the main non-invasive diagnostic imaging modality. Currently, especially in newborns and during childhood, echocardiography alone can be sufficient to accurately describe congenital heart defects even for complex cases, allowing to proceed with surgery based on echocardiography only[3]. Successful surgical and interventional treatment depends on accurate complete morphological and functional assessment of intracardiac and extracardiac structures. For specific cases complementary cardiac imaging modalities such as angiography, cardiac magnetic resonance imaging and computer assisted tomography may be indicated. Achieving a high level of diagnostic accuracy in echocardiographic imaging is imperative for effectively managing patients with CHD[4]. Diagnostic errors declined dramatically with improvements in cardiac ultrasound technology and operator expertise since the 1980s[5]. Long-term survival is influenced by the defect and its treatment with effects on cardiac structure and function. Patients with CHD are at long-term risk for heart failure,

arrhythmia and need life-long follow-up with monitoring of cardiac function and residual lesions related to CHD and its treatment.

These residual lesions can trigger cardiac remodeling, an adaptation involving molecular, cellular, and histological changes which affect cardiac dimensions, geometry, and function. Cardiac remodeling can be physiological to improve cardiac performance such as in athletes or pregnancy. In the case of residual lesions following congenital heart surgery, these adaptations often become pathological resulting in adverse remodeling negatively affecting cardiovascular function. Many research efforts aim to identify optimal timing for reinterventions at a stage of disease where this adverse cardiac remodelling can potentially be reversed or halted, without intervening too early and exposing patients to unnecessary risks[6–8]. The main indicators used in clinical practice to guide management have been dimensional changes such as increased ventricular volumes or wall thickness or even more recently deformation imaging using myocardial speckle-tracking echocardiography[9–12] as well as pressure gradients[13–15] . While these have all shown great promise and continue to, there remains many challenges.

A particular challenge is functional imaging of the right ventricle (RV), as the RV is often affected in CHD. Compared to the left ventricle, the right ventricle is much less studied. In addition, the right ventricle offers a unique imaging challenge by its crescentic shape and retrosternal position. Both echocardiography and cardiac magnetic resonance imaging (MRI) are commonly employed non-invasive methods for imaging the right ventricle. Among these, cardiac MRI is regarded as the gold standard for assessing RV volumetry and function[16,17].

In addition to anatomy, hemodynamic assessment of the right ventricle is an integral part of any functional assessment[18,19]. All cardiac electromechanical events have one goal: to propel blood forward in the vascular system. Color Doppler Imaging (CDI) and spectral Doppler are employed for blood flow visualization and quantification. However, CDI has limitations, such as angle dependency, restricting velocity measurement along the ultrasound beam. Additionally, aliasing artifacts occur when the Nyquist limit for blood velocity is reached, obscuring true velocity and flow direction[20,21]. Color Doppler also has limited temporal resolution depending on the region of interest, around 30-50 frames per second (fps), which is of capital importance in children as their heart rates are more elevated.

In Trondheim's ultrasound research environment, a flow modality called Blood Flow Imaging (BFI) was first developed to overcome CDI limitations[22,23]. The next step of the development was Blood Speckle Tracking (BST), a method designed to visualize and quantify blood flow velocities (figure 1) with higher temporal resolution.

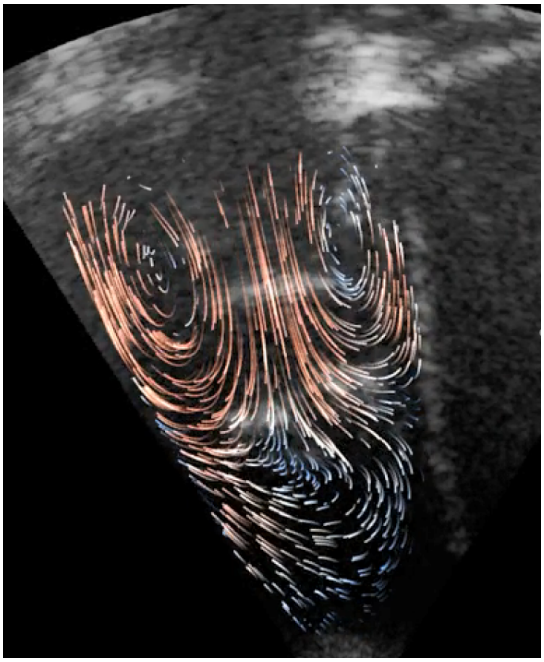

Figure 1: Example of BST in the right ventricle with particle animation

This allows to resolve very short-lived ventricular flow events and quantify blood flow velocities of speckles in the blood pool. This offers a novel perspective into the flow dynamics of hearts of patients with congenital heart disease.

The work in this thesis was conducted in collaboration with the engineers who developed the novel imaging technology and involved continuous refinement of the acquisitions as well as the analysis. This work was also the result of a collaboration between the Hospital for Sick Children

(SickKids) in Toronto and the Norwegian University of Science and Technology (NTNU) and St. Olavs University Hospital in Trondheim, Norway.

The unique challenges in congenital heart disease

The volume loaded right ventricle - Repaired tetralogy of Fallot and ASD

Tetralogy of Fallot (TOF), occurring in approximately 1 in 2,518 births[24], necessitates surgical repair to achieve a relatively normal lifespan. Relieving right ventricular outflow tract obstruction is among the main operative objectives. While efforts are made to preserve pulmonary valve function, when possible, severe pulmonary valve regurgitation is a frequent residual lesion. In the long term, this leads to right ventricular dilation and dysfunction, emphasizing the need for monitoring through various imaging modalities, mainly ultrasound and cardiac magnetic resonance imaging (CMR)[25–27].

Right ventricular (RV) failure significantly impacts the clinical condition and outcomes in both children and adults with rTOF[28]. Pulmonary valve replacement (PVR) is the main treatment approach to manage chronic RV volume and/or pressure overload in patients with rTOF, aiming to prevent RV failure. Nevertheless, in some cases, RV function remains compromised after PVR, even with the reduction of this haemodynamic stress. This suggests the possibility of irreversible cellular changes, or other factors contributing significantly to RV failure[29,30]. This highlights the role of detecting and preventing excessive adverse RV remodelling to maintain long-term RV function

and underscores the importance of exploring more sensitive and earlier biomarkers of RV function than the currently used volumetric data obtained for CMR or conventional echocardiography.

Recent advances in imaging techniques, including four-dimensional-flow CMR and vector flow mapping (VFM), have allowed the quantification of flow parameters such as vorticity and energy loss, contributing to a better understanding of RV flow dynamics[31,32]. High-frame-rate echocardiography and blood speckle tracking (BST) further enhances the ability to quantify blood flow vorticity and energy loss.

Large atrial septal defect (ASD) or pulmonary insufficiency (PI) after TOF repair results in right ventricular (RV) volume loading and dilatation. However, RV function remains preserved in ASD compared to progressive RV dysfunction in TOF patients[33]. Cardiac fluid disturbances are regarded as precursors of morphological changes[34]. The study of RV energetics in these two conditions with volume-loading of the RV and different long-term outcomes can help elicit differences in intraventricular fluid dynamics which could serve as early markers of adverse remodelling in the dilated, volume-loaded RV.

The pressure loaded right ventricle - Pulmonary arterial hypertension

In pediatric pulmonary artery hypertension (PAH), elevated pressure in the pulmonary artery and increased pulmonary vascular resistance negatively affect the morphology and function of the right ventricle (RV) by imposing a higher afterload. The impact of PAH on RV morphologic and functional parameters has been widely studied whereas data is scarce on the changes in flow dynamics associated with PAH[35–37]. Four-dimensional-flow CMR has been crucial in assessing flow characteristics, but its limitation in temporal resolution, especially in children, makes BST an

invaluable tool for studying short-lived flow events in the RV and MPA. The study of vortex formation and flow energetics in these patients could be a helpful, non-invasive marker of elevated pulmonary arterial pressure.

The volume underloaded univentricular heart - Fontan circulation

Functionally univentricular hearts (UVH) refer to a diverse spectrum of structural heart diseases, such as tricuspid atresia, mitral atresia, and double-inlet ventricles. UVH anatomy is characterized by insufficient functional and anatomical capacity for biventricular physiology, typically due to hypoplastic ventricles or a very large ventricular septal defect. Without surgery, some forms of UVH are fatal, contributing to 25% to 40% of neonatal deaths from congenital heart disease[38–40]. Survival rates have significantly improved with staged surgical palliation, approximately 88% at 10 years and around 84% at 15 years of age after Fontan palliation.[38,39,41–44]. As children transition into adulthood the risk of Fontan circulatory failure increases, affecting long-term morbidity and mortality[45–47]. Ongoing clinical and research efforts[48] focus on prognostication and longitudinal follow-up to identify determinants of successful palliation and transplantation-free survival.

Despite its success in directing systemic venous return to the pulmonary circulation, the Fontan circulation has many disadvantages, the first of which is the lack of ventricular pump to deliver pulsatile flow to the pulmonary circulation[49]. The movement of blood through the pulmonary circulation is dependent on systemic venous pressures which require a low trans-pulmonary gradient. Consequently, maintaining minimal pressure loss in pulmonary arteries and optimizing hemodynamic conditions are crucial for optimizing energetic efficiency in the Fontan

system[50,51]. It is typically associated with high central venous pressure and decreased cardiac output, particularly during exercise[52,53].

Diastolic ventricular dysfunction and other factors influencing transpulmonary pressure gradients are key determinants UVH function post-surgical palliation, with diastolic dysfunction being more prevalent than systolic dysfunction after the Fontan procedure[54–57]. Proposed mechanisms for diastolic dysfunction involve inherent myocardial abnormalities, including subendocardial fibrosis, conduction disturbances, or elevated ventricular compliance. Unfavourable mass-to-volume ratios persist throughout single ventricle palliation, resulting in hypertrophic changes to the volume-loaded ventricle after stage I palliation. This hypertrophy aims to minimize wall stress but subsequently leads to preload deficiency with gradual volume-unloading brought on during the Glenn and Fontan operations. The hemodynamic role of vortex formation patterns is unclear. The role of vortical flow in maintaining kinetic energy (KE) to minimize viscous energy loss (EL) remains theoretical, lacking direct quantitative assessment in both healthy subjects and patients with complex heart diseases. In addition, conventional echo-derived parameters of diastolic function are all load-dependant, limiting their applicability in UVH.[58]

Several CMR-based investigations have described the in vivo flow characteristics and categorize the phasic and temporal flow variations of Fontan circulation[48,59–62]. However, ultrasound is generally more accessible, particularly in younger patients who do not need sedation or anaesthesia as compared to CMR.

The exploration of altered cardiac flow dynamics has emerged as a potential early marker for adverse cardiac remodelling in both congenital and acquired heart diseases. In the realm of

clinical practice, cardiologists and cardiac imagers use ultrasound to quantify cardiac flow dynamics and energetics. However, these techniques, reliant on measuring pressure gradients and visualizing blood flow, often miss subtle changes due to their limited imaging speed, particularly in neonates and children with higher heart rates.

Despite being less accessible to non-invasive imaging, studying these subtle cardiac flow disturbances is crucial, as they are believed to precede morphological adaptation. This makes the study of cardiac flow dynamics a potential early, non-invasive marker of adverse cardiac remodeling, which is vital across all ages in congenital and acquired heart diseases. Current intervention cut-offs, based on morphological changes derived from echocardiography or CMR, may reflect a late stage in disease progression. The optimal timing for intervention could be better identified based on flow dynamics. Technological advancement in imaging has allowed for the exploration of novel hemodynamic parameters.

10. Non-invasive blood flow imaging

Doppler imaging is the mainstay of cardiac hemodynamic visualization and quantification, using Color Doppler and Spectral Doppler modalities. Doppler imaging has multiple limitations however such as angle-dependency, aliasing and a limited spatial and temporal resolution. In the last two decades, many novel blood flow imaging techniques have emerged using ultrasound imaging and CMR.

Echocardiography Particle Image Velocimetry

Echocardiography particle image velocimetry (echo-PIV)[63–65] involves injecting a small amount of ultrasound contrast agents, known as microbubbles, into the bloodstream. These particles are assumed to follow the movement of blood; hence the motion and velocity of these microbubbles can be calculated using image pattern matching techniques. This technique has been adapted from the PIV technology commonly used in fluid dynamics research. However, the use of ultrasound contrast in children has only recently been approved[66] in some countries, involves intravenous access and is readily accessible in clinical practice.

Vector flow mapping

Vector flow mapping (VFM) and its related technique called echodynamography[67] uses physics-based optimization to reconstruct the lateral flow velocity component by taking into consideration the spatial distribution of velocities obtained by color-Doppler, the endocardial border delineation as a boundary condition, and regularizing fluid physics terms. Itatani et al[68] and Garcia et al[69] further refined and improved the accuracy of this technique. Although this technique has allowed study of intracardiac dynamics and has had encouraging validation against PIV-echo[70], it still involves important mathematical assumptions and wall motion information to indirectly reconstruct components of blood velocities. One important assumption is that there is no out-of-plane flow component, which in most cases is not valid.

More recently, intracardiac flow analysis was made possible using retrospective, conventional echocardiographic acquisitions using a Doppler velocity reconstruction algorithm (DoVer)[71] which relies on both conservation of mass and momentum principles in contrast to VFM.

Although an innovative approach, the limited temporal resolution was identified as a major limitation in addition to most of the limitations of VFM.

4D-flow CMR

4D-flow MRI has become a valuable technology, offering in vivo, 4D imaging of complex intra cardiac and vascular blood flow patterns associated with congenital heart defects. This technology captures velocity fields in all three dimensions across any desired anatomical area, allowing for the assessment of new qualitative and quantitative hemodynamic parameters. Its main limitations are limited temporal resolution, length of acquisition time and accessibility of CMR, particularly in children who generally need sedation or general anaesthesia.

Blood speckle tracking

Conventional 2D ultrasound image reconstruction is based on transmitting focused ultrasound pulses through the tissue of interest and subsequent processing of the reflected ultrasound signals. Conventional image reconstruction requires multiple transmitted pulses, and the number of transmitted pulses required for reconstructing a complete color-Doppler image can lead to low image frame rates and limits the accuracy when measuring blood velocities. Plane wave imaging is based on sending broad, unfocused waves of ultrasound through the tissue of interest. By emitting a broad sound wave, ultrasound echoes are generated from the whole field of view, and a complete image can be formed in parallel for the region covered by the emitted pulse. This approach can significantly increase temporal resolution. This technological advancement is particularly advantageous in pediatric echocardiography, given that children have

higher heart rates compared to adults, necessitating superior temporal resolution to adequately resolve short-lived cardiac events. This however comes at the expense of image contrast, resolution, and penetration (figure2). Plane wave imaging has been applied for quantitative assessment of tissue properties (elastography)[72] and for imaging peripheral blood flow and vessel characteristics[73].

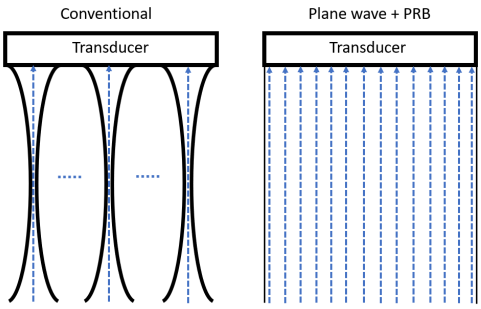

Figure 2: Conventional vs Plane wave ultrasound

PRB: Parallel receive beam

The engineering group at NTNU in Trondheim, Norway, has harnessed plane wave imaging to develop a high frame rate color Doppler technique[74]. When coupled with speckle-tracking analysis, this innovation facilitates the quantification and imaging of intracardiac blood velocities. Plane wave imaging enables cardiac imaging at exceptionally high frame rates[75] , theoretically increasing with a factor equal to the number of parallel receive beams, but lower in practice due

to real-time processing limitations of the ultrasound system[74]. In practice, our group has used 16 image lines in parallel, and a small number of transmit pulses (three to nine) for every image frame.

Originally designed to study myocardial motion, speckle tracking technology has been extended for the assessment of blood velocities in two-dimensional space. Given the weaker echoes coming from the blood pool compared to the adjacent myocardium, filtering stronger echo signals is an important process to allow blood speckles to become detectable. High-frame rate imaging, achievable with a plane wave ultrasound allows tracking of blood speckles by utilizing pattern-matching techniques (Figure 3) to quantify the movement of the blood speckles[76]. In this way, the velocity and direction of the blood flow can be calculated in an angle independent way with no upper aliasing limit.

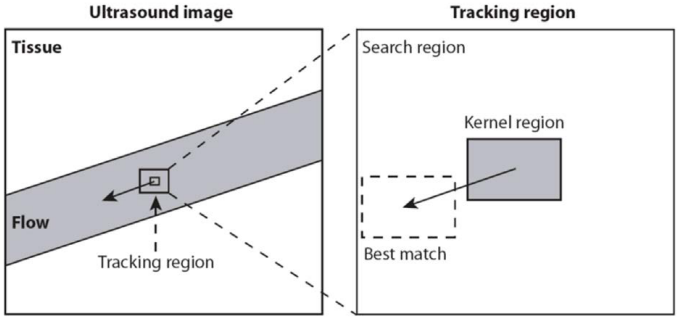

Figure 3: Blood speckle tracking. Reproduced from Fadnes et al 2014[77] with permissions. A spatial kernel region is defined in a first frame and the best match of this kernel is searched for in the next frame, which determines the velocity and direction.

Post-processing these high-frame rate images using speckle-tracking technology allows for the visualization of blood pool motion and the calculation of blood pool velocity vectors in 2D-space (Figure 4).

Initially developed using high-frequency linear transducers, these techniques have more recently been adapted to high-frequency phased array transducers[74], the standard probes used in pediatric echocardiography. This technological breakthrough offers a unique opportunity to visualize complex flow patterns in patients with congenital heart disease, shedding light on the underlying pathophysiology of the condition.

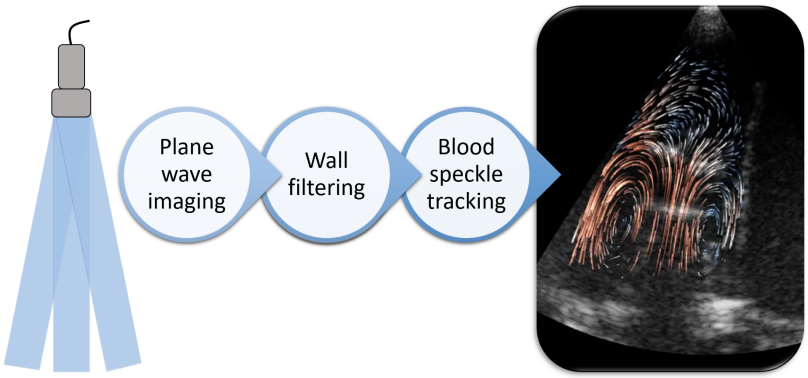

Figure 4: Blood flow imaging signal processing

Cardiovascular energetics

The heart is the source of mechanical energy in the cardiovascular system which is responsible for moving blood through it. This energy exists in three forms:[78,79]

1. Pressure potential energy: This is by the static pressure, measured invasively during cardiac catheterisation.

2. Kinetic energy: This energy of mass in motion, blood in the case of the cardiovascular system

3. Gravitational potential energy (or Hydrostatic Pressure): This is the energy a mass holds due to its position in a gravitational field.

Bernoulli's equation, rooted in the conservation of energy principle, dictates that in an ideal flow situation (steady and without friction), the energy entering and leaving a blood vessel should be equal. Thus, a drop in static pressure (like in blood pressure) should be compensated by an equivalent rise in either kinetic energy (dynamic pressure) or gravitational energy. Generally, gravitational energy changes have been considered negligible[80], leading to a simplified Bernoulli equation.

In the circulatory system, the primary source of mechanical energy is the work performed by the left and right ventricles. Ventricular contraction transfers mechanical energy to blood in the form of pressure. Conversion of pressure to kinetic energy leads to movement of a volume of blood. Energy losses are unavoidable in the cardiovascular system through friction, dissipating some mechanical energy irreversibly to thermal and acoustic energy. The ventricular contraction must give enough energy to blood to overcome these unavoidable energy losses within the system. Efficiency of the system is determined by how much energy is lost. Energy loss estimation

can help reflect global cardiac performance particularly when multiple lesions coexist as is often the case in congenital heart disease.

11. Quantitative cardiac flow parameters

The quantitative flow parameters obtained with BST describe different aspects of the flow field. Using the velocity information and the equations in Table 1 (page 43), different quantitative characteristics can be obtained.

Kinetic energy

The kinetic energy of blood refers to the energy it holds because of its movement. Given the absence of complete volumetric data, we integrate across a two-dimensional area to obtain the time trace of kinetic energy in J/m. Throughout various phases of the cardiac cycle, a fraction of this kinetic energy is dissipated due to viscous friction.

Energy loss

Mechanical energy, which can transform between pressure, gravitational, and kinetic types, also converts into heat due to the friction. The resulting heat cannot be turned back into mechanical energy, leading to an obligatory loss of energy. These losses stem from the shear interaction between adjacent layers of blood and the blood pool and the solid boundary of the cardiovascular structures.

Elevated energy loss in the cardiovascular system is thought to trigger genetic and biochemical alterations known as ventricular remodelling[78]. Initially, this process can be beneficial as it enhances cardiac performance. However, as mechanical stress and the related energy loss intensify or persist, these changes can become deleterious. These adverse effects include excessive thickening of the heart muscle (hypertrophy), significant enlargement (dilatation), or scarring of the heart tissue (fibrosis). The specific point at which remodelling shifts from being beneficial to harmful is not clearly defined in clinical, mechanical, or biochemical terms. Reducing mechanical stress and returning energy loss to more normal levels through various interventions such as valve repair or replacement, cardiac resynchronisation, can sometimes reverse detrimental ventricular remodelling. This is seen in cases such as rTOF and ASD, where pulmonary valve replacement or atrial septal defect closure can reverse ventricular dilation if done at the optimal moment.

In our study, viscous energy loss was considered and involved the assumption of only planar shear forces. Integration over the area of interest allows the quantification of EL.

Vorticity

Vorticity measures the rotation within a fluid around each point in the image at a specific time. It is a measure of blood flow complexity but is distinct from turbulence. It is calculated by the curl of the blood velocity vector field[81]. It is a central characteristic of intracardiac vortices. Cardiovascular vorticity results from blood-boundary interaction with formation of a shear layer resulting from velocity differences between the blood and the boundary. Vorticity is often present

in coherent flow structures, such as helices and ring vortices, and plays a critical role in the assessment of ventricular function and its pathophysiological implications[82,83]. Recently, vorticity has been studied by 4D-flow CMR in rTOF showing higher VO in rTOF[84] and relations to RV and LV dimensions[85].

Vector complexity

Vector complexity (VC) reflects the complexity of flow by measuring the angle spread of the blood velocity vectors within the flow and is adapted from Saris et al [86] who describe its use in carotid artery flow imaging. The resulting measures is a value between 0 and 1. When VC is equal to 0, the flow is the simplest with all vectors oriented in the same directions. When the VC value is 1, this represents the most complex flow, when none of the vectors are oriented in the same direction.

12. SAFETY OF PEDIATRIC ECHOCARDIOGRAPHY

Ultrasound has maintained an excellent safety record even with significant improvements in the various components of ultrasound imaging. The energy deposited in tissue by ultrasound leads to two primary bio-effects: heating and cavitation. Regulations focus on safety indices related to these effects, namely the thermal index (TI) and the mechanical index (MI).

The thermal index provides insight into tissue temperature rise due to ultrasound absorption, with bone and adjacent soft tissues being most susceptible. For neonatal cardiac

imaging, limiting exposure time is advised when TI exceeds 1. Manufacturers' declared maximum TI values are generally low, with pulsed Doppler mode having the highest values and B-mode imaging the least. It is crucial to adhere to recommended exposure times and stay within acceptable TI values to mitigate thermal effects.

The mechanical index assesses the likelihood of cavitation[87], the formation and collapse of gas bubbles resulting from shear forces. Tissues near gas, such as the lung and intestine surfaces and those involving contrast agents, are at risk of mechanical damage. Mechanical effects are best predicted by understanding individual pulses, specifically peak negative pressure. The FDA's maximum permitted MI is 1.9. Both TI and MI values are accessible on the ultrasound scanner screen, and when low values are unattainable, it is advisable to keep examination times short, staying within recommended limits.

Advancements in ultrasound technology have significantly improved image quality but have also led to some increases in acoustic output levels. Nonetheless, diagnostic ultrasound imaging remains safe when practitioners adhere to recommended limits. The ultrasound energy used for plane wave imaging is similar to regular ultrasound techniques. This new modality has been safety tested by GE Vingmed Ultrasound, with results provided to the ethical committees in Norway and Canada. All patient safety measurements were within the guidelines from the US Food and Drug Administration (FDA) and we received approval from Health Canada before enrolling patients. During the time period of this PhD, BST has been released for commercial use worldwide by GE as “Blood Speckle Imaging”.

13. AIMS

Using BST, we sought to describe the flow energetics and dynamics in the right heart, including the RV and MPA. We first proceeded to investigate and validate the quantitative measures using a 3D computer simulation and the describing the influence of smoothing parameters as well as imaging plane. We also assessed the interobserver and interobserver variability. After this, we studied the RV in three conditions:

1) The volume-loaded RV in ASD and rTOF. We hypothesised that both groups would have higher energy loss and vorticity compared to controls (CTL) given the increased RV stroke volume. However, we expected that EL and vorticity location would be different in rTOF compared to ASD and CTL because of the presence of severe pulmonary regurgitation.
2) The pressure-loaded RV and MPA in pulmonary arterial hypertension: We hypothesised that flow patterns would be different in the MPA of PAH compared to CTL with higher EL, VO and VC. We expected to observe the same differences in the RV.
3) The volume-underloaded ventricle in UVH after Fontan palliation: We hypothesized that in this context of lower ventricular preload, KE and EL would be lower in UVH, while inflow patterns would differ between the morphological subtypes.

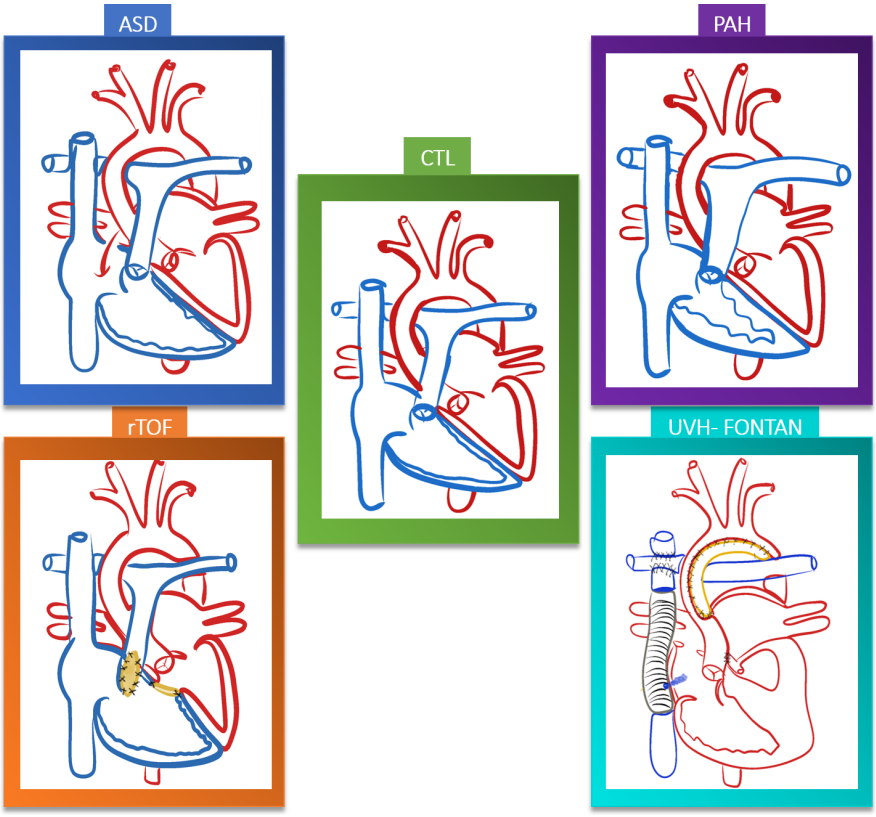

Figure 5: schematics of the study groups

14. MATERIALS AND METHODS

Study overview and design

The study relied on prospective, non-randomised high frame rate ultrasound (HFRUS) acquisitions on a research Vivid E-9 system (GE Ultrasound, Horten, Norway) as well as a Vivid E-

95/E90 utilizing plane-wave ultrasound images utilizing commercially available ultrasound probes (6 /12 MHz phased-array probes).

The studies were conducted on three sites: St. Olavs University Hospital and Ålesund Hospital in Norway and the Hospital for Sick Children in Canada. Under the leadership of Siri Ann Nyrnes and Luc Mertens on each site respectively.

Study participants were included from three sites with normal controls from Trondheim (Paper 1 and 2), Ålesund (Paper 3), Norway and cases with ASD, rTOF , PAH and UVH included from SickKids, Toronto, Canada.

Inclusion Criteria for all patient groups

1. Age ≤ 10 years
2. Patients scheduled for undergoing a clinically indicated echocardiography at the SickKids Echocardiography laboratory, St. Olavs and Ålesund Hospitals (normal controls).
3. Written informed consent has been obtained.

Exclusion criteria for all patient groups

1. Inability to lie still during the image acquisition.

Specific inclusion/exclusion criteria for subgroups

Patients with atrial septal defect (ASD)

1. Atrial septal defect (secundum or sinus venosus defect) with L-R shunt on atrial level causing significant RV dilatation (RVEDD z-score> 2.5)

Specific exclusion criteria:

a. Primum defect or atrioventricular septal defect b. Associated congenital heart defects.

Repaired tetralogy of Fallot (rTOF)

1. Severe pulmonary regurgitation as demonstrated by Doppler echocardiography.

Specific exclusion criteria:

1. No significant residual right ventricular outflow tract obstruction (Right ventricular outflow tract gradient < 35 mmHg)

2. No significant pulmonary artery branch stenosis (Peak gradient on branches > 35 mmHg)

Pulmonary arterial hypertension (PAH)

1. PAH as defined by an estimated mean pulmonary artery pressure by echocardiography above 25 mmHg.
2. No anatomic lesions causing right ventricular hypertension.

Functionally single ventricular heart after Fontan palliation

1. Univentricular hearts following Fontan palliation.

Specific exclusion criteria:

1. More than mild atrioventricular valve regurgitation

Healthy controls

1. Healthy children undergoing echocardiography with a normal cardiac structure and function.

Procedures and ethics

Studies were performed in accordance with national and international laws, regulations and conventions for research on humans. Patient representatives contributed to the elaboration of the study protocols and consent forms. Studies were conducted after ethics approval from the ethics review board in all centers. All data collected was de-identified, and coupling lists were not shared between centers. The patient/parent were initially approached by the treating team, who are within the patient's circle of care, to introduce the study. If the patient/parent agrees to learn more about the study, a regulated healthcare professional from the research team was introduced and explained the study directly to the patient/parent and obtained informed consent and, if applicable, assent.

Participants were imaged with the BST during their clinical visit. The participants also underwent routine echocardiography as per standard of care the same day. Both regular image data and RF (IQ) data were stored offline for analysis. At least 2 cardiac cycles on the E95 system and 3 cycles on the E9, were recorded with the 6S and 12S commercially available phased-array

probes (GE Healthcare, Milwaukee, WI, USA). In-phase and quadrature (IQ) data were stored and used offline for postprocessing and analysis with blood speckle tracking.

Quantitative and qualitative blood flow analysis

The raw echo data collected from both patients and controls underwent offline analysis using specialized in-house software designed for quantitative flow field analysis (PyUSview, NTNU, Norway).

Radial velocity measurements were obtained through color-Doppler, while lateral velocity estimates were determined using speckle tracking according to the method outlined by Wigen et al. in 2018[88]. To be included for analysis, apical right ventricular four-chamber (RV4C) views needed to include the RV inlet and apex, and RV3C views needed to include the inlet, outlet, and apex. Acquisitions with important signal dropout were excluded. Two observers (SAN, SF) evaluated the quality of acquisitions, with only RV4C and 3C views of good quality being subjected to analysis. In study 2, the flow field in the MPA was segmented and analysed.

Using PyUSview, a single observer (WM) performed segmentation of cardiac cycle and the flow field. Systole and diastole phases were identified based on the closure and opening of the tricuspid valve using a B-mode image and a timing tool within PyUSview. The start of systole was identified by the first frame where the tricuspid valve closed, while the initiation of diastole was defined by the first frame where the valve opened. After this timing was defined, the region of analysis was delineated using a domain which was drawn between the blood-endocardium border to the hinge-points of the atrioventricular valve. Following this, analysis of quantitative and qualitative data is possible. The processing steps are detailed in the figure 6. Utilizing the measured

velocities, ventricular flow parameters in the two-dimensional plane were calculated from the RV4C view according to the definitions and equations in table 1.

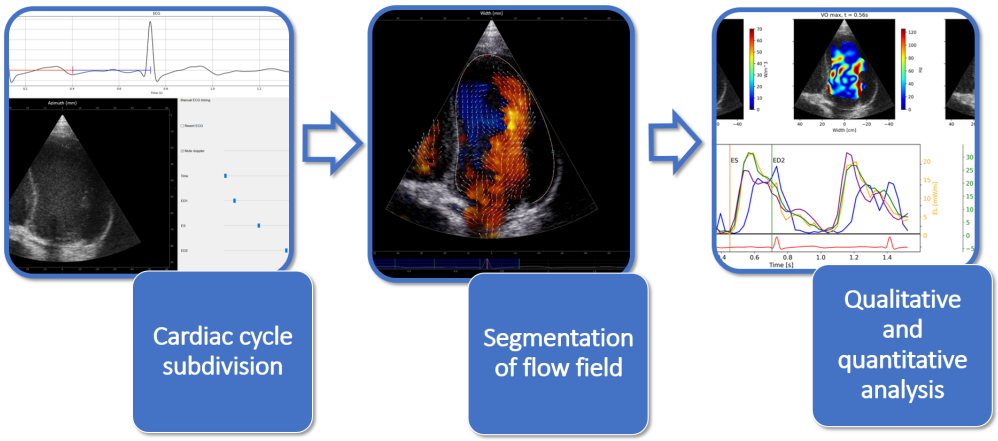

Figure 6: Summary of post-processing steps in PyUSview

Parameter	Description	Formula
Kinetic energy (KE)	Energy possessed by blood because of its motion (J/m)	$KE = \int q\, dA \quad ; \quad q = \frac{1}{2}\rho v^2$
	q: KE per unit of volume of fluid ρ = 1060 kg/m³ is the density of the blood and *v* is the velocity magnitude	
Energy loss (EL)	Rate of energy loss (W/m) Time integrated (J/m)	$\boldsymbol{EL = \mu \int 2\left(\frac{\partial v_x}{\partial x}\right)^2 + 2\left(\frac{\partial v_y}{\partial y}\right)^2 + \left(\frac{\partial v_x}{\partial y} + \frac{\partial v_y}{\partial x}\right)^2 dA,}$
	$v = [v_x, v_y]$ is the blood velocity vector and μ = 0.004 Pa·s is the blood viscosity	
Vorticity (VO)	Rate of rotation around each point in the image (Hz)	$\boldsymbol{VO = \lvert \vec{\omega} \rvert = \lvert (\partial v\_y)/\partial x - (\partial v\_x)/\partial y \rvert}$
Vector complexity (VC)	Measure of flow laminarity	1– r; Where $\boldsymbol{r = \sqrt{x^2 + y^2}}$; $\bar{x} = \frac{1}{n} \cdot \sum_{i=1}^{n} \cos(\theta_i)$; $\bar{y} = \frac{1}{n} \cdot \sum_{i=1}^{n} \sin(\theta_i)$ Θ *: flow angle*

Table 1: Quantitative flow parameter definitions and equations

The integration area in this study was defined by the color flow image, signifying integration of values wherever a color flow signal was present in each frame. Consistency in analysis was maintained through uniform temporal and spatial smoothing parameters (temporal smoothing: 40 ms; Gaussian spatial smoothing: 5x5 mm²). Energy loss values were ultimately determined by calculating the time-integrated values during systole and diastole, expressed in mJ/m.

Vorticity (VO) serves as a metric for the local rotation rate of blood in a two-dimensional flow field. Its computation was performed mathematically using the specified formula derived from the RV4C view and expressed in s^{-1}.

In study 1, localization of areas of high EL or VO was done using a RV3C view because it images simultaneously the RV inlet, apex and outlet flows in one acquisiton.

All acquisitions were also analysed qualitatively, describing patterns of ventricular and arterial vortex formation and dissipation during the cardiac cycle.

Reproducibility evaluation

To assess inter and intra-observer variability in quantification of flow parameters for the apical four chamber view, five subjects randomly selected from each group were included in study 1. Reproducibility assessment focused solely on energy loss (EL), as VO and VC rely on blood velocity measurements obtained through the same method.

The post-processing analysis steps were replicated after a four-week interval by the same observer and independently by a different observer (SAN). These steps encompassed:

1. Definition of timing points for systole and diastole, as previously outlined.
2. Segmentation of the flow domain by tracing the endocardial surface of RV
3. Calculation of EL in the selected cardiac cycle.

For each patient, both observers selected the same heart cycle from the RV4C cine-loop, and all data underwent analysis with consistent smoothing settings. This rigorous evaluation aimed to gauge the reliability and consistency of EL measurements in the specified context.

Validation and analysis of the energy loss measurement

In the first study, we aimed to verify the accuracy of the EL measurements and assess their sensitivity to variations related to imaging plane, data smoothing, and dropouts, a 3D computer simulation was conducted, as depicted in Figure 7 (bottom left panel). This simulation replicated key flow events (filling, vortex formation, and ejection) using a previously described ventricular model[89].

This simulation allowed for a comparison with a known ground truth for both 2D and 3D velocity fields, offering the flexibility to obtain standard and non-standard imaging views. The impact of small offsets (±5°) from standard cardiac views on 2D EL values was investigated. Additionally, the influence of dropouts and smoothing in the color-Doppler and BST data on EL was explored.

Study population characteristics

Approval from the ethics review boards of the Hospital for Sick Children in Toronto, Canada, and The Regional Committee for Medical and Health Research Ethics, REC Central, Trondheim, Norway, was obtained, and informed consent was collected before enrolment for all studies.

Materials - Study 1

Children with repaired tetralogy of Fallot (rTOF) and severe pulmonary insufficiency (PI), large secundum atrial septal defects (ASD) causing right ventricular (RV) dilatation (RV end-diastolic dimension Z score > 2.5), along with healthy controls (CTL), were enrolled from the Hospital for Sick Children in Toronto, Canada, and St. Olavs Hospital in Trondheim, Norway,

spanning December 2015 to January 2018. Parental consent was secured per the ethics review boards of both institutions with an upper age limit of 10 years. Conventional echocardiographic parameters were obtained before high-frame-rate acquisitions. The baseline characteristics can be found in table 2.

	CTL (n = 25)	rTOF (n = 21)	ASD (n = 11)
Age (months)	42 (26-76)	41 (21-74)	66 (33-99)
Male (%)	48%	52%	54%
Height (cm)	100 (85-124)	95 (82-109)	104 (88-134)
Weight (kg)	15.8 (12.3-23.6)	12.2 (10.0-19.5)	17.9 (10.5-27.3)
$BSA_{Haycock}$ (m^2)	0.94 (54-1.2)	0.84 (0.69-1.03)	0.74 (0.50-1.00)

Table 2: Baseline demographic data study 1

ASD: atrial septal defect; BSA: Body surface area; CTL: controls; rTOF: repaired tetralogy of Fallot; Values expressed as median, quartiles (Q1-Q3)

RV three-chamber (RV3C) and four-chamber (RV4C) views were acquired using a modified Vivid E-9 system (GE Vingmed Ultrasound, Horten, Norway). Three cardiac cycles were recorded with commercially available ultrasound probes. The acquired IQ (in-phase and quadrature) data were stored for offline postprocessing and analysis with blood speckle tracking.

To validate the energy loss (EL) measurement and assess its sensitivity to imaging plane changes, data smoothing, and dropouts, a 2D EL evaluation was conducted in a 3D computer simulation mimicking ventricular flow events. The effects of small offsets, dropouts, and smoothing in color-Doppler and blood speckle tracking data on EL were investigated.

The raw echo data from patients and controls underwent offline analysis using in-house software. Radial velocity was derived from color-Doppler, and lateral velocity estimates were determined by speckle tracking. Quality assessments were performed, excluding acquisitions with significant signal dropout, and only RV4C and 3C views of good quality were analyzed. Flow field segmentation was conducted, defining the region of analysis by delineating the endocardial border in both views.

Systole and diastole were identified by tricuspid valve closure and opening. EL in the two-dimensional plane was calculated from the RV4C view using a formula, and vorticity (VO) was computed mathematically using the RV4C view. A RV3C view was employed to localize areas of high EL. Reproducibility was assessed in five randomly selected subjects from each group, evaluating inter and intra-observer variability in EL measurement from an RV4C view, considering the timing points of systole and diastole, flow domain segmentation, and EL calculation.

Materials - Study 2

Between December 2015 and December 2020, we enrolled patients under 10 years of age with pulmonary arterial hypertension (PAH), defined by echocardiography showing an estimated mean pulmonary artery pressure exceeding 25 mmHg. Healthy controls (CTL) matched for age and sex were also included. The baseline characteristics can be found in Table 3.

	PAH (n=18)	CTL (n=18)
Male (%)	50	44
Age (years)	2.8 (0.5-4.2)	3.2 (0.5-4.8)
Height (m)	110 (89-125)	99 (80-122)
Weight (Kg)	18.9 (15.4-32.3)	15.8 (10.9-25.6)
BSA (m^2)	0.75 (0.65-0.81)	0.66 (0.50-0.94)

Table 3: Baseline characteristics study 2

BSA: Body surface area; CTL: controls; PAH (Pulmonary arterial hypertension); Values expressed as median, quartiles (Q1-Q3)

Utilizing a Vivid E9 or E95 system (GE Vingmed Ultrasound, Horten, Norway) with research software, we performed image acquisitions with a frame rate equal to the pulse repetition frequency, reaching the kHz range, combined with the B-mode modality. Short-axis views of the main pulmonary artery and RV-centred apical views were acquired using commercially available ultrasound probes. IQ (in-phase and quadrature) data storage enabled full offline postprocessing and blood speckle tracking analysis with dedicated in-house software tools (PyUSview, NTNU, Norway). Consistent temporal and spatial smoothing parameters (temporal smoothing = 40 ms, Gaussian spatial smoothing = 5x5mm2) were maintained for all analyses.

The main pulmonary artery flow field and RV were segmented, and vorticity, energy loss, and vector complexity were quantified in the main pulmonary artery (MPA) and the RV. The calculation of energy loss and its validation have been previously described, as well as the

definition of vorticity based on blood speckle tracking (BST). Vector complexity, indicating flow laminarity, was defined as 1-r, with measurements ranging from 0 (uniform flow direction) to 1 (varying flow directions). Conventional echocardiographic parameters were obtained using standard clinical methodology, and right pulmonary artery (RPA) distensibility was measured as the percentage difference between maximal and minimal RPA diameters in a parasternal short-axis view.

Materials - Study 3

Children with functional UVH and healthy controls (CTL) were included from the Hospital for Sick Children in Toronto, Canada and Ålesund Hospital, Ålesund, Norway, between December 2015 and March 2023. Consent from the parents of each participant was obtained before enrolment. Because of penetration limitations related to BST echocardiography, the upper age limit for inclusion was 10 years of age.[74] Conventional echocardiography was obtained from clinical studies done immediately before the high-frame-rate acquisitions. Ventricular apical four-chamber (V4C) and apical three-chamber (V3C) views were acquired using a modified Vivid E9 and E90/E95 systems (GE Vingmed Ultrasound, Horten, Norway) with research software. Flow data were acquired with a frame rate equal to the pulse repetition frequency, i.e. in the kHz range, and combined with the B-mode modality.[74] At least 2 cardiac cycles were recorded with commercially available 6S phased-array ultrasound probe (GE Healthcare, Milwaukee, WI, USA). Storage of IQ (in-phase and quadrature) data were required for the offline postprocessing. Quantitative flow parameters were obtained from the V4C, while both the V4C and V3C views were used to qualitatively describe both the inflow and outflow.

	UVH (n = 29)	SLV dominant (n = 9)	SRV dominant (n= 14)	SV DILV (n=6)	CTL (n = 30)
Age (months)	84 (60-113)	85 (57-127)	70 (60-112)	63 (59-89)	81 (70-87)
Fontan Fenestration	5/29 (left to right)				
NYHA class	Class 1: 23 Class 2: 6	Class 1: 7 Class 2: 2	Class 1:12 Class 2: 2	Class 1: 4 Class 2: 2	Class 1: 30
Paced rhythm	1: dual chamber	0	1: Dual chamber	0	0
Male (%)	79	78	70	83	51
Height (cm)	94 (33-117)	102 (23-144)	96 (38-117)	103 (36-123)*	126 (121-128)
Weight (kg)	24(17-119)	28 (16-122)	20 (15-118)	19 (15-82)	23 (22-27)
$BSA_{Haycock}$ (m^2)	0.83 (0.67-1.02)	0.75 (0.59-0.96)	0.81 (0.66-1.05)	0.69 (0.64-0.86)	0.88 (0.86-0.98)
HR (bpm)	79 (72 –100)	77 (70-96)	81 (68-92)	112 (111-113)*	82 (71-91)
QRS duration (ms)	98 (88-108)	90 (84-98)	98 (88-104)	114 (102-147)*	84 (80-95)
V FAC (%)	36 (28-50)		36 (28-53)	37 (27-46)	
TAPSE (mm)	7.6 (3.7 – 9.6)		7.7 (7.3 – 9.9)		
LVEF (%)		65 (55-70)			56 (51-60)
E wave velocity (cm/s)	81 (67-97)	71 (42-85)	94 (74-107)	77 (66-89)	92 (86-100)*
A wave velocity (cm/s)	50 (39-72)	41 (33-53)	56 (42-75)	49 (36-61)	45 (42-54)
E/A	1.44 (1.10-2.21)	1.65 (0.98-2.43)	1.39 (1.17-2.22)	1.57 (1.08-2.54)	1.92 (1.71-2.17)*
E/e'	8.3 (6.5-12.2)	5.0 (4.3-6.9)	10.9 (6.5-12.8)	8.3 (6.8-11.9)	6.8 (5.9-7.2)*

Table 4: Baseline characteristics study 3

BSA: Body surface area; CTL: controls; UVH: Univentricular heart; SRV: single right ventricle; SLV: single left ventricle; DILV: Double inlet left ventricle; NYHA: New York Heart Association; VFAC: ventricular fractional area change; HR: heart rate; RV: right ventricle; TAPSE; tricuspid annular plane systolic excursion; KE_S: systolic kinetic energy; KE_D: Diastolic kinetic energy VC_S: Systolic vector complexity; VC_D: Diastolic vector complexity; EL_S: Systolic energy loss; EL_D: Diastolic energy loss; VO_S: Systolic vorticity; VO_D: Diastolic vorticity. * When p value < 0.05; Values expressed as median, quartiles (Q1-Q3)

Statistical Methods

The statistical analyses were conducted using GraphPad Prism 8 (GraphPad Software, La Jolla, CA).

Study 1

Inter-and intra-observer analyses of energy loss (EL) was assessed using Bland-Altman plots. Demographic and echocardiographic data were expressed as median with quartiles (Q1-Q3). Kruskal-Wallis test was used to test the differences between the energy losses in three groups (CTL, rTOF and ASD). Comparison between two groups was done using the Mann-Whitney U test where a p-value < 0.05 was considered statistically significant. Spearman's rank test was used to test for correlations.

Study 2

Comparison between PAH and CTL groups was done using the Mann-Whitney U test with a p-value < 0.05 was considered statistically significant. Correlations were tested using Spearman's rank test.

Study 3

Data were expressed as median with quartiles (Q1-Q3). Comparison between two groups was done using the Mann-Whitney U test where a p-value < 0.05 was considered statistically significant. Correlations were tested using Spearman's rank test. Strength of correlations were classified depending on r values (>0.95: excellent, 0.85-0.95: strong, 0.70-0.85: good, 0.50-0.70: moderate and <0.5: poor)

15. SUMMARY OF RESULTS

Results - Study 1

Validation of EL using computational fluid dynamics

The validation and analysis of EL calculations using computational fluid dynamics (CFD) are summarized in Figure 7. Our primary objective was to assess the alignment of 2D EL for standard views with the true 3D EL and to explore how deviations from these imaging planes impact the 2D EL measurement.

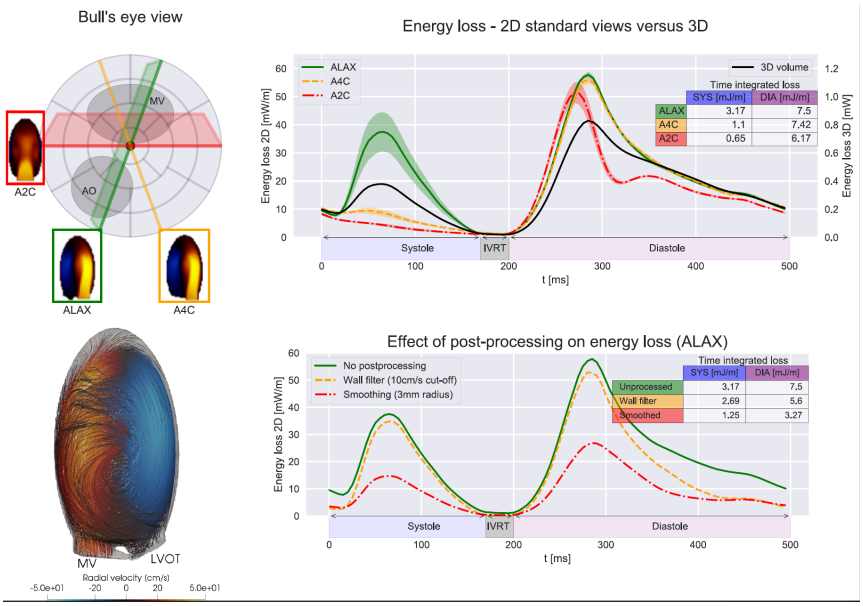

Figure 7: An analysis of the energy loss metric in a computer simulation model mimicking 3D ventricular flow.

The 3D EL curve indicated that most of the energy loss in the model occurs during diastole, characterized by the filling jet leading to vortex formation and associated shearing fluid losses. For the standard 2D views, specifically the apical long-axis view (ALAX) and apical four-chamber view (A4C), both provided a relatively accurate representation of diastolic 3D EL (with a relative error of ±5% and ±4%, respectively). These 2D views exhibited similar integrated EL values, demonstrating limited sensitivity to imaging view misalignment (Figure 7, upper right panel, shaded color regions around the curves). In contrast, the apical two-chamber view (A2C) showed the highest error (±9%) during diastole. For systole, both the EL traces and integrated values exhibited substantial variation between imaging planes (relative error ALAX ±19%; A4C ±13%; A2C

±17%). These findings supported the preference for A4C views in diastole for our patient population.

Our secondary objective was to analyze the impact of post-processing changes on the estimated 2D EL, illustrated for the ALAX view in Figure 7 (lower right plot). Notably, spatial smoothing reduced the EL magnitude while preserving the curve shape, and the wall filter had minimal influence in systole but could lead to some underestimation of EL in mid-to-late diastole.

In summary, the computational simulation of EL analysis revealed that, firstly, 2D diastolic EL measures from A4C and ALAX views closely matched the 3D EL shape, while the 2D systolic EL measure from the ALAX view demonstrated good agreement with the 3D EL shape. Secondly, the effect of post-processing primarily resulted in a change in EL magnitude, facilitating the comparison of relative changes. Consistency in post-processing parameters is crucial and providing clear baseline values is essential.

Energy Loss in the volume-loaded RV of repaired Tetralogy of Fallot (rTOF) and Atrial Septal Defect (ASD)

The study included a total of 21 repaired TOF (rTOF) patients (16 with a transannular patch repair and 5 with an RV-to-pulmonary artery conduit), 11 ASD patients, and 25 control subjects, all possessing a suitable RV4C view for analysis. All rTOF subjects exhibited severe pulmonary insufficiency (PI) without residual right ventricular outflow tract obstruction. The RV3C view, defined as a loop with high-quality Blood Speckle Tracking (BST) measurements in the inflow, outflow, and apex, was suitable in 11/25 controls, 9/11 ASD, and 15/21 rTOF patients.

Baseline demographic characteristics were comparable across the three groups (Table 2). The rTOF group had a longer QRS duration compared to the other groups. Echocardiographic parameters of RV size and function indicated enlarged RVs in ASD and rTOF patients compared to controls. While RV fractional area change (FAC) showed no notable differences among the three groups, tricuspid annular plane systolic excursion (TAPSE) was reduced in patients with rTOF compared to both groups, while it was highest in ASD (Table 5). Tricuspid early diastolic inflow velocity (TV E) did not differ between the groups. Left ventricular (LV) systolic function parameters were similar in all three groups.

	CTL (n = 25)	rTOF (n = 21)	ASD (n = 11)
HR (bpm)	97 (85-108)	93 (85-100)	97 (89-101)
QRS duration (ms)	81 (77-93)	114 (80-128)*	82 (72-92)†
RV EDd (mm)	13 (10-16)	19 (17-23)	25 (21-32)
RV EDd Z-score	-0.4 (-1.4-0.9)	3.3 (2.7-3.5)*	4.6 (2.8-5.1)*
TAPSE (mm)	20 (18-23)	11 (10-13) *	23 (17-27) *†
RV Diastolic area (cm^2)	9.0 (7.6-13.3)	15.2 (8.8-17.6)*	18.2 (14.2-20.3) *†
RV Systolic area (cm^2)	5.6 (4.0-7.7)	8.7 (5.9-10.7)*	14.1 (10.5-20.3)*
RV FAC (%)	40 (37-46)	37 (33-42)	45 (37-48)
TV E (cm/s)	84 (72-126)	84 (71-100)	80 (70-101)
LVEF (%)	69 (64-74)	64 (61-68)	66 (61-70)
LVSF (%)	36 (32-39)	34 (32-37)	35 (31-38)
EL_S (mJ/m)	0.17 (0.10-0.48)	0.29 (0.07-0.51)	0.44 (0.29-0.68)
EL_D (mJ/m)	1.34 (0.55-2.06)	1.93 (1.46-2.74)*	2.86 (1.47-3.65)*
VO_S (Hz)	3.66 (2.02-5.98)	6.57 (1.52-11.19)	13.90 (6.13-18.41)
VO_D (Hz)	14.09 (8.36-17.61)	23.01 (17.73-28.52)*	28.74 (21.55-33.80)*

Table 5: Right ventricular energy loss and vorticity in the four-chamber view

ASD: atrial septal defect; CTL: controls; rTOF: repaired tetralogy of Fallot; EDd: end-diastolic dimension; EF: ejection fraction; FAC: fractional area change; HR: heart rate; LV: Left ventricle; RV: right ventricle; SF: shortening fraction; TAPSE; tricuspid annular plane systolic excursion; TV E: tricuspid valve E wave velocity EL_S: Systolic energy loss; EL_D: Diastolic energy loss; VO_S: Systolic vorticity; VO_D: Diastolic vorticity; p-value < 0.05: ***** ASD or rTOF vs CTL; Values expressed as median, quartiles (Q1-Q3)

Quantitative Results from Right Ventricular Four-Chamber Views

Table 5 and Figure 8 provide a comparison of flow characteristics among the three groups based on blood speckle tracking. Both ASD and rTOF patients exhibited significantly higher diastolic EL compared to controls. Systolic EL, however, was similar across all groups. Diastolic vorticity was also higher in ASD and rTOF patients compared to controls, while maximal systolic vorticity was similar across all groups. Heart rate, body surface area (BSA), or QRS duration did not correlate with EL or vorticity in any group. Weak statistically significant correlations of systolic and diastolic EL with age were noted in rTOF and controls, but not in ASD, with a wide spread of values as age increased. Energy loss and vorticity did not correlate with any conventional RV functional parameters.

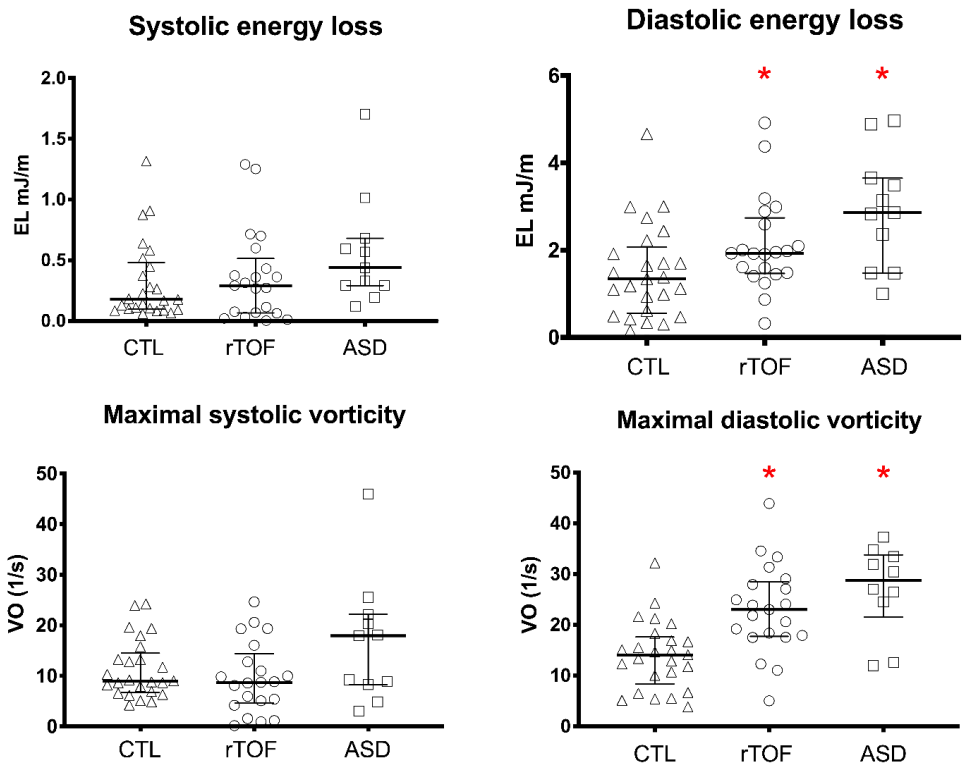

Figure 8: Scatter plot of right ventricular flow energetics in the four-chamber view

Scatter plot of energy loss and vorticity with median (thick line) and quartiles (Q1-Q3, thin line); ASD: atrial septal defect; CTL: controls; EL: energy loss; rTOF: repaired tetralogy of Fallot; p-value < 0.05:***** ASD or rTOF vs CTL, **†** rTOF vs ASD

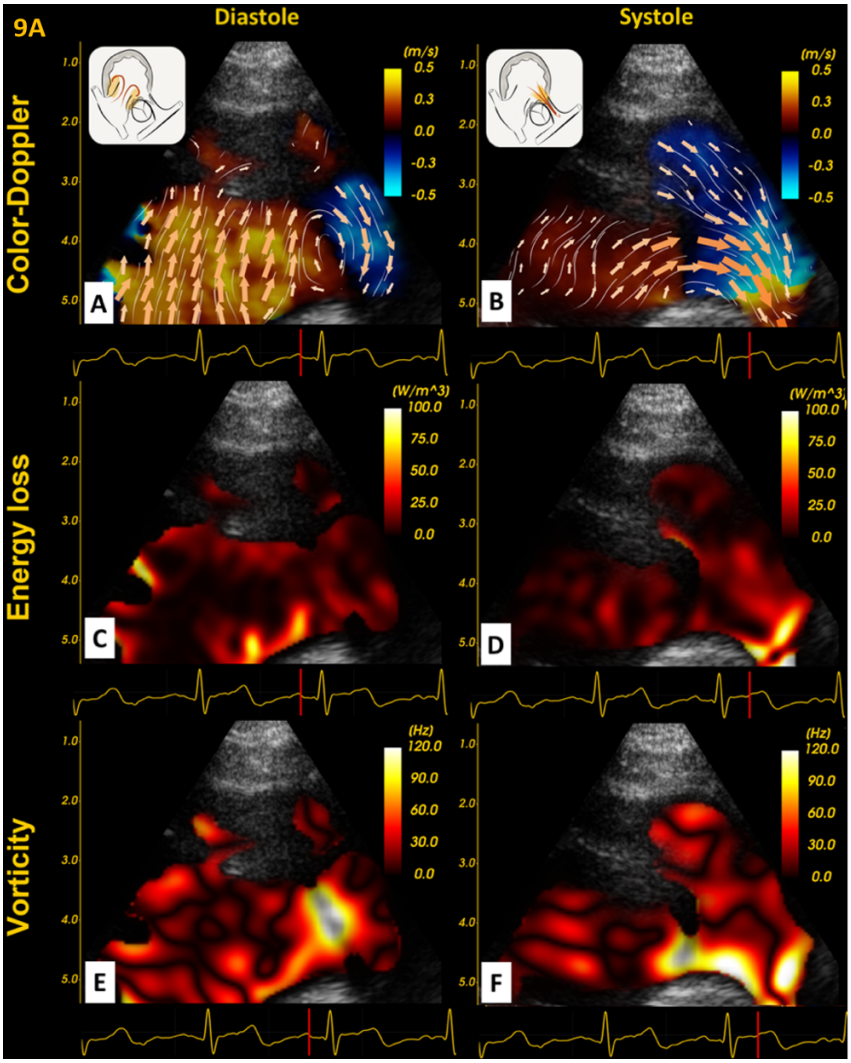

Figure 9A: Typical examples of right ventricular intracardiac velocities, energy-loss and vorticity mapping in diastole and systole in controls

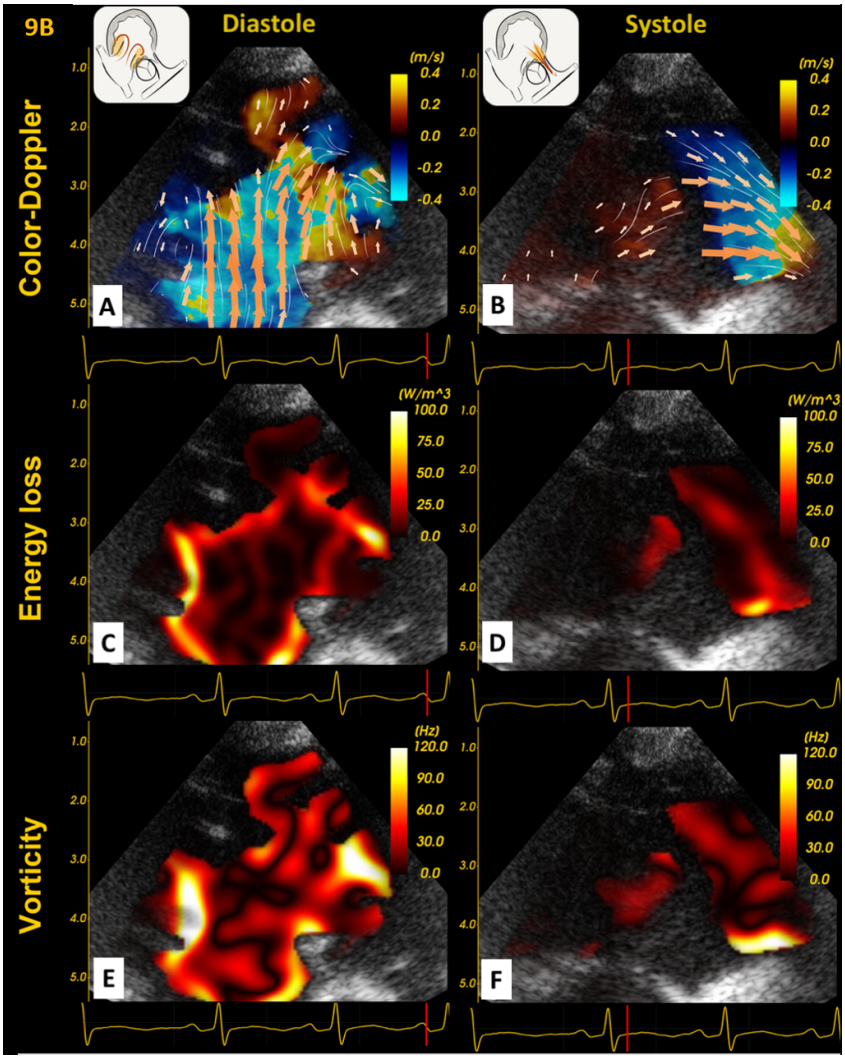

Figure 9B: Typical examples of right ventricular intracardiac velocities, energy-loss and vorticity mapping in diastole and systole in ASD

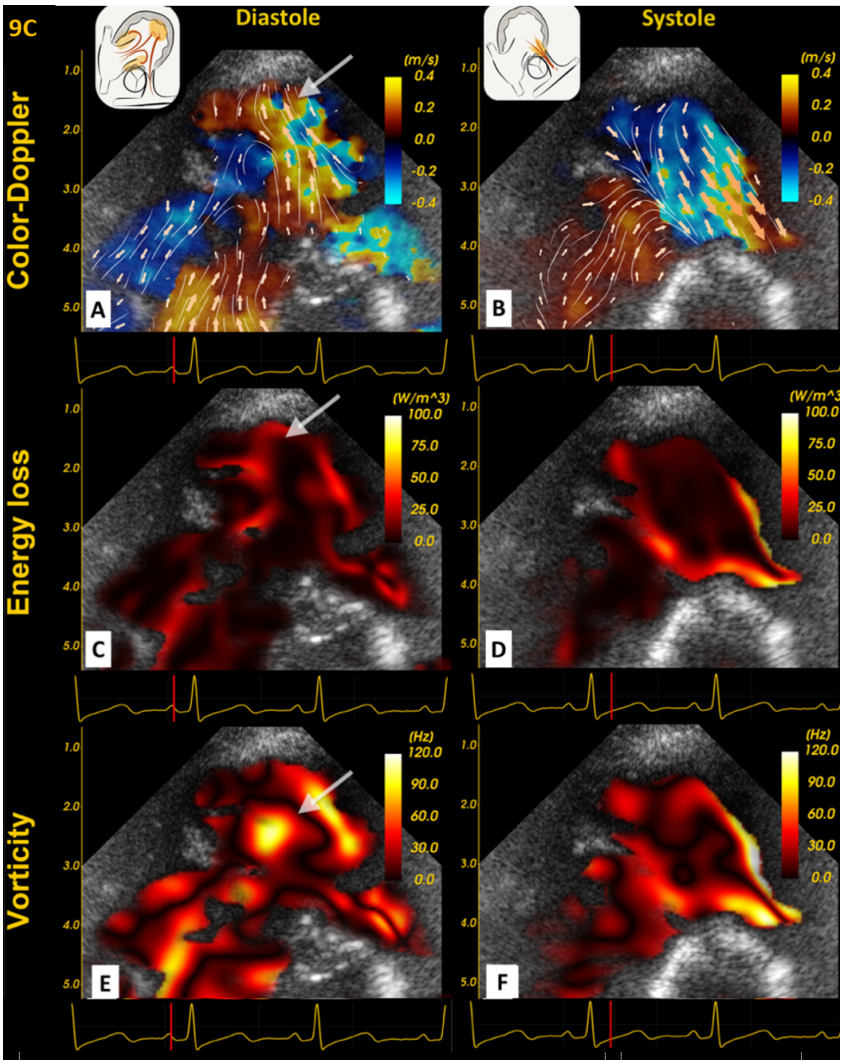

Figure 9C: Typical examples of right ventricular intracardiac velocities, energy-loss and vorticity mapping in diastole and systole in rTOF

The systolic and diastolic flow patterns were similar in CTL and ASD, with diastolic vortices forming around the tricuspid valve leaflets in early diastole (9A-B , A and B,) with corresponding areas of high energy loss and vorticity (9A-B , C -E). In rTOF, systolic flow patterns were also similar to those

of the other groups (9C, B, D, F), but in diastole, regurgitant pulmonary flow collides with the tricuspid inflow, resulting in disorganized apical vortices (9C, A, indicated by white arrow) with an additional area apical energy loss and vorticity (9C, C and D, indicated by white arrow). The schematic in the upper left of each panel illustrates the imaging plane and areas of high EL in orange.

Qualitative Results from Right Ventricular Three-Chamber Views

When identifying regions of highest EL from the RV3C, all groups exhibited a similar region of high systolic EL and vorticity in the right ventricular outflow tract. In diastole, all groups demonstrated high EL and vorticity around the tricuspid valve leaflets, corresponding to vortex formation at the edge of the tricuspid valve leaflets (Figure 9A-C). However, in rTOF, an additional region of high EL and vorticity was present in the RV apex (Figure 9C, panels C-E) in most cases (11/15), corresponding to colliding pulmonary insufficiency and tricuspid inflow. The cardiac blood speckle tracking findings are summarized schematically in Figure 10 and illustrated in typical examples in figures 9A-C.

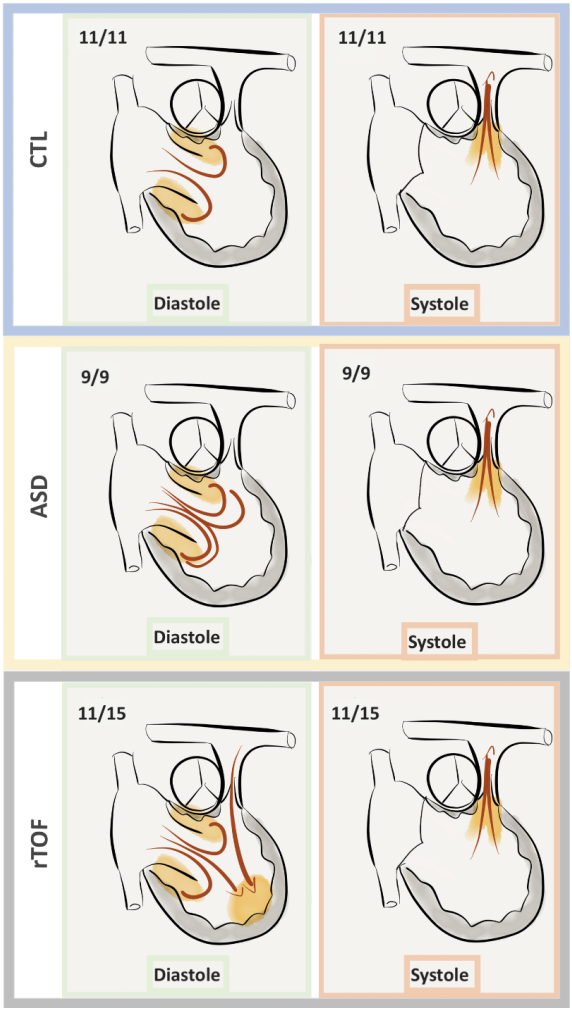

Figure 10: Schematic of energy loss regions in right ventricular three-chamber views

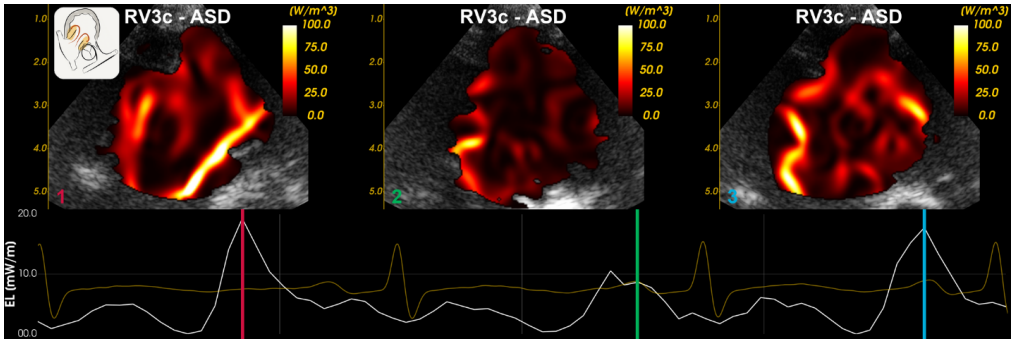

Figure 11A: Beat to beat variation of energy loss patterns

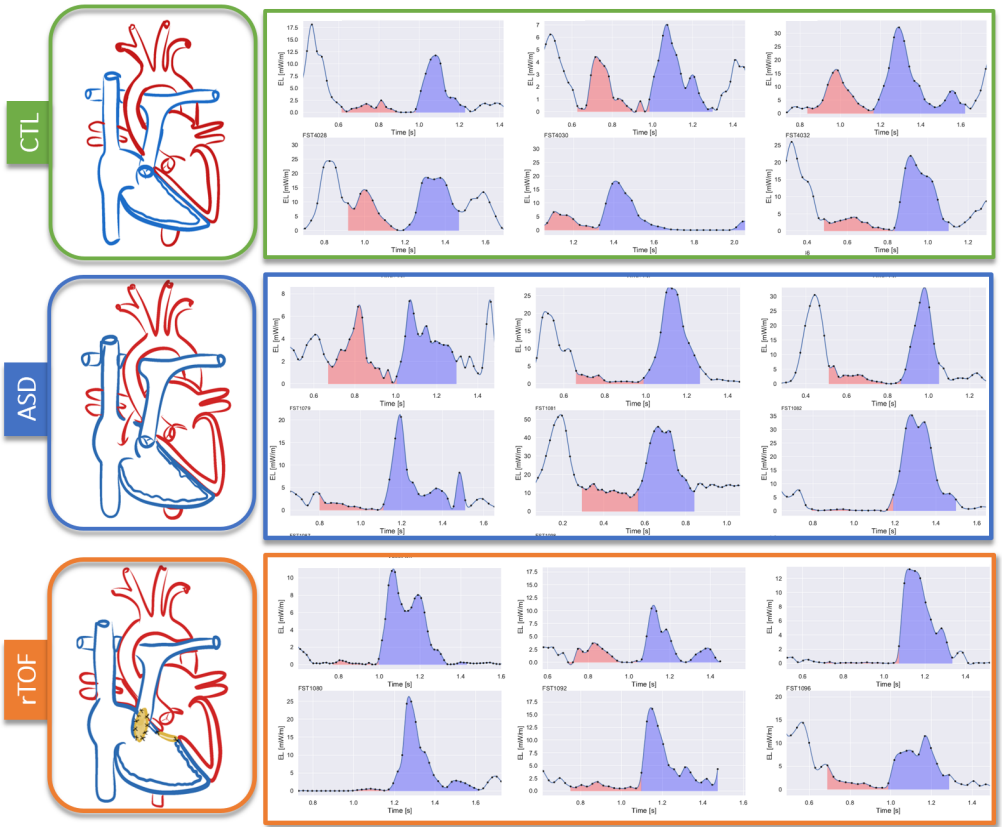

Figure 11B: Beat to beat variation of energy loss

Systolic and diastolic flow patterns were similar in controls and ASD, with diastolic vortices forming around the tricuspid valve leaflets in early diastole, accentuating with atrial systole, followed by streaming towards the right ventricular outflow tract. In rTOF, systolic flow patterns were also similar to the other groups, but in diastole, regurgitant pulmonary flow collided with tricuspid inflow, resulting in disorganized apical vortices. The pattern of EL could also vary from beat to beat, as illustrated in Figure 11A. This figure shows varying regions of high EL from one beat to the next. This is likely due to translational motion, respiration and motion of the probe on

the chest. We illustrated this by also analyzing the EL curves over the cardiac cycle (Figure 11B), showing that variation from one cycle to another.

Inter- and Interobserver Variability

Excellent intraobserver reproducibility was demonstrated for both diastolic and systolic EL measurements, with an average systematic measurement error of -0.1% and 0.0%, respectively, and narrow limits of agreement within a 5% variation. Interobserver variability was also good for both diastolic and systolic EL, with an average systematic error of 0.0% for both parameters and narrow limits of agreement within a 5% variation from the RV4C view (Figure 12). Inter- and intraobserver variability was not conducted for the RV3C, as it served to provide a qualitative measure, although findings were reviewed by co-authors (WM, SAN, LL, SF).

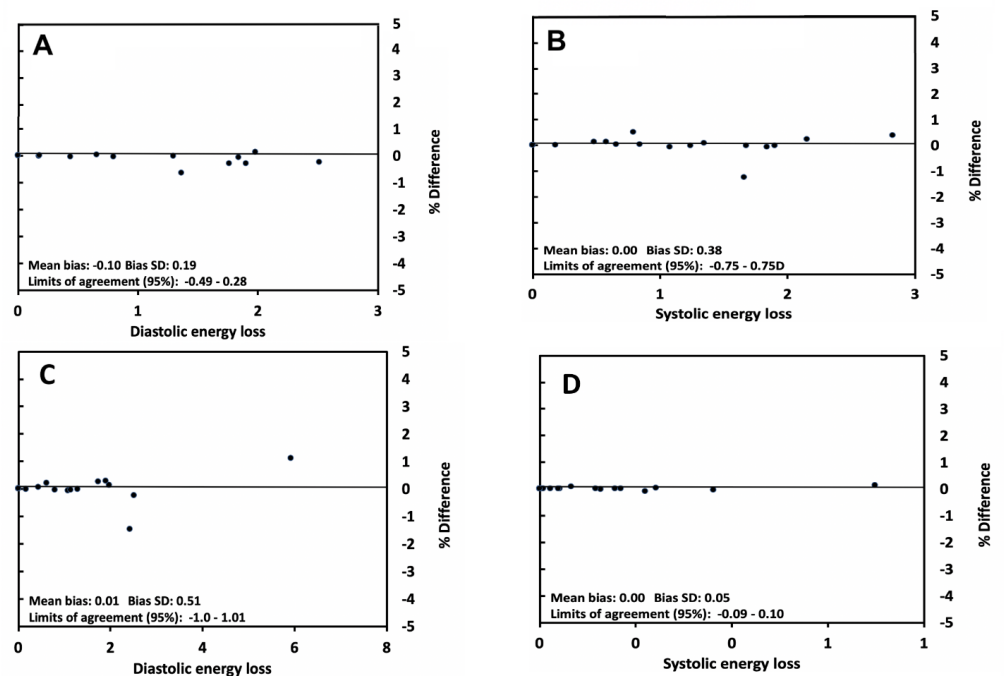

Figure 12: Bland-Altman plots showing intraobserver (A and B) and interobserver (C and D) agreement

Intraobserver (A and B) and interobserver (C and D) variability diastolic and systolic energy loss. In these Bland Altman plots, the solid line represents the average measurement error in percentage. The calculated mean bias and the limits of agreement are displayed in the lower left corner of each graph. The average error in measurement in all cases is well below 5%.

Results - Study 2

Demographic and Hemodynamic Characteristics

Table 6 provides a summary of demographic and hemodynamic characteristics for a total of 36 subjects, comprising 18 patients with pulmonary arterial hypertension (PAH) and 18 controls. All cases had idiopathic PAH and no history of cardiac surgery. The majority (13/18) of PAH patients were undergoing anti pulmonary hypertensive therapy, including sildenafil (4), sildenafil with oxygen (8), and a combination of sildenafil, bosentan, macitentan, and selexipag (1). Baseline characteristics were similar between the two groups. However, the PAH group exhibited a larger main pulmonary artery (MPA) size and lower tricuspid annular systolic excursion (TAPSE) and right ventricular fractional area change (RVFAC).

Qualitatively, laminar flow in the main pulmonary artery during systole was observed in both groups. Notably, a diastolic vortex in the MPA was observed in 16 out of 18 PAH patients, whereas it was absent in all controls. The diastolic vortex initially appeared in the right pulmonary artery (RPA) origin in 6 out of 16 PAH patients and in the MPA in the remaining 10. All vortices exhibited a clockwise rotation and dissipated as they migrated toward the pulmonary valve. In contrast, diastolic flow in controls remained laminar without detectable rotation. Figure 13 illustrates typical examples from each group, showcasing the distinct flow patterns.

		PAH (n=18)	CTL (n=18)
Male (%)		50	44
Age (years)		2.8 (0.5-4.2)	3.2 (0.5-4.8)
Height (m)		110 (89-125)	99 (80-122)
Weight (Kg)		18.9 (15.4-32.3)	15.8 (10.9-25.6)
BSA (m^2)		0.75 (0.65-0.81)	0.66 (0.50-0.94)
HR (BPM)		86 (75-108)	97 (81-110)
MPA Zscore		2.77 (1.62-3.26)	-0.20 (-1.74-1.01) *
RPA distensibility (%)		23.9 (12.7-31.7)	24.5 (17.2-30.4)
RV systolic pressure (mmHg)		82 (42-105)	
RV systolic pressure (% of systemic)		79 (46-104)	
TAPSE Zscore		-1.30 (-3.83-6.80)	0.02 (-1.18-4.71) *
RVFAC (%)		33.5 (30-38)	37 (36-40) *
MPA	Diastolic MPA vortex	16/18	0/18
	MPA diastolic vortex duration (ms)	150 (121-171)	
	Avg. VC_S	0.21 (0.08-0.42)	0.04 (0.02-0.06)*
	Avg. VC_D	0.13 (0.06-0.30)	0.05 (0.02-0.16)*
	Avg EL_S (mW/m)	4.84 (2.16-11.67)	2.42 (1.11-3.86)*
	Avg EL_D (mW/m)	0.69 (0.28-2.17)	0.14 (0.03-0.39)*
	Avg VO_S (Hz)	17.1 (15.8-21.6)	27.7 (20.6-35.1)
	Avg VO_D (Hz)	15.2 (11.1-20.9)	4.4 (0.2-8.4)*
RV	Avg. VC_S	0.27 (0.12-0.42)	0.13 (0.09-0.28)*
	Avg. VC_D	0.27 (0.15-0.34)	0.12 (0.09-0.16)*
	Avg EL_S (mW/m)	1.54 (0.32-2.67)	0.68 (0.25-1.12)
	Avg EL_D (mW/m)	4.08 (2.19-7.20)	2.87 (1.44-4.86)
	Avg VO_S (Hz)	22.8 (17.9-27.3)	22.1 (18.3-27.5)
	Avg VO_D (Hz)	25.1 (18.5-31.3)	24.2 (17.8-28.2)

Table 6: Demographic and echocardiographic data

BSA: Body surface area; CTL: controls; FAC: fractional area change; HR: heart rate; RV: right ventricle; TAPSE; tricuspid annular plane systolic excursion; MPA: Main pulmonary artery; VCS: Systolic vector complexity; VC_D: Diastolic vector complexity; EL_S: Systolic energy loss; EL_D: Diastolic energy loss; VO_S: Systolic vorticity; VO_D: Diastolic vorticity. * When p value < 0.05; Values expressed as median, quartiles (Q1-Q3)

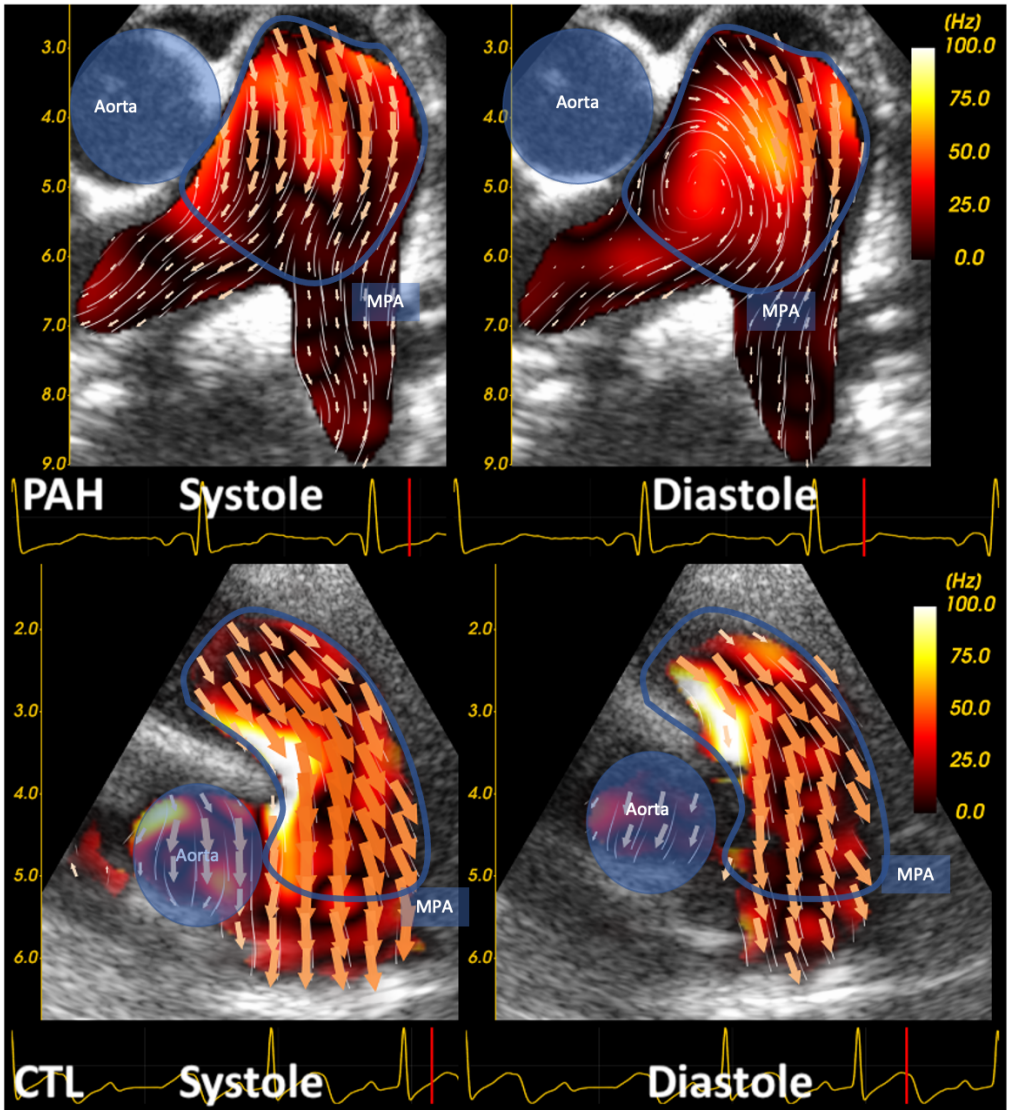

Figure 13: Typical main pulmonary artery flow patterns as shown by high frame rate ultrasound imaging and blood speckle tracking. The vorticity map is seen in the background.

CTL; Control, PAH; Pulmonary arterial hypertension

Quantitative Flow Parameters in the hypertensive RV and MPA

Quantitative flow parameters, as shown in Figure 14, revealed higher rates of energy loss in the main pulmonary artery for PAH in both systole (4.84 vs 2.42 mW/m) and diastole (0.69 vs 0.14 mW/m) compared to controls. Vector complexity was also elevated in both systole (0.21 vs 0.04) and diastole (0.13 vs 0.05) in PAH compared to controls. However, vector complexity did not correlate with MPA z-score (r=0.37, p=0.15). Diastolic vorticity was significantly higher in PAH compared to controls (15.2 vs 4.4 Hz). In the right ventricle (RV), diastolic vector complexity was higher in PAH compared to controls, but RV energy loss and RV vortex output were not statistically significant between the groups.

The duration of vortex time did not exhibit significant correlations with RV functional parameters (TAPSE: r=0.22, p=0.40; RVFAC: r=-0.45, p=0.11), right ventricular systolic pressure (RVSP: r=-0.01, p=0.11), or pulmonary artery dimensions (RPAd: r=0.17, p=0.51; MPA z-score: r=-0.21, p=0.41). Main pulmonary artery energy loss did not correlate with any RV functional parameters or RV flow parameters (RV energy loss, vortex output, and vector complexity). Quantitative flow parameters in the MPA and RV did not exhibit significant correlations with RVSP.

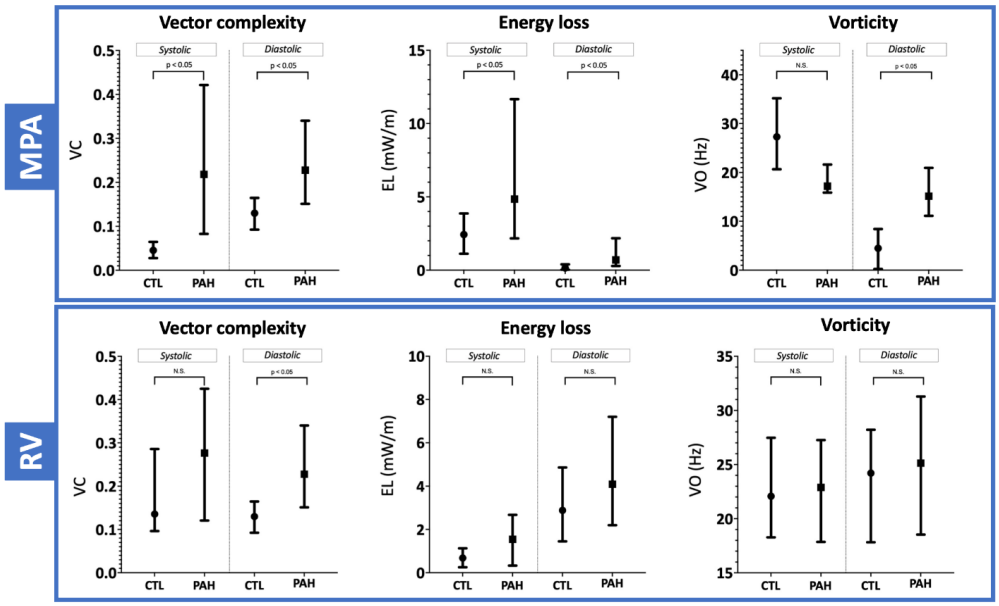

Figure 14: Quantitative flow parameters in the main pulmonary artery and right ventricle

RV: right ventricle; MPA: Main pulmonary artery; VC: vector complexity; EL: energy loss; VO: vorticity; Values expressed as median, quartiles (Q1-Q3)

Right Pulmonary Artery Distensibility Index (RPAD) and Correlations

When comparing the right pulmonary artery distensibility index (RPAD, Figure 15), no significant differences were observed between the control and PAH groups (CTL 23.9% vs PAH 24.5%). In PAH patients, diastolic MPA energy loss negatively correlated with RPAD (r=-0.48; p=0.04) and positively correlated with MPA z-score (r=0.68; p=0.03) (Figure 16).

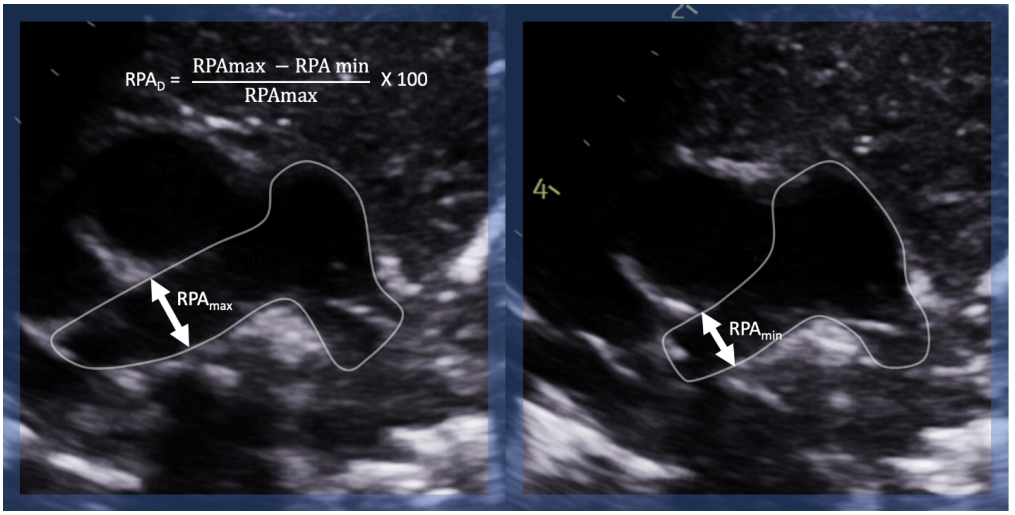

Figure 15: Right pulmonary artery distensibility index (RPA_D) measurement in a parasternal short axis view of the pulmonary arteries.

max: maximal measurement; min: minimum measurement; RPA: Right pulmonary artery

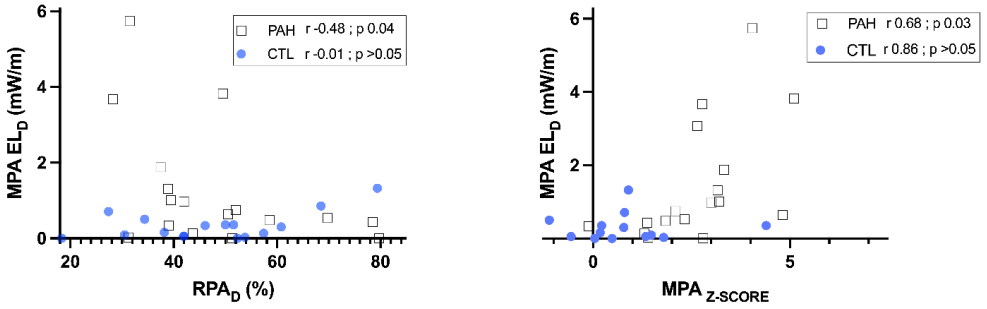

Figure 16: Correlation of main pulmonary artery diastolic energy loss with right pulmonary artery distensibility index and main pulmonary artery Z-score

MPA: Main pulmonary artery; EL_D: Diastolic energy loss; CTL: controls; PAH: Pulmonary arterial hypertension; RPA_D: right pulmonary artery distensibility index

Results - Study 3

The univentricular heart group (UVH) included 29 patients after exclusion of 2 patients with insufficient image quality. Nine patients had a dominant left ventricle (SLV), 14 had a dominant right ventricle (SRV) and six had double inlet left ventricles (DILV). Although the systemic ventricle is a morphological LV, we considered DILV separately as these patients have two separate atrioventricular valves connecting to a single LV contrary to the other UVH in this study. They were compared to 30 healthy controls of similar age, height, weight and sex distribution. Heart rate (DILV 112 [111-113] vs CTL 82 [71-91] bpm; p= 0.05) and QRS duration (DILV 114 [86-147] vs CTL 84 [80-95] bpm; p= 0.002) were statistically higher in the DILV group compared to CTL. These parameters did not differ between the other subgroups. Most UVH patients (23/29) were asymptomatic with NYHA class I status, while a smaller proportion (6/29) reported NYHA class 2 status. These patients did not differ for KE, EL, VO or VC from the rest of the UVH. Only one patient in the UVH group was paced in a dual chamber mode with atrioventricular synchrony and six patients had a Fontan fenestration shunting left to right. None of the patients had more than mild atrioventricular valve regurgitation, and all had qualitatively normal systolic function. E wave velocity (CTL 92 [86-100] vs UVH 81 [67-97] bpm; p= 0.001) and E/A ratio (CTL 1.92 [1.71-2.17] vs UVH 1.44 [1.10-2.21] bpm; p= 0.001) were higher in CTL compared to UVH, while E/e' was higher in UVH (CTL 6.8 [5.9-7.2] vs UVH 8.3 [6.5-12.2] bpm; p= 0.01).

Qualitative intracardiac flow analysis

Examples of typical flow patterns in the V4C and V3C views are shown in figure 17. The systolic flow patterns from the V3C views were similar between UVH and controls, consisting of

laminar flow towards the ventricular outflow tract and through the semilunar valve. In diastole, SLV had similar flow patterns compared to LV in controls. Vortices form around the leaflets of the atrioventricular valve in early diastole and rotate away from the inflow. The single RV group had similar diastolic vortex formation along the leaflets of the tricuspid valve curling away from the tricuspid valve opening and migrating to the apex or outflow tract. These flow patterns were also similar to those observed in the RV of CTL. The most complex diastolic flow patterns were observed in the DILV group, with multiple diastolic vortices forming in early diastole, some colliding together before migrating towards the apex and outflow tract.

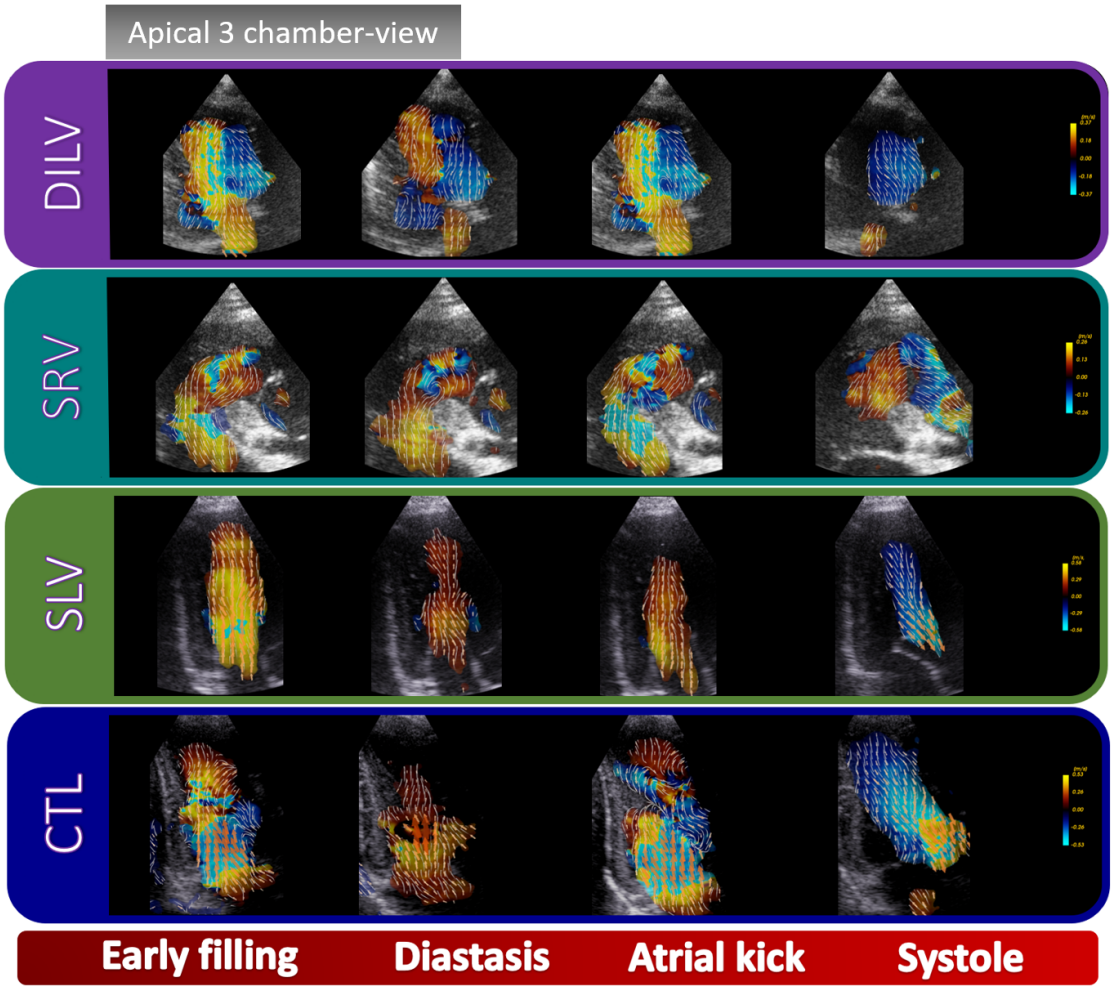
Apical 3 chamber-view
DILV
SRV
SLV
CTL
Early filling
Diastasis
Atrial kick
Systole

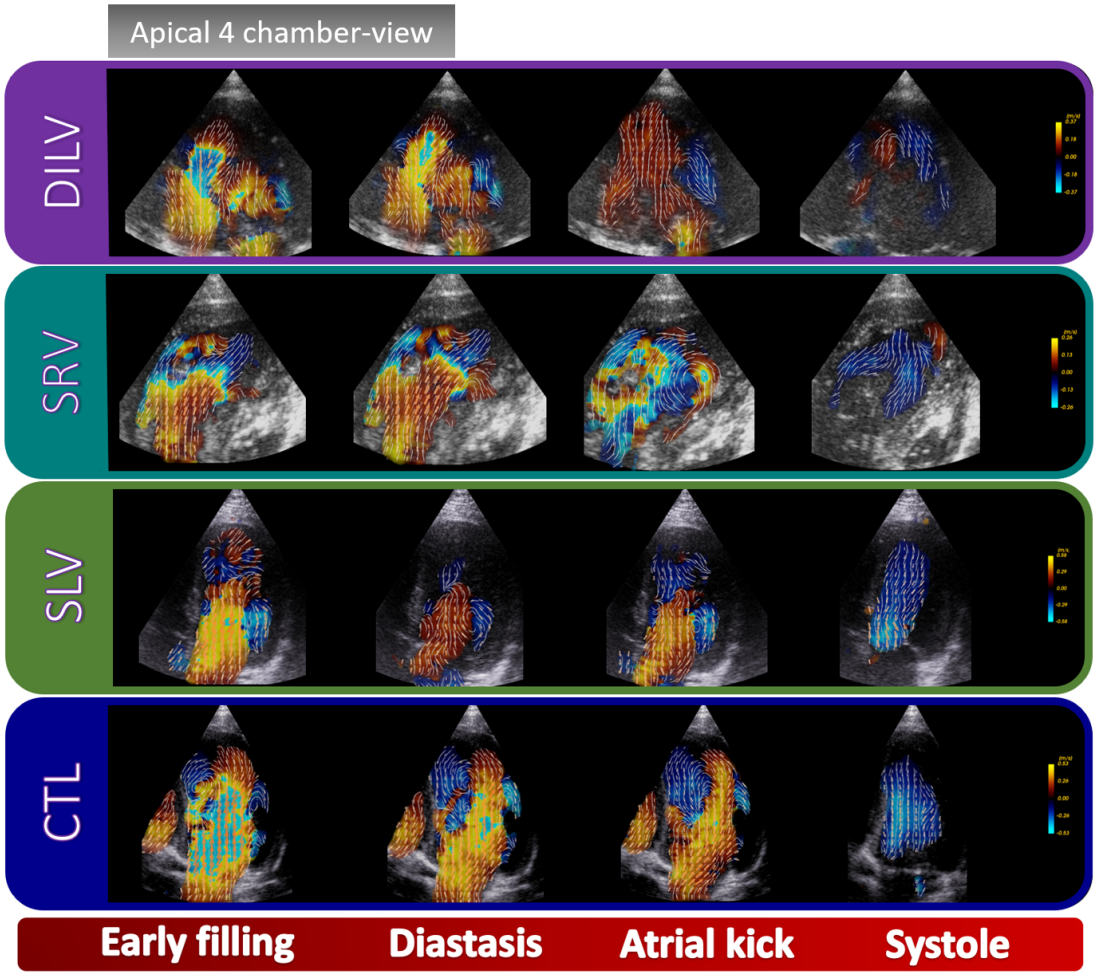

Figure 17: Typical examples of ventricular intracardiac velocities and vortex formation

Quantitative intracardiac flow analysis

Quantitative flow parameters were obtained from V4C views and are summarized in table 7. Systolic (KE_S) and diastolic KE (KE_D), systolic (EL_S) and diastolic EL (EL_D) and systolic (VO_S) and diastolic VO (VO_D)were significantly higher in controls versus UVH (KE_S CTL 55.6 [45.0-68.7] vs UVH

29.2 [16.8-53.8] mJ/m; p= 0.0001, KE_D CTL 134 [105.2-154.4] vs UVH 83.2 [49.5-111.0]; p<0.0001), EL_S CTL 2.55 [1.64-3.45] vs UVH 1.32 [0.68 -2.53] mW/m; p<0.0001, EL_D CTL 10.46 [7.79-12.48] vs UVH 5.11 [2.14-8.44]; p<0.0001), VO_S CTL 5.43 [3.91-6.64] vs UVH 3.40 [2.30-6.07] Hz; p=0.006, VO_D CTL 16.99 [14.25-19.81] vs UVH 10.64 [8.20-13.72]; p<0.0001) (figure 18). The subgroup analysis comparing these parameters between SRV, SLV and DILV did not show significant differences. When inspecting the location of highest diastolic KE, we observed similar patterns around the atrioventricular valve leaflets where vortex formation was observed and where maximal EL is observed SRV, SLV and CTL. In contrast to the other subgroups, where maximal EL and VO tended to be aligned with the ventricular inflow, in DILV these regions were more dispersed within the ventricle. They also coincided with regions of colliding inflows in early filling. Figure 19 summarizes typical patterns of maximal KE, EL and VO. The parameter of VC did not differ significantly between the groups during the cardiac cycle but tended to be higher in diastole for SRV compared to other subgroups (Figure 18).

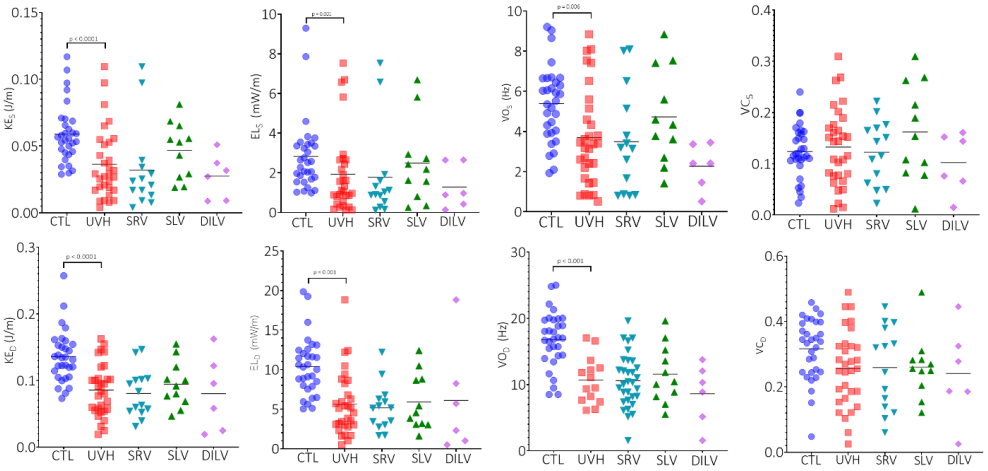

Figure 18: Scatter plot of ventricular flow energetics in the four-chamber view

KE_S: systolic kinetic energy; KE_D: Diastolic kinetic energy VC_S: Systolic vector complexity; VC_D: Diastolic vector complexity; EL_S: Systolic energy loss; EL_D: Diastolic energy loss; VO_S: Systolic vorticity; VO_D: Diastolic; CTL: controls; UVH: Univentricular heart; SRV: single right ventricle; SLV: single left ventricle; DILV: Double inlet left ventricle

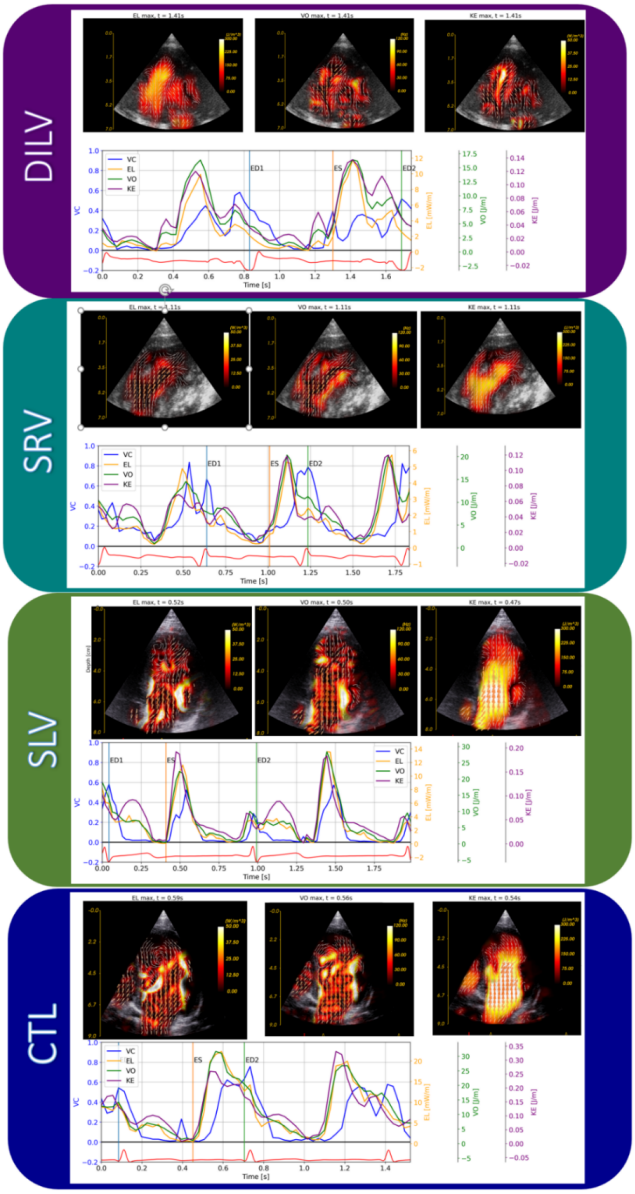

Figure 19: Typical examples of highest kinetic energy, energy loss and vorticity

KE: kinetic energy; EL: Energy loss; VO: Vorticity; CTL: controls; UVH: Univentricular heart; SRV: single right ventricle; SLV: single left ventricle; DILV: Double inlet left ventricle

	UVH (n = 29)	SLV dominant (n = 9)	SRV dominant (n= 14)	SV DILV (n=6)	CTL (n = 30)
PRF	5000 (3500-5000)	3500 (2750 -5000)	4500 (3500-5000)	3500 (3500-3875)	4000 (3500-4125)
KE_s (mJ/m)	29.2 (16.8-53.8)	54.8 (31.1-66.7)	27.3 (16.0-42.3)	22.0 (9.0-37.1)	55.6 (45.0-68.7)*
KE_D (mJ/m)	83.8 (49.5-111.0)	80.1 (61.9-131.7)	93.5 (56.5-120.7)	34.9 (20.3-67.7)	134.2 (105.2-154.4)*
EL_S (mW/m)	1.32 (0.68 -2.53)	2.43 (0.98-4.37)	1.03 (0.55-1.93)	0.65 (0.21-0.95)	2.55 (1.64-3.45) *
EL_D (mW/m)	5.11 (2.14-8.44)	3.84 (3.06-9.63)	5.16 (3.03-6.79)	1.67 (0.63-4.86)	10.46 (7.79-12.48) *
VO_S (Hz)	3.40 (2.30-6.07)	4.5 (2.91-7.47)	3.20 (0.87-6.51)	1.93 (0.75-3.19)	5.43 (3.91-6.64) *
VO_D (Hz)	10.64 (8.20-13.72)	10.04 (7.59-12.71)	11.04 (7.65-13.58)	7.74 (2.46-11.63)	16.99 (14.25-19.81) *
VC_S	0.14 (0.07-0.17)	0.18 (0.09-0.26)	0.14 (0.06-0.17)	0.11 (0.03-0.16)	0.12 (0.10-0.16)
VC_D	0.26 (0.13-0.35)	0.26 (0.20-0.29)	0.30 (0.13-0.38)	0.23 (0.07-0.40)	0.34 (0.24-0.39)

Table 7: Intraventricular flow energetics

CTL: controls; UVH: Univentricular heart; SRV: single right ventricle; SLV: single left ventricle; DILV: Double inlet left ventricle; KE_S: systolic kinetic energy; KE_D: Diastolic kinetic energy VC_S: Systolic vector complexity; VC_D: Diastolic vector complexity; EL_S: Systolic energy loss; EL_D: Diastolic energy loss; VO_S: Systolic vorticity; VO_D: Diastolic vorticity; Values expressed as median, quartiles (Q1-Q3); * When p value < 0.05 CTL vs UVH

Interactions of blood flow energetic

There were significant positive correlations between KE, EL and VO in both systole and diastole. These correlations were noted in the CTL (KE_S vs VO_S: r=0.45 , p <0.001; KE_D vs VO_D: r=0.74 , p=0.001; EL_S vs VO_S: r=0.72 , p <0.001; EL_D vs VO_D: r=0.55 , p=0.001) and in UVH (KE_S vs VO_S: r=0.87 , p <0.001; KE_D vs VO_D: r=0.58 , p<0.001; EL_S vs VO_S: r=0.86 , p <0.001; EL_D vs VO_D: r=0.69 , p<0.001). VC did not correlate significantly with the other flow parameters. We also did not observe a significant correlation between, HR, QRS duration and any of the blood flow energetic parameters. The details for this analysis can be found in figure 20.

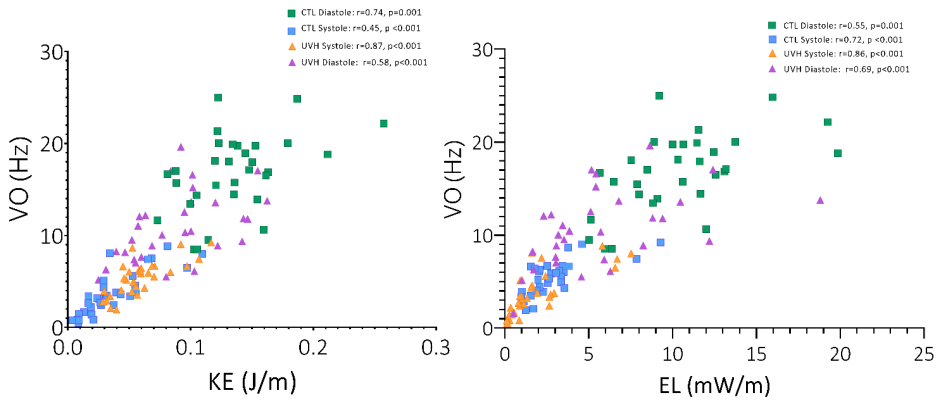

Figure 20: Correlation between vorticity and kinetic energy and energy loss

KE: kinetic energy; EL: Energy loss; VO: Vorticity; CTL: controls; UVH: Univentricular heart

16. DISCUSSION

In this work, we used BST to describe right ventricular flow dynamics in various hemodynamic conditions. We studied the right ventricle in groups with increased right ventricular volume loading, namely ASD and rTOF (Study 1), then the pressure-loaded RV and MPA due to increased afterload in PAH (Study 2) and finally the UVH with the unique Fontan circulation leading to reduced preload (Study 3).

Our findings in all studies demonstrated an added value of blood visualization and quantification compared to conventional echocardiography. We showed that both qualitative and quantitative assessment of blood flow are valuable in characterizing intraventricular flow

dynamics. When quantitative energetics were similar between groups, we demonstrated differences in intracardiac flow patterns and location of high energy losses and vorticity (Study 1). Conversely, we showed that the opposite is possible, where qualitative assessment between controls and patients is similar, such as it was our UVH patients, the quantitative blood flow parameters differed (Study 3). We also demonstrated that these novel imaging tools can be applied to vessels and that vascular quantitative and qualitative characteristics can help differentiate patents from controls, as on our PAH patients (Study 2)

During the study period, significant improvements were made to image optimization, postprocessing and analysis thanks to a close collaboration between the clinical and engineering team members. The quantitative measurements obtained from the velocity field were validated both *in vivo* and *in silico*. Perhaps even more important than the demonstration of the advantages and unique capabilities of this novel imaging technology, we also explored and described many limitations and factors which can influence the data obtained. We found that image acquisition was the most impactful on data quality compared to post-processing, which demonstrated very low inter and intra-observer variability. The effect of imaging planes and beat-to-beat variations on such quantitative flow parameters was explored and described (study 1 and 2). The smoothing parameters were also kept standard across all analysis to avoid potential effects. Some patients (Study 3) were included from the E95, a scanner which offered blood speckle imaging and direct visualization at the time of acquisition, which was a major improvement for optimization of these acquisitions.

Qualitative blood flow dynamics

The qualitative description of intracardiac and vascular flow phenomena demonstrates unique hemodynamics in our studies. Vortex formation in the RV of patients with ASDs, rTOF, PAH and UVH were all similar and in keeping with descriptions founds in the literature using other imaging modalities and computational flow modeling[90–92]: Similar diastolic filling and systolic flow patterns within the ventricles were also observed in SRV and SLV and PAH. Diastolic vortex formation started at the tips of the atrioventricular valve leaflets in early diastole and curled away from the inflow, with the greater component towards the outflow tract. In diastasis this vortex persisted before being progressing further in the outlet in atrial systole and finally dissipating through the semilunar valve in systole. These similarities were surprisingly also present in the UVH group compared to CTL. The similarities in intracardiac flow dynamics seen between SRV, SLV and CTL are in keeping with recent findings pointing to preserved ventricular mechanics in UVH, regardless of the ventricular morphology[93–95]. Pathological findings have shown adverse SRV remodelling including hypertrophy and myocyte disarray. Although these changes ultimately become deleterious, they produce a shift from a longitudinal pattern of contraction to and LV-like circumferential pattern[96 97]. This is perhaps an explanation to the similar qualitative flow energetics we've observed in this study. Another explanation is that in the Fontan circulation with low atrial pressure, as is likely the case in our groups, the atrioventricular axis of early filling does not change significantly compared to CTL. There is laminar flow with low pressure gradients across the valve with preserved vortex formation around the atrioventricular valve at that stage.

There were two groups where diastolic flow patterns were disturbed, namely rTOF and DILV with Fontan circulation. Both these groups had abnormal areas of colliding flows, which corresponded to distinct regions of maximal EL which differed from the other groups. In rTOF this corresponded tricuspid inflow and severe pulmonary insufficiency jets colliding at the RV apex. This also corresponded to the maximal region of energy loss, not seen in the ASD or CTL groups. Abnormal flow patterns and energetics within the RV apex of rTOF could affect remodeling and function. Apical dysfunction has been shown to preferentially affect rTOF when compared to equally volume loaded ASD and healthy controls[33]. In DILV, the collision was related to the two inflows with maximal area of energy loss corresponding to collision points of these vortices.

We also demonstrated the value of qualitative blood flow assessment in the vascular compartment. The non-invasive quantification of PAH relies on quantification of RV-RA gradient measurement. However, this is limited when the spectral Doppler is incomplete because of insufficient degree of tricuspid valve regurgitation. This work focused on the MPA vortex formation in PAH, but our group also studied this in the ascending aorta of children with bicuspid aortic valve[98]. In study 2, we demonstrated that despite having similar ventricular quantitative flow parameters between CTL and PAH, the latter group had a distinct diastolic vortex in the MPA as well as higher EL and VC in the MPA, even for milder forms of PAH (less than 50% systemic pulmonary artery pressure). Diastolic vortex duration in CMR studies was though to correlate with pulmonary artery pressure[11], this could not be demonstrated in our study. A possible explanation of this is the two-dimensional nature of our echocardiographic acquisitions which may not capture through-plane motion of the vortices and therefore leading to an underestimation of their duration compared to a three-dimensional imaging modality such as CMR. Although this study

could not validate the value of vortex duration as a non-invasive marker of PAH severity, vortex detection as a diagnostic sign for PAH requires further validation.

Quantitative blood flow parameters

Quantification of blood flow parameters also provided new insights into the cardiac flow dynamics of these groups. In the volume-loaded RV of ASD and rTOF, as expected diastolic EL and VO was higher compared to CTL, while not significantly different from each other. From a fluid mechanics standpoint, this phenomenon can be explained by mechanical energy loss (EL) due to abrupt flow expansion, a concept believed to be applicable to EL in the ascending aorta of individuals with aortic stenosis[99]. In our study, this sudden flow expansion happens during early diastole via the tricuspid valve, and it would be amplified in cases where the right ventricle (RV) is dilated. These observations suggest that dilated RVs are less efficient compared to non-dilated ones, as more kinetic energy is dissipated during diastole.

The lack of difference between ASD and rTOF could be related to the small sample size but also reveals the additional value of qualitative visualization tools in addition to quantitative parameter. One without the other would not permit the differentiation of flow dynamics between these two groups of volume-loaded right ventricles.

These results align with previous findings from a canine study on volume-loaded right ventricles, which indicated diminished diastolic vortex strength and extent, quantitative measures believed to correlate with kinetic energy[100].

In systole, there were no discernible differences in energy loss between the groups. This finding was surprising as more energy losses would be expected in rTOF and ASD with increased RV stroke volume compared to controls. The absence of a difference could be attributed to the mostly out of plane direction of blood flow in systole when the RV is imaged from the RV4C.

In PAH, MPA diastolic EL, VC and VO were higher than in CTL. Higher energy loss could potentially be explained by higher friction forces related to more complex flow patterns in the MPA. Our findings indicate that MPA flow exhibited more complexity with wider distribution of vector directions, suggested by higher vector complexity. Vortices in the MPA may differ from an energetic perspective from the ones observed in the ventricles where they can serve as conservers of kinetic energy from diastole to systole. We speculate that the diastolic vortex observed in most PAH contributes to increased energy loss and to inefficiencies in the pulmonary arterial circulation compared to controls.

In PAH, diastolic EL correlated negatively with RPA_D and positively with MPA Z-score while no such correlations were found in CTL. These findings could point to increased vascular stiffness as a more dilated and less distensible pulmonary arterial system in PAH offers diminished elastic recoil to continue propelling blood forward in diastole and predisposes it to more complex flow patterns with higher energy losses. Although the literature is scant, the role of such a measurement has been shown to be valuable in humans and dogs[17,18] with PAH as an additional non-invasive marker of pulmonary arterial stiffness.

In the third study we demonstrated that despite the similar intracardiac vortex formation, UVH groups had significantly lower energetics, including EL, KE and VO in both systole and diastole. This is in keeping with published CMR studies[61,103,104] and with the pathophysiology of a univentricular circulation, characterized by the absence of a sub-pulmonary ventricle to transfer energy to the blood pool to propel in into the pulmonary circulation. This elevates the central venous pressure (CVP) chronically and results in a state of chronic preload deficiency in the UVH[105]. This adverse loading affects cardiac performance which is limits myocardial energy transfer to the blood pool. Although not the design of our study, we suspect this difference to become greater during exercise compared to CTL[106] as healthy controls are able to increase ventricular preload significantly compared to UVH. Although our study did not have large numbers of DILV, this is where quantitative flow parameters tended to be lowest. This is also congruent with the qualitative flow assessment of vortex formation and localisation of highest KE and EL in this group. These findings also highlight the added value of quantitative flow analysis as UVH are energetically different from CTL while have similar ventricular mechanics.

We also observed a positive correlation between VO and KE and EL in both CTL and UVH. These correlations were strongest in the UVH compared to CTL. Elevated diastolic VO has been thought of as hemodynamic diastolic-to-systolic coupling mechanism [61]. By maintaining elevated diastolic VO, diastolic KE is stored in the blood pool to allow necessary EL to be compensated and thus facilitating systolic ejection[107]. This mechanism becomes more important in an energy-deprived circulation such as the Fontan. In the UVH patient, VO with VC is in favour of an energy conserving function of diastolic vortices seen, as opposed to the ones seen in the MPA of PAH,

which are accompanied by higher VC, indicating less laminarity and higher energy loss in the pulmonary arterial circulation.

The influence of blood flow patterns on cardiac morphology and function is intricate[108,109]. Increased fluid shear stress is believed to modulate endocardial signalling pathways implicated in cardiac remodelling and function[110,111]. Disturbances in flow dynamics are thought to precede morphological and functional changes[112]. Advancements in CMR and ultrasound technologies are enabling the study of energy-based imaging biomarkers[84,113]. This could provide novel insights in the relationship between flow dynamics and RV remodelling. Our work demonstrates that the use of BST for cardiac flow dynamics is feasible, reproducible and provides novel, early insights into adverse intracardiac and vascular hemodynamics. These flow dynamics could help detect adverse RV hemodynamic at an earlier, more adaptive stage of disease which would otherwise have been missed using the current imaging biomarkers used.

17. LIMITATIONS

There were several limitations in this work. The relatively small sample sizes limit the generalisability of results. Analysis of subgroup, particularly in the univentricular heart group was limited because of the small numbers of DILV. The image acquisitions were planned amidst clinical visits to better suit the participants and their families as per our institutions ethics boards. The consequence of this is that we lacked contemporaneous invasive hemodynamic data from cardiac

catheterisation or consistent complementary imaging such as CMR, of relevance in PAH, rTOF and UVH after Fontan.

The very significant increase in temporal resolution made possible by plane wave imaging comes with the trade-off of lower contrast and lateral resolution, particularly in B-mode. Thankfully, as our focus is the blood pool, lower B-mode quality was acceptable. The availability of BST only using higher frequency probes limited inclusion of older and bigger children. Indeed, beyond 10 cm of depth, significantly affected the quality of the blood flow imaging. This affected particularly our UVH group as the Fontan pathway was often at or beyond this depth limit.

Capturing a three-chamber view of the right ventricle (RV3C) was especially difficult in subjects without ventricular enlargement. However, the RV4C view was more feasible. Reliable EL and vorticity measurements depends on similar imaging planes. Therefore, we chose to exclude 22/57 RV3C views with differences in imaging planes in the first study. The absence of real-time BST visualization on the modified research scanner used for this study further aggravated this limitation. Quality control was only possible off-line, precluding any optimization. As with other Doppler-based techniques, multiple acquisitions are analysed to optimize alignment with the blood flow direction. Similarly, velocities obtained with BST benefit from real-time visualization and analysis. This technology has now become commercially available on the E95 GE scanners.

Another limitation is the two-dimensional nature of the imaging technique, thus not accounting for through-plane blood flow. This is highlighted in the systolic EL scatter plots with many values near zero when assessed in the RV4C view (figure 8). Because of the crescentic shape of the RV, the imaging plane of the RV4C view is nearly perpendicular to the direction of systolic

flow towards the outflow tract so that the through-plane component of systolic RV flow is lost as illustrated in the following schematic (figure 21).

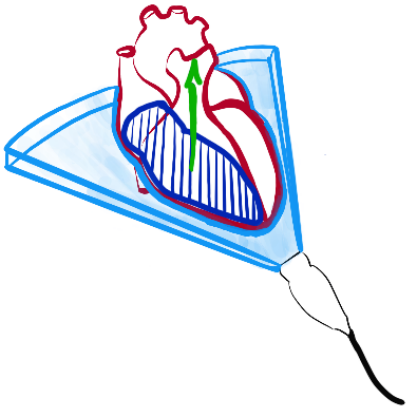

Figure 21: Schematic demonstrating through plane flow

Smoothing parameters influence EL calculations. The same smoothing parameters were used across our analysis to avoid this source of error. Awareness of this limitation is important for longitudinal studies and for group comparisons in future studies.

Data analysis is currently done on PyUSview, an in-house software which is not commercially available. Although done manually, the postprocessing resulted in low intra and interobserver variability.

18. FUTURE PERSPECTIVES AND INNOVATIONS

Continued technological improvements addressing some of the current limitations are already underway. Adapting the image acquisition process to make this imaging modality available

on lower frequency probes with improved signal at lower depth would open many possibilities, namely the study of Fontan pathways more reliably in older patients as well as other vessels, such as the aortic arch, where flow dynamics are being studied using 4D-flow CMR.

A major limitation of BST is it's 2D nature missing important flow characteristics which can only be demonstrated in 3D data sets. Work is already underway showing promising results when compared to 4D-flow CMR[74]. Further work is required to assess this imaging technology in congenital heart disease and children as well as compare its blood flow quantification to that of 4D-flow CMR.

During the course of this work, links with industry lead to important exchanges which helped in the commercialization of BST into GE scanners, with continued improvements allowing real-time visualization of blood speckle tracking. Our group contributed to this advancement through a multidisciplinary, international collaboration, which is becoming ever stronger with many collaborators in Norway and Canada continuing to utilize and perfect this novel imaging tool to study cardiac flow dynamics in the setting of congenital heart disease. We foresee that the trajectory will follow with regards to flow quantification parameters becoming commercially available. As we've demonstrated, both qualitative and quantitative flow dynamics are important to precisely describe cardiac hemodynamics.

Improvements in automation of postprocessing, which is quite time-consuming and currently not commercially available are required. We believe this is an area uniquely suited to workflow optimization through the integration of machine-learning pathways, to allow real-time quantification of blood flow parameters. The study of other quantitative flow parameters is also an exciting next step. Our group has already published data on IVPG estimations using BST with

excellent validation data. This is a potential major breakthrough in non-invasive diastolic function assessment, particularly univentricular hearts [114].

The continued study of current quantitative flow data is necessary to better understand their physiological implications and more importantly their potential roles in clinical decision making for challenging patient populations. This will require larger, prospective cohorts studied before and after interventions to assess clinical utility of these parameters. The integration of multiple flow parameters is also suited to the application of artificial intelligence to propose, early, sensitive and personalized cardiac energetics for an individual patient.

19. CONCLUSIONS

Blood speckle tracking enables the visualisation and description of flow dynamics in the right ventricle and main pulmonary arteries of children with congenital heart disease. Quantitative flow parameters are measurable, validated and highly reproducible. There are important limitations and technical aspects to be considered when acquiring and analysing BST data. Both quantitative and qualitative flow analysis are complementary and can demonstrate differences in flow energetics between groups of healthy controls and patient with abnormal right ventricular loading.

Even though the clinical significance of our findings is not yet clear, the study of cardiac flow disturbances using ultrasound at the bedside is a novel tool which can provide novel, sensitive and personalized biomarkers of adverse cardiovascular function in congenital cardiology and

beyond, allowing earlier more timely interventions. Ongoing technological advancements will hopefully address some of the current limitations and help development of new frameworks for improved clinical management.

20. REFLECTIONS

At the close of these projects, I have come to many realizations regarding medical technologies and practice. We are truly living in an era of unpreceded technological abundance with excessive amounts of information and advances which often far outpace our ability to see a useful purpose for them. I have come to realize the vast workload that precedes introduction and use of new technologies in clinical practice. More importantly, the value of strong collaborations between the clinical and technical world to bring about the best and most useful tools. The development and improvement of the PyUSview analysis tool is a great example of this type of collaboration. The clinician and technical sides of the team collaborated intensely to constantly improve this tool. In addition, collaboration between centres, in this case between NTNU, SickKids, St Olavs Hospital and Ålesund Hospital enriched everyone and brought forward the best in everyone. I believe that this model of collaboration over competition is the best way forward for innovation in medical technology, particularly in the realm of pediatric and congenital heart disease.

Seeing something in a new light is exciting in so far as it opens a pathway of deeper understating of a phenomenon. After working on this project, I must admit to standing over the

Nidelva river at the “Gate to Happiness” and wondering what the energetics were in the different areas of the river.

In this work, we studied the right ventricle of patients with challenging physiologies not fully described with conventional parameters. Repaired TOF, UVH and PAH, are all conditions with insufficient non-invasive markers of early adverse cardiac function. We described promising results for this novel visualization and quantification tool of ventricular flow dynamics as well as important shortcomings and limitations.

It is an immense privilege to be in this position and we therefore have the responsibility to push our understanding of these novel technologies to ultimately benefit the center of all our efforts, our patients’ lives. I believe this work has been fruitful in expanding the boundaries of our knowledge slightly, but the journey continues.

21. REFERENCES

1. Dolk H, Addor MC, Loane M, et al. Congenital heart defects in Europe: prevalence and perinatal mortality, 2000 to 2005. *Circulation TA - TT* -. 2011;123(8):841-849. doi:10.1161/CIRCULATIONAHA.110.958405 LK - https://mcgill.on.worldcat.org/oclc/711695356
2. O’Leary JMMD, Siddiqi OKMD, de Ferranti SMD, Landzberg MJMD, Opotowsky MPH ARMD. The Changing Demographics of Congenital Heart Disease Hospitalizations in the United States, 1998 Through 2010. *JAMA: the Journal of the American Medical Association*

TA - TT -. 309(10):980-986. doi:10.1001/jama.2013.564 LK - https://mcgill.on.worldcat.org/oclc/10059403967

3. Tworetzky W, McElhinney DB, Brook MM, Reddy VM, Hanley FL, Silverman NH. Echocardiographic diagnosis alone for the complete repair of major congenital heart defects. LK - https://mcgill.on.worldcat.org/oclc/118680371. *Journal of the American College of Cardiology TA - TT* -. 1999;33(1):228-233.
4. Mertens L, Miller O, Fox K, Simpson J. Certification in echocardiography of congenital heart disease: experience of the first 6 years of a European process. *European Heart Journal - Cardiovascular Imaging TA - TT* -. 2013;14(2):142-148. doi:10.1093/ehjci/jes126 LK - https://mcgill.on.worldcat.org/oclc/4948196618
5. Stanger P, Silverman NH, Foster E. Diagnostic accuracy of pediatric echocardiograms performed in adult laboratories. LK - https://mcgill.on.worldcat.org/oclc/119430089. *The American journal of cardiology TA - TT* -. 1999;83(6):908-914.
6. Therrien J, Siu SC, McLaughlin PR, Liu PP, Williams WG, Webb GD. Pulmonary valve replacement in adults late after repair of tetralogy of Fallot: Are we operating too late? *J Am Coll Cardiol*. 2000;36(5):1670-1675. doi:10.1016/S0735-1097(00)00930-X
7. Bokma JP, Geva T, Sleeper LA, et al. Improved Outcomes After Pulmonary Valve Replacement in Repaired Tetralogy of Fallot. *J Am Coll Cardiol*. 2023;81(21):2075-2085. doi:10.1016/j.jacc.2023.02.052
8. Beroukhim RS, Graham D a, Margossian R, Brown DW, Geva T, Colan SD. An echocardiographic model predicting severity of aortic regurgitation in congenital heart

disease. *Circ Cardiovasc Imaging*. 2010;3(5):542-549. doi:10.1161/CIRCIMAGING.110.957175

9. Dragulescu A, Friedberg MK, Grosse-Wortmann L, Redington A, Mertens L. Effect of Chronic Right Ventricular Volume Overload on Ventricular Interaction in Patients after Tetralogy of Fallot Repair. *Journal of the American Society of Echocardiography*. 2014;27:896-902. doi:10.1016/j.echo.2014.04.012
10. Dragulescu A, Mertens L, Friedberg MK. Interpretation of left ventricular diastolic dysfunction in children with cardiomyopathy by echocardiography: Problems and limitations. *Circ Cardiovasc Imaging*. 2013;6(2):254-261. doi:10.1161/CIRCIMAGING.112.000175
11. Zhong SW, Zhang YQ, Chen LJ, Wang SS, Li WH, Sun YJ. Ventricular Twisting and Dyssynchrony in Children with Single Left Ventricle Using Three-Dimensional Speckle Tracking Imaging after the Fontan Operation. *Echocardiography*. 2015;(Lv). doi:10.1111/echo.13103
12. Khoo NS, Tham EB, Kantor PF. Newer imaging modalities in the assessment of heart function in single ventricle hearts. *Canadian Journal of Cardiology*. 2013;29(7):886-889. doi:10.1016/j.cjca.2013.03.025
13. Keane JF, Driscoll DJ, Gersony WM, et al. Second natural history study of congenital heart defects. Results of treatment of patients with aortic valvar stenosis. *Circulation*. 1993;87(2 Suppl):I16-27.

14. Feltes TF, Bacha E, Beekman RH 3rd, et al. Indications for cardiac catheterization and intervention in pediatric cardiac disease: a scientific statement from the American Heart Association. *Circulation*. 2011;123(22):2607-2652. doi:10.1161/CIR.0b013e31821b1f10

15. Rao PS, Galal O, Smith PA, Wilson AD. Five- to nine-year follow-up results of balloon angioplasty of native aortic coarctation in infants and children. *J Am Coll Cardiol*. 1996;27(2):462-470. doi:10.1016/0735-1097(95)00479-3

16. Valsangiacomo Buechel ER, Mertens LL. Imaging the right heart: the use of integrated multimodality imaging. *Eur Heart J*. 2012;33(8):949-960. doi:10.1093/eurheartj/ehr490

17. Mawad W, Mertens LL. Recent Advances and Trends in Pediatric Cardiac Imaging. *Curr Treat Options Cardiovasc Med*. 2018;20(1). doi:10.1007/s11936-018-0599-x

18. Lai WW, Geva T, Shirali GS, et al. Guidelines and Standards for Performance of a Pediatric Echocardiogram: A Report from the Task Force of the Pediatric Council of the American Society of Echocardiography. *Journal of the American Society of Echocardiography*. Published online 2006. doi:10.1016/j.echo.2006.09.001

19. Lai WW, Mertens L, Cohen M, Geva TTATT. Echocardiography in pediatric and congenital heart disease : from fetus to adult LK - https://mcgill.on.worldcat.org/oclc/1257314132. Published online 2022.

20. Mitchell DG. Color Doppler imaging: principles, limitations, and artifacts. *Radiology*. 1990;177(1):1-10. doi:10.1148/radiology.177.1.2204956

21. Ferrara K, DeAngelis G. Color flow mapping. *Ultrasound Med Biol*. 1997;23(3):321-345. doi:10.1016/s0301-5629(96)00216-5

22. Edler I, Lindström K. The history of echocardiography. LK - https://mcgill.on.worldcat.org/oclc/111739507. *Ultrasound in medicine & biology TA - TT -*. 2004;30(12):1565-1644.

23. Løvstakken L, Bjaerum S, Martens D, Torp H. Blood flow imaging--A new real-time, 2-D flow imaging technique. *IEEE Trans Ultrason Ferroelectr Freq Control*. 2006;53(2):289-299. doi:10.1109/tuffc.2006.1593367

24. Zaragoza-Macias E, Stout KK. Management of pulmonic regurgitation and right ventricular dysfunction in the adult with repaired Tetralogy of Fallot. *Curr Treat Options Cardiovasc Med*. 2013;15(5):575-586. doi:10.1007/s11936-013-0258-1

25. van der Bom T, Bouma BJ, Meijboom FJ, Zwinderman AH, Mulder BJM. The prevalence of adult congenital heart disease, results from a systematic review and evidence based calculation. *Am Heart J*. 2012;164(4):568-575. doi:10.1016/j.ahj.2012.07.023

26. Marelli AJ, Mackie AS, Ionescu-Ittu R, Rahme E, Pilote L. Congenital heart disease in the general population: Changing prevalence and age distribution. *Circulation*. 2007;115(2):163-172. doi:10.1161/CIRCULATIONAHA.106.627224

27. Marelli AJ, Ionescu-Ittu R, Mackie AS, Guo L, Dendukuri N, Kaouache M. Lifetime prevalence of congenital heart disease in the general population from 2000 to 2010. *Circulation*. 2014;130(9):749-756. doi:10.1161/CIRCULATIONAHA.113.008396

28. Reddy S, Bernstein D, Newburger JW. Renin-angiotensin-aldosterone system inhibitors for right ventricular dysfunction in tetralogy of fallot: Quo Vadis? *Circulation*. 2018;137(14):1472-1474. doi:10.1161/CIRCULATIONAHA.117.032285

29. Tang D, Yang C, Del Nido PJ, et al. Mechanical stress is associated with right ventricular response to pulmonary valve replacement in patients with repaired tetralogy of Fallot. *Journal of Thoracic and Cardiovascular Surgery*. 2016;151(3):687-694.e3. doi:10.1016/j.jtcvs.2015.09.106

30. Yu H, del Nido PJ, Geva T, et al. A Novel Pulmonary Valve Replacement Surgery Strategy Using Contracting Band for Patients With Repaired Tetralogy of Fallot: An MRI-Based Multipatient Modeling Study. *Front Bioeng Biotechnol*. 2021;9(May):1-15. doi:10.3389/fbioe.2021.638934

31. Shibata M, Itatani K, Hayashi T, et al. Flow Energy Loss as a Predictive Parameter for Right Ventricular Deterioration Caused by Pulmonary Regurgitation After Tetralogy of Fallot Repair. *Pediatr Cardiol*. 2018;39(4):731-742. doi:10.1007/s00246-018-1813-z

32. Schäfer M, Barker AJ, Morgan GJ, et al. Increased systolic vorticity in the left ventricular outflow tract is associated with abnormal aortic flow formations in Tetralogy of Fallot. *Int J Cardiovasc Imaging*. 2020;36(4):691-700. doi:10.1007/s10554-019-01764-w

33. van der Ven JPG, van den Bosch E, Bogers AJCC, Helbing WA. Current outcomes and treatment of tetralogy of Fallot. *F1000Res*. 2019;8:1530. doi:10.12688/f1000research.17174.1

34. Pedrizzetti G, Martiniello AR, Bianchi V, D'Onofrio A, Caso P, Tonti G. Cardiac fluid dynamics anticipates heart adaptation. *J Biomech*. 2015;48(2):388-391. doi:10.1016/J.JBIOMECH.2014.11.049

35. Swift AJ, Rajaram S, Hurdman J, et al. Noninvasive Estimation of PA Pressure, Flow, and Resistance With CMR Imaging Derivation and Prospective Validation Study From the ASPIRE Registry. JACC Cardiovasc Imaging. 2013;6(10):1036-1047. doi:10.1016/J.JCMG.2013.01.013

36. Foris V, Kovacs G, Tscherner M, Olschewski A, Olschewski H. Biomarkers in pulmonary hypertension: What do we know? *Chest*. 2013;144(1):274-283. doi:10.1378/chest.12-1246

37. Schäfer M, Barker AJ, Kheyfets V, et al. Helicity and vorticity of pulmonary arterial flow in patients with pulmonary hypertension: Quantitative analysis of flow formations. *J Am Heart Assoc*. 2017;6(12):14-16. doi:10.1161/JAHA.117.007010

38. Birth Defects Research - 2019 - Mai - National population-based estimates for major birth defects 2010 2014.pdf.

39. Giannakou A, Sicko RJ, Kay DM, et al. Copy number variants in hypoplastic right heart syndrome. *Am J Med Genet A*. 2018;176(12):2760-2767. doi:10.1002/ajmg.a.40527

40. Barron DJ, Kilby MD, Davies B, Wright JGC, Jones TJ, Brawn WJ. Hypoplastic left heart syndrome. *The Lancet*. 2009;374(9689):551-564. doi:https://doi.org/10.1016/S0140-6736(09)60563-8

41. Anderson PAW, Sleeper LA, Mahony L, et al. Contemporary Outcomes After the Fontan Procedure. A Pediatric Heart Network Multicenter Study. *J Am Coll Cardiol*. 2008;52(2):85-98. doi:10.1016/j.jacc.2008.01.074

42. Schwartz I, McCracken CE, Petit CJ, Sachdeva R. Late outcomes after the Fontan procedure in patients with single ventricle: A meta-analysis. *Heart*. 2018;104(18):1508-1514. doi:10.1136/heartjnl-2017-312807

43. Rychik J, Atz AM, Celermajer DS, et al. Evaluation and Management of the Child and Adult With Fontan Circulation: A Scientific Statement From the American Heart Association. *Circulation*. Published online July 2019. doi:10.1161/CIR.0000000000000696

44. Meza JM, Blackstone EH, Argo MB, et al. A dynamic Norwood mortality estimation: Characterizing individual, updated, predicted mortality trajectories after the Norwood operation. *JTCVS Open*. 2023;14(June):426-440. doi:10.1016/j.xjon.2023.04.010

45. Dennis M, Zannino D, du Plessis K, et al. Clinical Outcomes in Adolescents and Adults After the Fontan Procedure. *J Am Coll Cardiol*. 2018;71(9):1009-1017. doi:10.1016/j.jacc.2017.12.054

46. Cardoso B, Kelecsenyi A, Smith J, et al. Improving outcomes for transplantation in failing Fontan—what is the next target? *JTCVS Open*. 2021;8(C):565-573. doi:10.1016/j.xjon.2021.08.006

47. Baker DW, Dennis MR, Zannino D, et al. Path ahead for € low risk' adolescents living with a Fontan circulation. *Heart*. 2021;107(7):556-562. doi:10.1136/heartjnl-2020-317619

48. Alsaied T, Allen KY, Anderson JB, et al. The Fontan outcomes network: first steps towards building a lifespan registry for individuals with Fontan circulation in the United States – CORRIGENDUM. *Cardiol Young*. 2020;30(9):1381. doi:DOI: 10.1017/S1047951120002462

49. Gewillig M, Brown SC. The Fontan circulation after 45 years: Update in physiology. *Heart*. 2016;102(14):1081-1086. doi:10.1136/heartjnl-2015-307467

50. Gewillig M. The Fontan circulation. *Heart*. 2005;91(6):839-846. doi:10.1136/hrt.2004.051789

51. de Leval MR, Deanfield JE. Four decades of Fontan palliation. *Nat Rev Cardiol*. Published online 2010. doi:10.1038/nrcardio.2010.99

52. Stephenson EA, Lu M, Berul CI, et al. Arrhythmias in a contemporary Fontan cohort: Prevalence and clinical associations in a multicenter cross-sectional study. *J Am Coll Cardiol*. 2010;56(11):890-896. doi:10.1016/j.jacc.2010.03.079

53. Randall WC, Wehrmacher WH. Early and late arrhythmias after the Fontan operation: Predisposing factors and clinical consequences [2]. *Br Heart J*. 1993;69(6):572. doi:10.1136/hrt.69.6.572-a

54. Schlangen J, Fischer G, Petko C, et al. Arterial elastance and its impact on intrinsic right ventricular function in palliated hypoplastic left heart syndrome. *International Journal of Cardiology TA - TT -*. 2013;168(6):5385-5389. doi:10.1016/j.ijcard.2013.08.052 LK - https://mcgill.on.worldcat.org/oclc/5902511120

55. Cools B, Brown SC, Sluysmans T, DeWolf D, Dessy H, Gewilliga M. When coronary arteries need systolic pressure: Surgical considerations. *European Journal of Cardio-thoracic Surgery*. 2013;43(4):737-742. doi:10.1093/ejcts/ezs531

56. Gewillig M, Goldberg DJ. Failure of the fontan circulation. *Heart Fail Clin*. 2014;10(1):105-116. doi:10.1016/j.hfc.2013.09.010

57. Goldstein BH, Connor CE, Gooding L, Rocchini AP. Relation of Systemic Venous Return, Pulmonary Vascular Resistance, and Diastolic Dysfunction to Exercise Capacity in Patients

With Single Ventricle Receiving Fontan Palliation. *American Journal of Cardiology*. 2010;105(8):1169-1175. doi:10.1016/j.amjcard.2009.12.020

58. Mawad W, Friedberg MK. The continuing challenge of evaluating diastolic function by echocardiography in children. *Curr Opin Cardiol*. 2017;32(1):93-100. doi:10.1097/HCO.0000000000000346

59. Rijnberg FM, Westenberg JJM, van Assen HC, et al. 4D flow cardiovascular magnetic resonance derived energetics in the Fontan circulation correlate with exercise capacity and CMR-derived liver fibrosis/congestion. *Journal of Cardiovascular Magnetic Resonance*. 2022;24(1):1-10. doi:10.1186/s12968-022-00854-4

60. Trusty PM, Wei Z, Rychik J, et al. Impact of hemodynamics and fluid energetics on liver fibrosis after Fontan operation. *Journal of Thoracic and Cardiovascular Surgery*. 2018;156(1):267-275. doi:10.1016/j.jtcvs.2018.02.078

61. Kamphuis VP, Roest AAW, van den Boogaard PJ, et al. Hemodynamic interplay of vorticity, viscous energy loss, and kinetic energy from 4D Flow MRI and link to cardiac function in healthy subjects and Fontan patients. *Am J Physiol Heart Circ Physiol*. 2021;320(4):H1687-H1698. doi:10.1152/AJPHEART.00806.2020

62. Stone ML, Schäfer M, DiMaria M V., et al. Diastolic inflow is associated with inefficient ventricular flow dynamics in Fontan patients. *Journal of Thoracic and Cardiovascular Surgery*. 2022;163(3):1195-1207. doi:10.1016/j.jtcvs.2021.06.064

63. Mele D, Smarrazzo V, Pedrizzetti G, et al. Intracardiac Flow Analysis: Techniques and Potential Clinical Applications. *Journal of the American Society of Echocardiography*. 2019;32(3):319-332. doi:10.1016/j.echo.2018.10.018

64. Hong GR, Pedrizzetti G, Tonti G, et al. Characterization and quantification of vortex flow in the human left ventricle by contrast echocardiography using vector particle image velocimetry. *JACC Cardiovasc Imaging*. 2008;1(6):705-717. doi:10.1016/j.jcmg.2008.06.008

65. Kim HB, Hertzberg JR, Shandas R. Development and validation of echo PIV. *Exp Fluids*. 2004;36(3):455-462. doi:10.1007/s00348-003-0743-5

66. Kutty S, Biko DM, Goldberg AB, Quartermain MD, Feinstein SB. Contrast-enhanced ultrasound in pediatric echocardiography. *Pediatr Radiol*. 2021;51(12):2408-2417. doi:10.1007/s00247-021-05119-3

67. Tanaka M, Sakamoto T, Sugawara S, et al. Blood flow structure and dynamics, and ejection mechanism in the left ventricle: Analysis using echo-dynamography. *J Cardiol*. 2008;52(2):86-101. doi:10.1016/j.jjcc.2008.05.005

68. Itatani K, Okada T, Uejima T, et al. Intraventricular flow velocity vector visualization based on the continuity equation and measurements of vorticity and wall shear stress. *Jpn J Appl Phys*. 2013;52(7 PART 2). doi:10.7567/JJAP.52.07HF16

69. Garcia D, Juan JC, Tanné. D, et al. Two-dimensional intraventricular flow mapping by digital processing conventional color-doppler echocardiography images. *IEEE Trans Med Imaging*. 2010;29(10):1701-1713. doi:10.1109/TMI.2010.2049656

70. Asami R, Tanaka T, Kawabata K ichi, Hashiba K, Okada T, Nishiyama T. Accuracy and limitations of vector flow mapping: left ventricular phantom validation using stereo particle image velocimetory. *J Echocardiogr*. 2016;15(2):57-66. doi:10.1007/s12574-016-0321-5

71. Meyers B, Nyce J, Zhang J, et al. Intracardiac Flow Analysis of the Right Ventricle in Pediatric Patients With Repaired Tetralogy of Fallot Using a Novel Color Doppler Velocity Reconstruction. *Journal of the American Society of Echocardiography*. 2023;36(6):644-653. doi:10.1016/j.echo.2023.02.008

72. Tanter M, Bercoff J, Sandrin L, Fink M. Ultrafast compound imaging for 2-D motion vector estimation: application to transient elastography. *IEEE Trans Ultrason Ferroelectr Freq Control*. 2002;49(10):1363-1374. doi:10.1109/tuffc.2002.1041078

73. Bercoff J, Montaldo G, Loupas T, et al. Ultrafast compound Doppler imaging: providing full blood flow characterization. *IEEE Trans Ultrason Ferroelectr Freq Control*. 2011;58(1):134-147. doi:10.1109/TUFFC.2011.1780

74. Nyrnes SA, Fadnes S, Wigen MS, Mertens L, Lovstakken L. Blood Speckle-Tracking Based on High–Frame Rate Ultrasound Imaging in Pediatric Cardiology. *Journal of the American Society of Echocardiography*. Published online 2020. doi:https://doi.org/10.1016/j.echo.2019.11.003

75. Fadnes S, Wigen MS, Nyrnes SA, Lovstakken L. In Vivo Intracardiac Vector Flow Imaging Using Phased Array Transducers for Pediatric Cardiology. 2017;64(9):1318-1326.

76. Fadnes S, Nyrnes SA, Torp H, Lovstakken L. Shunt flow evaluation in congenital heart disease based on two-dimensional speckle tracking. *Ultrasound Med Biol*. 2014;40(10):2379-2391. doi:10.1109/ULTSYM.2012.0471

77. Fadnes S, Nyrnes SA, Torp H, Lovstakken L. Shunt Flow Evaluation in Congenital Heart Disease Based on Two-Dimensional Speckle Tracking. *Ultrasound Med Biol*. 2014;40(10):1-13. doi:10.1016/j.ultrasmedbio.2014.03.029

78. Akins CW, Travis B, Yoganathan AP. Energy loss for evaluating heart valve performance. *Journal of Thoracic and Cardiovascular Surgery*. 2008;136(October):820-833. doi:10.1016/j.jtcvs.2007.12.059

79. Bird 1924- RB (Robert B, Stewart WE 1924, Lightfoot EN 1925. *Transport Phenomena LK - Https://Mcgill.on.Worldcat.Org/Oclc/46456316*. 2nd, Wiley ed. J. Wiley; 2002.

80. Grigioni M, D'Avenio G, Amodeo A, Di Donato RM. Power dissipation associated with surgical operations' hemodynamics: Critical issues and application to the total cavopulmonary connection. *J Biomech*. 2006;39(9):1583-1594. doi:10.1016/j.jbiomech.2006.04.008

81. Sengupta PP, Pedrizzetti G, Kilner PJ, et al. Emerging trends in CV flow visualization. *JACC Cardiovasc Imaging*. 2012;5(3):305-316. doi:10.1016/j.jcmg.2012.01.003

82. Pedrizzetti G, La Canna G, Alfieri O, Tonti G. The vortex--an early predictor of cardiovascular outcome? *Nat Rev Cardiol*. 2014;11(9):545-553. doi:10.1038/nrcardio.2014.75

83. Garcia J, Larose E, Pibarot P, Kadem L. On the evaluation of vorticity using cardiovascular magnetic resonance velocity measurements. *J Biomech Eng*. 2013;135(12):1-6. doi:10.1115/1.4025385

84. Hirtler D, Garcia J, Barker AJ, Geiger J. Assessment of intracardiac flow and vorticity in the right heart of patients after repair of tetralogy of Fallot by flow-sensitive 4D MRI. *Eur Radiol*. 2016;26(10):3598-3607. doi:10.1007/s00330-015-4186-1

85. Elsayed A, Gilbert K, Scadeng M, Cowan BR, Pushparajah K, Young AA. Four-dimensional flow cardiovascular magnetic resonance in tetralogy of Fallot: a systematic review. *J Cardiovasc Magn Reson*. 2021;23(1):59. doi:10.1186/s12968-021-00745-0

86. Saris AECM, Hansen HHG, Fekkes S, Menssen J, Nillesen MM, de Korte CL. In Vivo Blood Velocity Vector Imaging Using Adaptive Velocity Compounding in the Carotid Artery Bifurcation. *Ultrasound Med Biol*. 2019;45(7):1691-1707. doi:10.1016/j.ultrasmedbio.2019.03.008

87. Karzova MM, Yuldashev P V., Khokhlova VA, Nartov FA, Morrison KP, Khokhlova TD. Dual-Use Transducer for Ultrasound Imaging and Pulsed Focused Ultrasound Therapy. *IEEE Trans Ultrason Ferroelectr Freq Control*. 2021;68(9):2930-2941. doi:10.1109/TUFFC.2021.3070528

88. Wigen MS, Fadnes S, Rodriguez-molares A, et al. 4-D Intracardiac Ultrasound Vector Flow Imaging – Feasibility and Comparison to Phase-Contrast MRI. 2018;37(12):2619-2629. doi:10.1109/TMI.2018.2844552

89. Van Cauwenberge J, Lovstakken L, Fadnes S, et al. Assessing the Performance of Ultrafast Vector Flow Imaging in the Neonatal Heart via Multiphysics Modeling and <italic>In Vitro</italic> Experiments. *IEEE Trans Ultrason Ferroelectr Freq Control*. 2016;63(11):1772-1785. doi:10.1109/TUFFC.2016.2596804

90. Faludi R, Szulik M, D'hooge J, et al. Left ventricular flow patterns in healthy subjects and patients with prosthetic mitral valves: An in vivo study using echocardiographic particle image velocimetry. *Journal of Thoracic and Cardiovascular Surgery*. 2010;139(6):1501-1510. doi:10.1016/j.jtcvs.2009.07.060

91. Collia D, Zovatto L, Tonti G, Pedrizzetti G. Comparative Analysis of Right Ventricle Fluid Dynamics. *Front Bioeng Biotechnol*. 2021;9(July):1-10. doi:10.3389/fbioe.2021.667408

92. Pasipoularides A, Vlachos PP, Little WC. Vortex formation time is not an index of ventricular function. *J Cardiovasc Transl Res*. 2015;8(1). doi:10.1007/s12265-015-9607-7

93. Lopez C, Mertens L, Dragulescu A, et al. Strain and Rotational Mechanics in Children With Single Left Ventricles After Fontan. *Journal of the American Society of Echocardiography*. 2018;31(12):1297-1306. doi:10.1016/j.echo.2018.09.004

94. Grattan M, Mertens L, Grosse-Wortmann L, Friedberg MK, Cifra B, Dragulescu A. Ventricular Torsion in Young Patients With Single-Ventricle Anatomy. *Journal of the American Society of Echocardiography*. 2018;31(12):1288-1296. doi:10.1016/j.echo.2018.07.018

95. Grattan M, Mertens L. Mechanics of the Functionally Univentricular Heart – How little do we understand and why does it matter? *Canadian Journal of Cardiology*. Published online 2015:1-8. doi:10.1016/j.cjca.2015.11.001

96. Khoo NS, Smallhorn JF, Kaneko S, Myers K, Kutty S, Tham EB. Novel insights into RV adaptation and function in hypoplastic left heart syndrome between the first 2 stages of surgical palliation. *JACC Cardiovasc Imaging*. 2011;4(2):128-137. doi:10.1016/j.jcmg.2010.09.022

97. Broberg CS, van Dissel A, Minnier J, et al. Long-Term Outcomes After Atrial Switch Operation for Transposition of the Great Arteries. *J Am Coll Cardiol*. 2022;80(10):951-963. doi:10.1016/j.jacc.2022.06.020

98. Henry M, Fadnes S, Lovstakken L, Mawad W, Mertens L, Nyrnes SA. Flow Dynamics in Children With Bicuspid Aortic Valve: A Blood Speckle Tracking Study. *Ultrasound Med Biol*. 2023;49(11):2354-2360. doi:10.1016/j.ultrasmedbio.2023.07.012

99. Binter C, Gotschy A, Sündermann SH, et al. Turbulent Kinetic Energy Assessed by Multipoint 4-Dimensional Flow Magnetic Resonance Imaging Provides Additional Information Relative to Echocardiography for the Determination of Aortic Stenosis SeverityCLINICAL PERSPECTIVE. *Circ Cardiovasc Imaging*. 2017;10(6). doi:10.1161/CIRCIMAGING.116.005486

100. Pasipoularides A, Shu M, Shah A, Womack MS, Glower DD. Diastolic right ventricular filling vortex in normal and volume overload states. *Am J Physiol Heart Circ Physiol*. 2003;284(4):H1064-H1072. doi:DOI 10.1152/ajpheart.00804.2002

101. Visser LC, Im MK, Johnson LR, Stern JA. Diagnostic Value of Right Pulmonary Artery Distensibility Index in Dogs with Pulmonary Hypertension: Comparison with Doppler Echocardiographic Estimates of Pulmonary Arterial Pressure. *J Vet Intern Med*. 2016;30(2):543-552. doi:10.1111/jvim.13911

102. Venco L, Mihaylova L, Boon JA. Right Pulmonary Artery Distensibility Index (RPAD Index). A field study of an echocardiographic method to detect early development of pulmonary hypertension and its severity even in the absence of regurgitant jets for Doppler evaluation in heartworm-infec. *Vet Parasitol*. 2014;206(1-2):60-66. doi:10.1016/j.vetpar.2014.08.016

103. Sjöberg P, Heiberg E, Wingren P, et al. Decreased Diastolic Ventricular Kinetic Energy in Young Patients with Fontan Circulation Demonstrated by Four-Dimensional Cardiac

Magnetic Resonance Imaging. *Pediatr Cardiol*. 2017;38(4):669-680. doi:10.1007/s00246-016-1565-6

104. Sjöberg P, Töger J, Hedström E, et al. Altered biventricular hemodynamic forces in patients with repaired tetralogy of fallot and right ventricular volume overload because of pulmonary regurgitation. *Am J Physiol Heart Circ Physiol*. 2018;315(6):H1691-H1702. doi:10.1152/ajpheart.00330.2018

105. Heying R, d'Udekem Y, Gewillig M, Rychik J. Editorial: The fontan circulation: Problems and solutions. *Front Pediatr*. 2022;10(December):1-5. doi:10.3389/fped.2022.1087739

106. Van De Bruaene A, Claessen G, Salaets T, Gewillig M. Late Fontan Circulatory Failure. What Drives Systemic Venous Congestion and Low Cardiac Output in Adult Fontan Patients? *Front Cardiovasc Med*. 2022;9(March):1-9. doi:10.3389/fcvm.2022.825472

107. Kheradvar A, Rickers C, Morisawa D, Kim M, Hong GR, Pedrizzetti G. Diagnostic and prognostic significance of cardiovascular vortex formation. *J Cardiol*. 2019;74(5):403-411. doi:10.1016/j.jjcc.2019.05.005

108. Pasipoularides A. Diastolic filling vortex forces and cardiac adaptations: Probing the epigenetic nexus. *Hellenic Journal of Cardiology*. 2012;53(6):458-469.

109. Pasipoularides A. Evaluation of right and left ventricular diastolic filling. *J Cardiovasc Transl Res*. 2013;6(4):623-639. doi:10.1016/j.biotechadv.2011.08.021.Secreted

110. Tseng H, Peterson TE, Berk BC. Fluid Shear Stress Stimulates Mitogen-Activated Protein Kinase in Endothelial Cells. *Circ Res*. 1995;77(5):869 LP - 878.

111. Ueba H, Kawakami M, Yaginuma T. Shear Stress as an Inhibitor of Vascular Smooth Muscle Cell Proliferation. *Arterioscler Thromb Vasc Biol*. 1997;17(8):1512 LP - 1516.

112. Pedrizzetti G, Sengupta PP. Vortex imaging: New information gain from tracking cardiac energy loss. *Eur Heart J Cardiovasc Imaging*. 2015;16(7):719-720. doi:10.1093/ehjci/jev070

113. Azarine A, Garcon P, Stansal A, et al. Four-dimensional Flow MRI: Principles and Cardiovascular Applications. *Radiographics*. 2019;39(3):632-648. doi:10.1148/rg.2019180091

114. Sørensen K, Fadnes S, Mertens L, et al. Assessment of Early Diastolic Intraventricular Pressure Difference in Children by Blood Speckle-Tracking Echocardiography. *Journal of the American Society of Echocardiography*. 2023;36(5):523-532.e3. doi:10.1016/j.echo.2022.12.025

22. PAPERS

PAPER 1

Ultrasound in Med. & Biol., Vol. 47, No. 6, pp. 1514–1527, 2021

0301-5629/$ - see front matter

https://doi.org/10.1016/j.ultrasmedbio.2021.02.004

● *Original Contribution*

RIGHT VENTRICULAR FLOW DYNAMICS IN DILATED RIGHT VENTRICLES: ENERGY LOSS ESTIMATION BASED ON BLOOD SPECKLE TRACKING ECHOCARDIOGRAPHY—A PILOT STUDY IN CHILDREN

Wadi Mawad,*[,†,‡] Lasse Løvstakken,[†] Solveig Fadnes,[†] Thomas Grønli,[†] Patrick Segers,[§] Luc Mertens,* and Siri Ann Nyrnes[†,¶]

* The Hospital for Sick Children, Toronto, Ontario, Canada; [†] Department of Circulation and Medical Imaging, Norwegian University of Science and Technology (NTNU), Trondheim, Norway; [‡] Department of Paediatrics, Montreal Children's Hospital, McGill University Health Centre, Montreal, Quebec, Canada; [§] Biommeda, University of Ghent, Ghent, Belgium; and [¶] Children's Clinic, St. Olav's University Hospital, Trondheim, Norway

(*Received* 14 *September* 2020; *revised* 24 *December* 2020; *in final from* 6 *February* 2021)

Abstract—Using blood speckle tracking (BST) based on high-frame-rate echocardiography (HFRE), we compared right ventricle (RV) flow dynamics in children with atrial septal defects (ASDs) and repaired tetralogy of Fallot (rTOF). Fifty-seven children with rTOF with severe pulmonary insufficiency (PI) (n = 21), large ASDs (n = 11) and healthy controls (CTL, n = 25) were included. Using a flow phantom, we studied the effects of imaging plane and smoothing parameters on 2-D energy loss (EL). RV diastolic EL was similar in ASD and rTOF, but both were greater than in CTL. Locations of high EL were similar in all groups in systole, occurring in the RV outflow tract and around the tricuspid valve leaflets in early diastole. An additional apical early diastolic area of EL was noted in rTOF, corresponding to colliding tricuspid inflow and PI. The flow phantom revealed that EL varied with imaging plane and smoothing settings but that the EL trend was preserved if kept consistent. (E-mail: wadi.mawad@mcgill.ca)

Key Words: **Blood flow imaging, Energy loss, Flow dynamics, Blood speckle tracking, High-frame-rate imaging.**

INTRODUCTION

Volume loading caused by a large atrial septal defect (ASD) or pulmonary insufficiency (PI) after tetralogy of Fallot repair (rTOF) results in right ventricle (RV) dilation. Although the RV is dilated in these two conditions, RV function generally remains preserved in ASD patients whereas progressive RV dysfunction can occur in rTOF patients (van der Ven et al. 2019). When RV longitudinal function is studied using strain imaging, RV longitudinal strain is typically reduced in rTOF patients but preserved or even increased in ASD patients (Dragulescu et al. 2013). Our group also reported that reduction in RV longitudinal function preferentially affects the RV apex in rTOF (Dragulescu et al. 2014). Right ventricular function is an important prognostic factor in patients with rTOF, and an early imaging biomarker anticipating later failure is still lacking. Disturbances in cardiac fluid dynamics and energetics are thought to precede morphologic changes (Pedrizzetti et al. 2015). Flow patterns within the left ventricle have been studied, mainly by cardiac magnetic resonance imaging (MRI) or particle imaging velocimetry echocardiography (echo-PIV) and, more recently, vector flow mapping (VFM) (Zhong et al. 2016; Nakashima et al. 2017). RV flow dynamics, however, have not been well characterized in humans. Four-dimensional-flow MRI has revealed increased RV vorticity in rTOF patients, compared with healthy controls (Hirtler et al. 2016). Energy-based descriptions of RV flow dynamics in rTOF have been proposed but have until recently relied on MRI and invasive pressure measurements (Fogel et al. 2012). With the use of VFM, energy loss (EL) was found to be predictive of RV function after tetralogy of Fallot repair (Shibata et al. 2018).

Recent advances in ultrasound technologies allow the study of cardiac fluid dynamics with a temporal resolution higher than ever before. A combination of high-

Address correspondence to: Wadi Mawad, B04.2656-1001 Décarie Boulevard, Montreal, QC, Canada H4 A3 J1. E-mail: wadi.mawad@mcgill.ca

frame-rate echocardiography (HFRE), obtained by plane wave imaging, with blood speckle tracking (BST) allows quantification of blood speckle velocities (Fadnes et al. 2017; Nyrnes et al. 2020), ultimately enabling direct quantification and visualization of blood flow vorticity and EL. The aim of this pilot study was to use blood speckle tracking to compare cardiac flow dynamics between patients with dilated RVs secondary to large ASD or PI after rTOF. To this end, we aimed to compare RV vorticity and to quantify and localize EL in both groups of volume-loaded RVs. To provide more insight into the practical use of the energy loss parameter, we further analyzed its sensitivity to positioning of the imaging plane and the effects of post-processing (smoothing) in a computer simulation model, as well as inter and intraobserver variability *in vivo*.

METHODS

Children with rTOF and severe PI, children with a large secundum ASD causing RV dilation (RV end-diastolic dimension Z score > 2.5) and healthy controls (CTL) from the Hospital for Sick Children in Toronto, Canada, and St. Olavs Hospital in Trondheim, Norway, between December 2015 and January 2018, were included. Consent from the parents of each participant was obtained before enrollment, as specified by the ethics review boards of both institutions (Toronto Hospital for Sick Children No. 1000050095; St. Olav's No. 2010/499). The upper age limit for inclusion was 10 y. Conventional echocardiographic parameters were obtained from clinical studies done immediately before the high-frame-rate acquisitions. RV three-chamber (RV3C) and four-chamber (RV4C) views were acquired using a modified Vivid E-9 system (GE Vingmed Ultrasound, Horten, Norway) with research software enabling high-frame-rate acquisitions using plane (unfocused) transmit beams and parallel receive beamforming (Nyrnes et al. 2020). The principle underlying our image acquisition is illustrated in Figure 1. At least three cardiac cycles were recorded with commercially available ultrasound probes, including the 6 S and 12 S phased-array probes (GE Healthcare, Milwaukee, WI, USA). Storage of IQ (in-phase and quadrature) data was required for the offline postprocessing and analysis with blood speckle tracking.

Validation and analysis of the energy loss measurement

To validate the EL measurement and analyze its sensitivity to changes related to imaging plane, as well as for data smoothing and dropouts, the 2-D EL was evaluated in a 3-D computer simulation as illustrated in Figure 2 (bottom left), mimicking the main flow events (filling, vortex formation and ejection) in a previously described ventricular model (Van Cauwenberge et al. 2016). This allowed for comparison with a known ground truth for both 2-D and 3-D velocity fields, with the flexibility to obtain standard and non-standard imaging views. We investigated the effect of small offsets ($\pm 5^{\circ}$) from the standard cardiac views on the 2-D EL values. Furthermore, we investigated the influence of dropouts and smoothing in the color Doppler and BST data on EL.

Energy-loss calculations and localization

The raw echo data obtained in patients and controls were transferred for offline analysis using in-house software developed for quantitative flow field analysis. The radial velocity measurement was derived from color Doppler, and the lateral velocity estimate was determined by speckle tracking (Wigen et al. 2018). For further analysis, the RV4C views needed to include the RV inlet and apex; the RV3C views needed to include the inlet, outlet and apex. Acquisitions with significant signal dropout were excluded. Quality of the acquisitions was assessed by two observers (SAN, SF), and only RV4C and RV3C views of good quality were analyzed. Segmentation of the flow field was performed by a single observer (WM). This was done to define the region of analysis and was achieved by delineating the endocardial border in both views. Systole and diastole were identified by closure and opening of the tricuspid valve. The first frame in which the tricuspid valve closed defined the start of systole, and the first frame in which the valve was open defined the start of diastole. By use of the measured velocities, EL in the 2-D plane was calculated from the RV4C view using the formula (Akiyama et al. 2017)

$$\mathrm{EL} = \mu \int 2\left(\frac{\partial v_x}{\partial x}\right)^2 + 2\left(\frac{\partial v_y}{\partial y}\right)^2 + \left(\frac{\partial v_x}{\partial y} + \frac{\partial v_y}{\partial x}\right)^2 dA \quad (1)$$

where $v = [v_x,\ v_y]$ is the blood velocity vector, $\mu = 0.004$ Pa · s is the blood viscosity, and dA indicates that the values are integrated over an area. The area of integration was in this work determined by the color flow image; that is, values were integrated where there is color flow signal for each frame. Temporal and spatial smoothing parameters were kept identical for all analyses (temporal smoothing = 40 ms, Gaussian spatial smoothing = 5×5 mm^2). The final energy loss values were calculated as the time-integrated values in systole and diastole, expressed in millijoules per meter. Vorticity (VO) quantifies the local rotation rate of blood in a

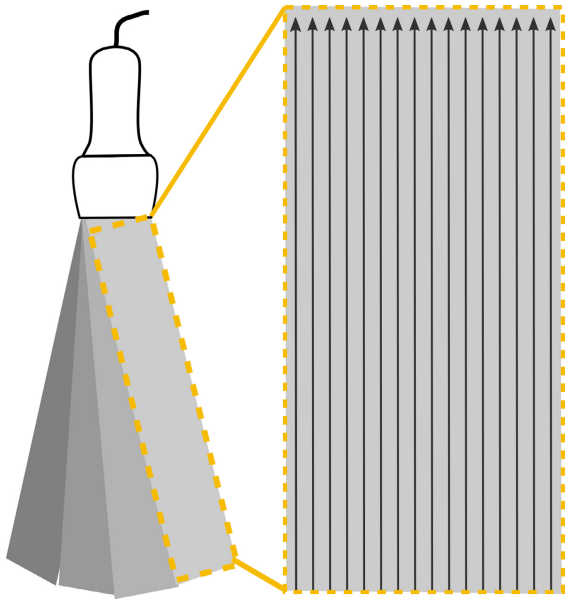

Fig. 1. Plane wave imaging and parallel receive beam forming. In this study, we used three to nine plane wave directions to cover the Doppler sector width. For each plane wave transmitted, multiple image lines (16 in our setup) were received simultaneously. Tracking can be done within the region covered by the 16 receive lines, where the frame rate equals the pulse repetition frequency.

2-D flow field. It was computed mathematically using the formula from the RV4C view and expressed in reciprocal seconds:

$$\mathrm{VO} = |\vec{\omega}| = \left| \frac{\partial v_y}{\partial x} - \frac{\partial v_x}{\partial y} \right| \quad (2)$$

An RV3C view was used to localize the areas of high EL because it provided simultaneous visualization of the RV inlet, apex and outlet flows in one 2-D cine loop. Only views including all three RV components were analyzed.

Reproducibility

A total of five randomly selected patients from each group were used to assess inter- and intra-observer variability in EL measurement from an RV4C view. We assessed this for EL only because both EL and VO rely on blood velocity measurements obtained with the same method. All the postprocessing analysis steps were repeated at an interval of 4 wk for the same observer and by a different observer (SAN). These were (i) definition of the timing points of systole and diastole as defined above; (ii) segmentation of a flow domain by tracing the endocardial surface of the RV; and (iii) calculation of EL in the selected cycle. For each patient, the same heart cycle in the RV4C cine loop was chosen by both observers, and all data were analyzed with the same smoothing settings.

Statistical analysis

Inter- and intra-observer analyses were assessed using Bland–Altman plots. Demographic and echocardiographic data were expressed as medians with quartiles (Q1–Q3). The Kruskal–Wallis test was used to test the differences in energy losses in three groups (CTL, rTOF and ASD). Comparison between two groups was done using the Mann–Whitney *U*-test, where a p value < 0.05 was considered to indicate statistical significance.

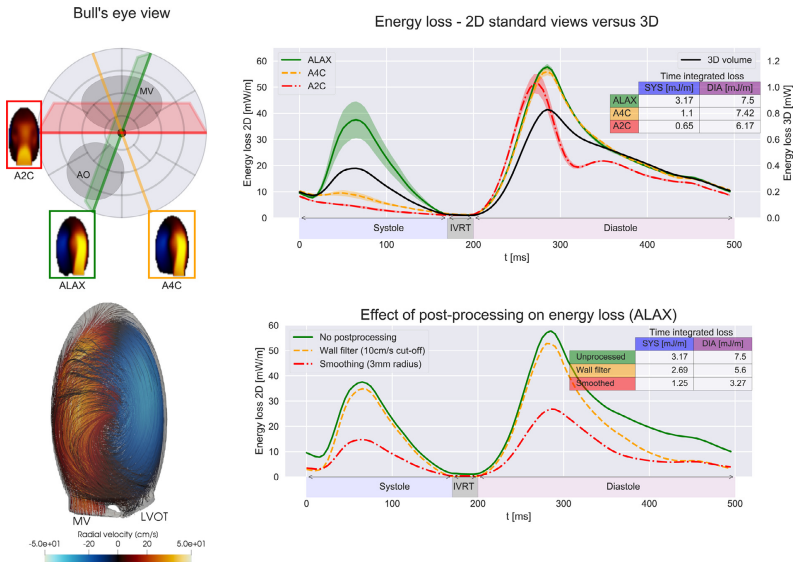

Fig. 2. Analysis of the energy loss metric in a computer simulation model mimicking 3-D ventricular flow. Bottom left: Snapshot of the flow pattern in the model in late diastole. In the Upper left: Bull's-eye view marking the mitral valve and outflow tract of the phantom along with the imaging plane/position of the selected standard examination views. Top right: The energy losses for standard views are traced along with variation resulting from the ±5˚ change in angle in the shaded lines. Little variation is noted in diastole, with some more important variations in systole from the ALAX view. Bottom right: The influence of the estimated values after postprocessing operations is plotted for the ALAX view with varying degrees of smoothing parameters. This indicates that increasing spatial smoothing reduces the EL magnitude but retains the curve shape (*red dotted line*). Wall filtering (*yellow line*) has little effect on EL magnitude and curve shape. ALAX = apical long axis; A2C = apical two-chamber; A4C = apical four-chamber; DIA = diastolic; EL = energy loss; IVRT = isovolumic relaxation time; LVOT = left ventricle outflow tract; MV = mitral valve; SYS = systole.

Correlations were tested using Spearman's rank test. The analyses were conducted using GraphPad Prism 8 (GraphPad Software, San Diego, CA, USA).

RESULTS

Validation and analysis of EL calculations using CFD

The computer-simulated validation and analysis of the EL measure are summarized in Figure 2. Our first aim was to evaluate how closely the 2-D EL for standard views compares with the true 3-D EL and to investigate how deviations from these imaging planes influence the 2-D EL measurement.

The 3-D EL curve indicates that most energy loss in the model occurs in diastole, where the filling jet leads to vortex formation with added shearing fluid losses. For the standard 2-D views, both the apical long-axis (ALAX) and apical four-chamber (A4C) views provided a fair representation of the diastolic 3-D EL (relative error: ±5% and ±4%, respectively). These 2-D views had similar integrated EL values with limited sensitivity to imaging view alignment (Fig. 2, upper right panel, *shaded color regions* around the curves). The apical two-chamber view (A2C), however, had the highest error (±9%). For systole, both the EL traces and integrated values varied substantially among imaging planes (relative error ALAX: ±19%, A4C: ±13%, A2C: ±17%). These findings supported the use of A4C views in our patients in diastole.

Our second aim was to analyze the influence of changes in postprocessing on the estimated 2-D EL and is shown for the ALAX view in Figure 2 (lower right plot). It can be observed that (i) spatial smoothing reduces EL magnitude but retains the curve shape, and (ii) the wall

filter has little influence in systole but may lead to some underestimation of EL in mid-to-late diastole.

To summarize, the computer simulation EL analysis revealed that, first, 2-D diastolic EL measures from A4C and ALAX views agree well with the 3-D EL shape, and the 2-D systolic EL measure from the ALAX view agrees well with the 3-D EL shape. Second, the effect of postprocessing is mainly a change in EL magnitude and can be used to compare relative changes. Consistent postprocessing parameters should be used, and clear baseline values should be provided.

RV energy loss calculations in TOF and ASD patients

In total, 21 rTOF (16 had received a transannular patch repair, 5 with an RV-to-pulmonary artery conduit), 11 ASD and 25 control patients were included, all with a suitable RV4C view for analysis. All rTOF patients had severe PI and no residual right ventricular outflow tract obstruction. The RV3C view was suitable (defined as a loop including high-quality BST measurements in the inflow, outflow and apex) only in 11 of 25 controls, 9 of 11 patients with ASD and 15 of 21 patients with rTOF.

Baseline demographic characteristics were similar among the three groups (Table 1). QRS duration was longer in the rTOF group compared with the other groups. When echocardiographic parameters of RV size and function were compared, the RVs were enlarged in ASD and rTOF patients compared with controls. Although RV fractional area change (FAC) was similar among the three groups, tricuspid annular plane systolic excursion (TAPSE) was significantly lower in the rTOF group compared with the other groups, whereas it was higher in the ASD patients compared with the other groups (Table 2). Tricuspid early diastolic inflow velocity (TVE) did not significantly differ among the groups. Left ventricular (LV) systolic function parameters did not significantly differ among the three groups.

Quantitative results from RV four-chamber views

Table 2 and Figure 3 compare the flow characteristics among the three groups as derived from blood speckle tracking. Compared with the CTL group, both the ASD and rTOF groups had significantly higher diastolic EL. Systolic EL, on the other hand, was similar in all groups. Diastolic vorticity was also significantly higher in ASD and rTOF as compared with CTL, whereas maximal systolic vorticity was similar in all groups. No significant correlation of heart rate, BSA or QRS duration with EL or vorticity was noted in any group. There were weak statistically significant correlations of systolic and diastolic EL with age in rTOF and CTL but not in ASD, with a wide spread of values as age increased. Energy loss and vorticity did not correlate with any conventional RV functional parameter.

Qualitative results from RV three-chamber views

When localizing regions of highest EL from the RV3C, all groups had a similar region of high systolic EL (Supplementary Videos S1, S2 and S3 [online only] for CTL, ASD and rTOF, respectively) and VO (Supplementary Videos S4, S5 and S6 [online only] for CTL, ASD and rTOF, respectively) in the right ventricular outflow tract. In diastole, all groups had high EL and VO around the tricuspid valve leaflets, corresponding to

Table 1. Demographic and echocardiographic data

	CTL (n = 25)	rTOF (n = 21)	ASD (n = 11)
Age (mo)	42 (26–76)	41 (21–74)	66 (33–99)
Male (%)	48%	52%	54%
Height (cm)	100 (85–124)	95 (82–109)	104 (88–134)
Weight (kg)	15.8 (12.3–23.6)	12.2 (10.0–19.5)	17.9 (10.5–27.3)
$BSA_{Haycock}$ (m^2)	0.94 (54–1.2)	0.84 (0.69–1.03)	0.74 (0.50–1.00)
Heart rate (bpm)	97 (85–108)	93 (85–100)	97 (89–101)
QRS duration (ms)	81 (77–93)	114 (80–128)*	82 (72–92)†
RV EDd (mm)	13 (10–16)	19 (17–23)	25 (21–32)
RV EDd Z-score	−0.4 (−1.4 to 0.9)	3.3 (2.7–3.5)*	4.6 (2.8–5.1)*
TAPSE (mm)	20 (18–23)	11 (10–13)*	23 (17–27)*,†
RV diastolic area (cm^2)	9.0 (7.6–13.3)	15.2 (8.8–17.6)*	18.2 (14.2–20.3)*,†
RV systolic area (cm^2)	5.6 (4.0–7.7)	8.7 (5.9–10.7)*	14.1 (10.5–20.3)*
RV FAC (%)	40 (37–46)	37 (33–42)	45 (37–48)
TV E (cm/s)	84 (72–126)	84 (71–100)	80 (70–101)
LV ejection fraction (%)	69 (64–74)	64 (61–68)	66 (61–70)
LV shortening fraction (%)	36 (32–39)	34 (32–37)	35 (31–38)

ASD = atrial septal defect; BSA = body surface area; CTL = controls; EDd = end-diastolic dimension; FAC = fractional area change; LV = left ventricle; RV = right ventricle; rTOF = repaired tetralogy of Fallot; TAPSE = tricuspid annular plane systolic excursion; TV E = tricuspid valve E-wave velocity.

Values are expressed as the median (quartiles Q1–Q3).

* p value < 0.05 versus CTL.

† p value < 0.05 versus rTOF.

Table 2. Right ventricular energy loss and vorticity in the four-chamber view

	CTL (n = 25)	rTOF (n = 21)	ASD (n = 11)
Systolic energy loss (mJ/m)	0.17 (0.10–0.48)	0.29 (0.07–0.51)	0.44 (0.29–0.68)
Diastolic energy loss (mJ/m)	1.34 (0.55–2.06)	1.93 (1.46–2.74)*	2.86 (1.47–3.65)*
Maximal systolic vorticity (1/s)	3.66 (2.02–5.98)	6.57 (1.52–11.19)	13.90 (6.13–18.41)
Maximal diastolic vorticity (1/s)	14.09 (8.36–17.61)	23.01 (17.73–28.52)*	28.74 (21.55–33.80)*

ASD = atrial septal defect; CTL = controls; rTOF = repaired tetralogy of Fallot.
Values are expressed as the median (quartiles Q1–Q3).
p-value < 0.05: *ASD or rTOF versus CTL.

vortex formation at the edge of the tricuspid valve leaflets. In rTOF, however, an additional region of high EL and VO was present in most cases (11/15) in the RV apex, corresponding to colliding PI and tricuspid inflow. Cardiac blood speckle tracking findings are summarized in schematic form in Figure 4 and in typical examples in Figure 5. The systolic and diastolic flow patterns were similar in CTL (Supplementary Video S7, online only) and ASD (Supplementary Video S8, online only), with diastolic vortices forming around the tricuspid valve leaflets in early diastole and accentuated with atrial systole followed by streaming toward the right ventricular outflow tract. In rTOF, systolic flow patterns were also similar to those of the other groups, but in diastole,

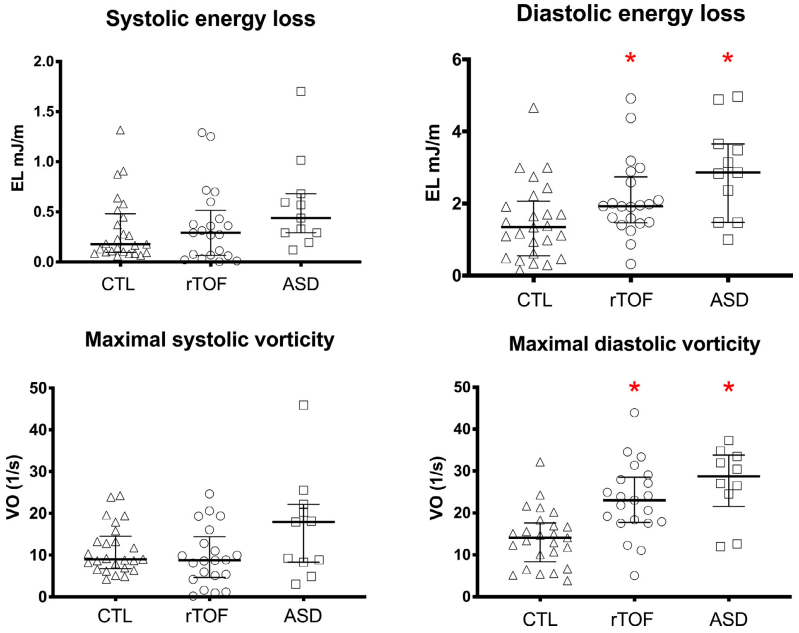

Fig. 3. Scatterplot of right ventricular flow energetics in the four-chamber view. Scatterplots of energy loss and vorticity with median (*thick line*) and quartiles (Q1–Q3, *thin line*). ASD = atrial septal defect; CTL = controls; EL = energy loss; rTOF = repaired tetralogy of Fallot; VO = vorticity. **p* Value < 0.05, ASD or rTOF versus CTL. †*p* Value < 0.05, rTOF versus ASD.

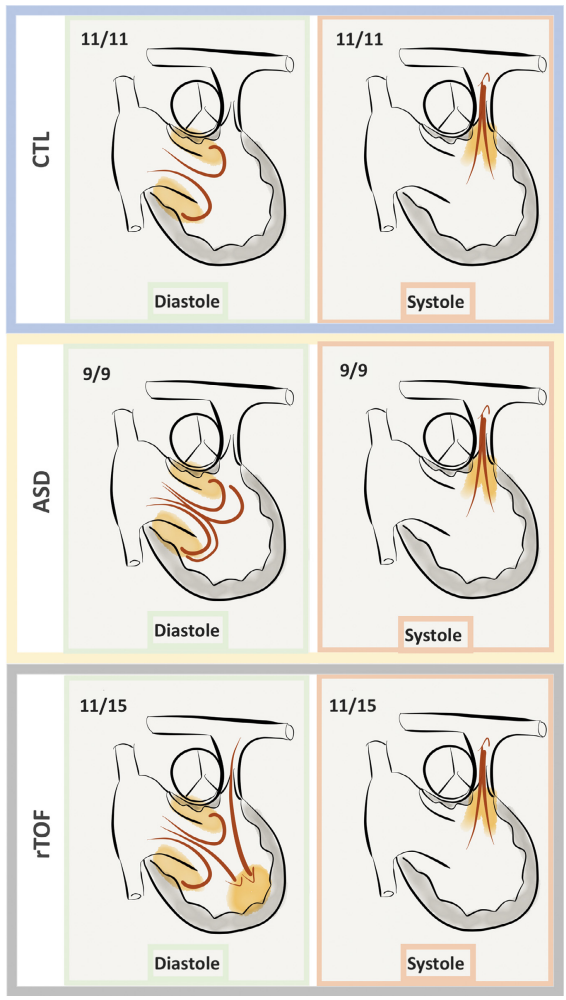

Fig. 4. Schematic of regions of high energy loss (*yellow shadowed areas*) as seen in the right ventricular three-chamber view. ASD = atrial septal defect; CTL = controls; rTOF = repaired tetralogy of Fallot.

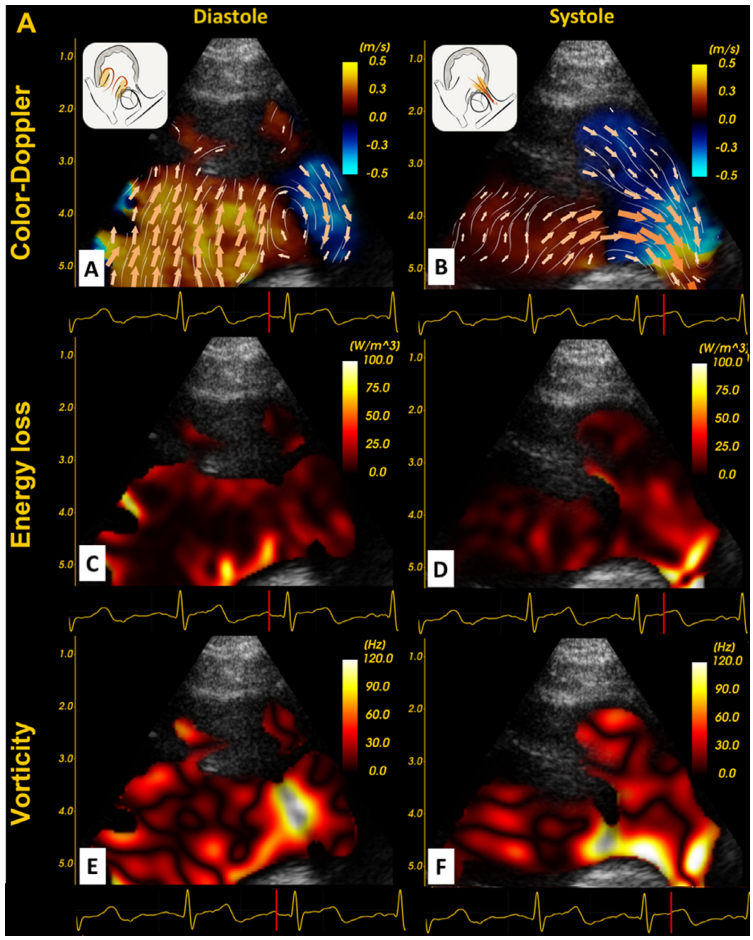

Fig. 5. Typical examples of right ventricle intracardiac velocities, energy loss and vorticity mapping in diastole and systole in controls (5A), patients with atrial septal defect (ASD) (5B) and patients with repaired tetralogy of Fallot (rTOF) (5C). The systolic and diastolic flow patterns were similar in CTL and ASD, with diastolic vortices forming around the tricuspid valve leaflets in early diastole (A and B, panel A) with corresponding areas of high energy loss and vorticity (A and B, panels C–E). In rTOF, systolic flow patterns were also similar to those of the other groups (A– C, panel B), but in diastole, regurgitant pulmonary flow collides with the tricuspid inflow, resulting in disorganized apical vortices (C, panel A, indicated by *white arrow*) with an additional area apical energy loss and vorticity (C, panels C and D, indicated by *white arrow*). The schematic in the upper left of each panel illustrates the imaging plane and areas of high EL in *orange.*

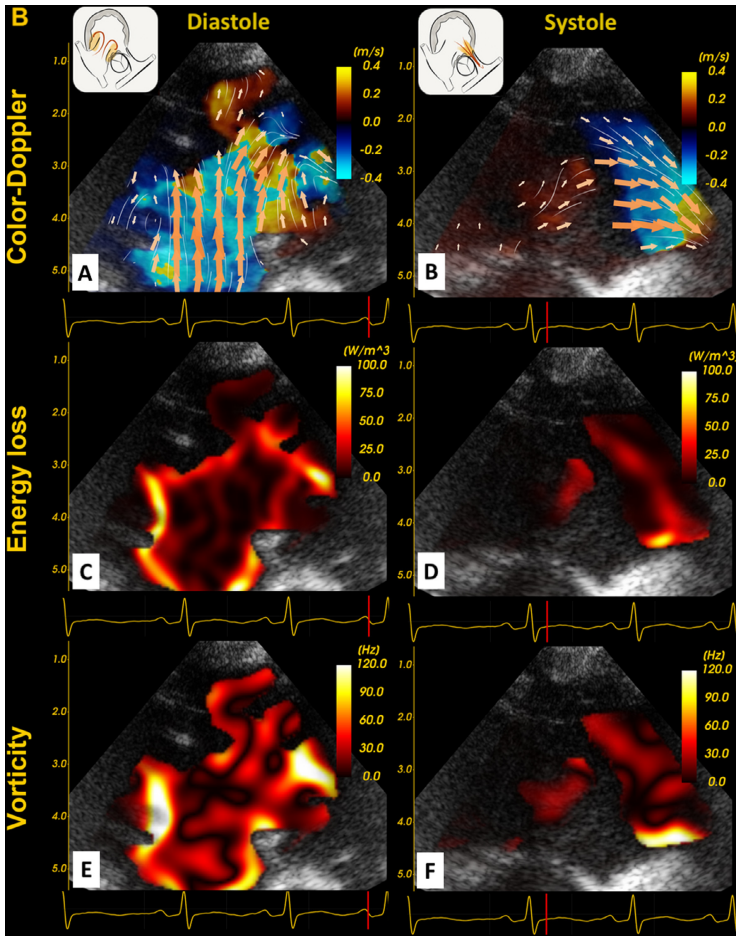

Fig. 5. Continued

regurgitant pulmonary flow collides with the tricuspid inflow, resulting in disorganized apical vortices (Supplementary Video S9, online only). The pattern of EL could also vary from beat to beat, as illustrated in Figure 6.

Inter- and intra-observer variability

Analysis of intra-observer variability revealed very good reproducibility for both diastolic and systolic EL measurements, with average systematic measurement

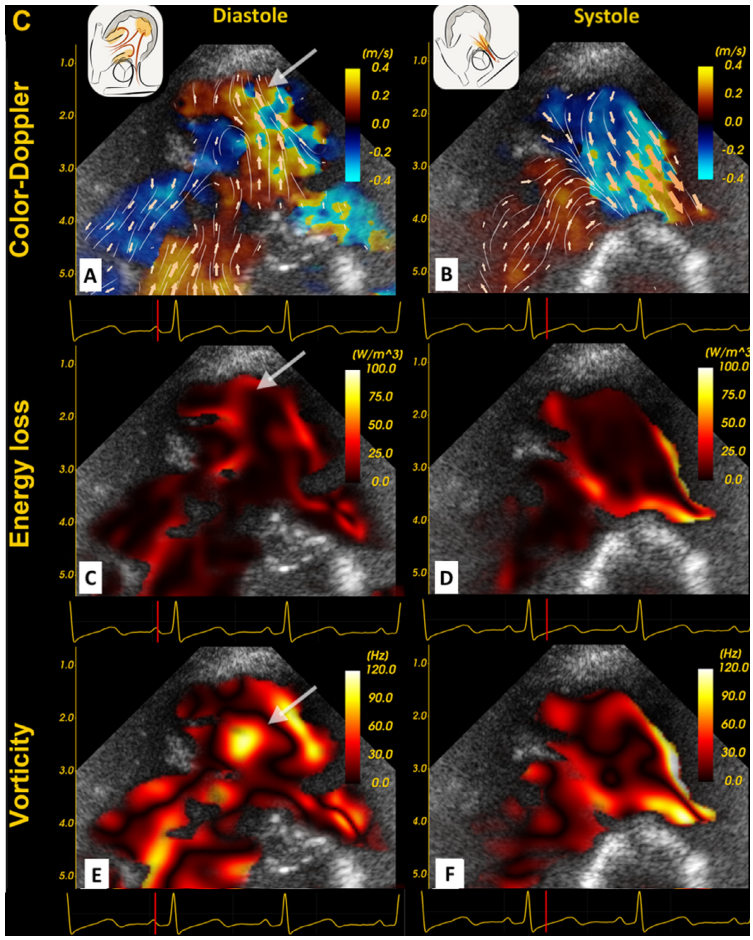

Fig. 5. Continued

errors of −0.1% and 0.0%, respectively, and very narrow limits of agreement, well within 5% variation. Analysis of inter-observer variability also revealed good reproducibility for both diastolic and systolic EL, with an average systematic error of 0.0% for both parameters and a narrow limit of agreement within 5% variation from the RV4C view (Fig. 7). The inter- and intra-observer variability was not determined for the RV3C view because this served to supply a qualitative measure, although findings were reviewed by co-authors (WM, SAN, LL, SF).

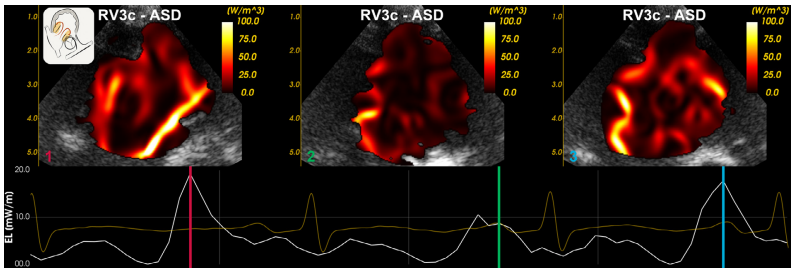

Fig. 6. Beat-to-beat variation of energy loss patterns. Energy loss mapping from a right ventricle three-chamber view revealing different patterns of energy loss from beat to beat in an example of a patient with ASD. RV3C = right ventricular three-chamber view; ASD = atrial septal defect.

DISCUSSION

In this study we compared cardiac blood flow energy losses between two groups with volume-loaded RVs and controls using high-frame-rate ultrasound imaging and blood speckle tracking. We studied the feasibility and reproducibility of blood speckle tracking and validated energy loss measurements. We described different blood flow dynamics and energetics in volume-loaded RVs compared with controls.

Although the EL parameter varied for different patient groups, it could also vary substantially because of changes in image plane and postprocessing (smoothing). Beat-to-beat variation in EL patterns could also be

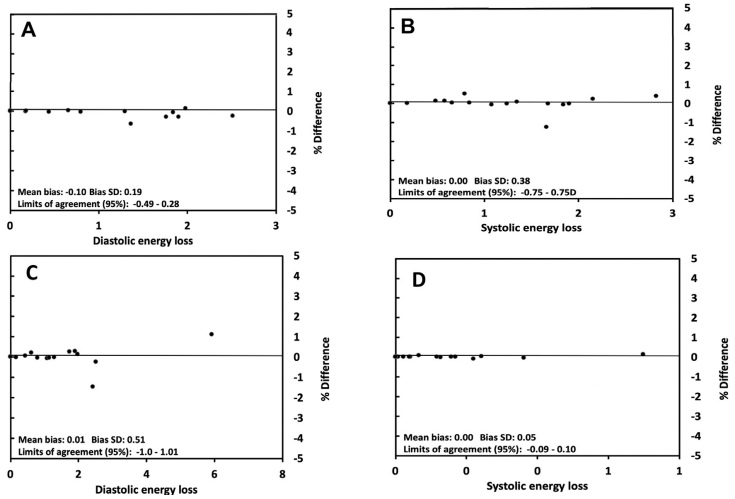

Fig. 7. Bland–Altman plots of intra-observer (A,B) and inter-observer (C, D) agreement. Intra-observer (A,B) and inter-observer (C,D) variability in diastolic and systolic energy loss. In these Bland–Altman plots, the *solid line* represents the average measurement error as a percentage. The calculated mean bias and limits of agreement are displayed in the lower left corner of each graph. The average error in measurement in all cases is well below 5%. SD = standard deviation.

seen and could stem from translational motion of the heart or slight variation of imaging planes (Fig. 6). Computer simulation analysis of the velocity and EL measurements in a ventricular model highlighted some determinants of measurement errors, among which the most important is the alignment with blood flow, but also post-processing settings (*e.g.,* smoothing). Because the postprocessing steps are not major sources of variability, as highlighted by excellent inter- and intraobserver variability, careful and consistent imaging technique become a very important prerequisite for useful and accurate quantitative measures such as energy loss and vorticity in 2-D views. The computer simulation analysis also revealed that diastolic EL was reliable when assessed from a 4CV, as we did here.

Our data indicate that volume-loaded RVs in both rTOF and ASD patients have higher energy losses in diastole compared with those in controls, without being different from each other. In diastole, energy loss occurred at the tricuspid valve leaflets for all groups. This can be understood from a fluid mechanics perspective by the mechanical EL as a result of sudden flow expansion, as it is thought to apply to EL in the ascending aorta of patients with aortic stenosis (Binter et al. 2017). In our study, this sudden flow expansion occurs in early diastole through the tricuspid valve and would be accentuated when the RV is dilated. These findings would support the notion that dilated RVs are less efficient than non-dilated RVs because more kinetic energy is lost during diastole. These findings are in keeping with earlier observations in volume-loaded RVs in a canine study finding reduced diastolic vortex strength and extent, which are quantitative vortical measures thought to correlate with kinetic energy (Pasipoularides et al. 2003).

Even though total diastolic EL was similar in both ASD and rTOF, the two groups exhibited different diastolic flow patterns. In all groups, the tricuspid leaflets were regions of disturbed flow and higher EL. In rTOF, however, an additional region of high EL is present in most cases at the RV apex, associated with colliding flow from the inflow and the PI. These abnormal flow patterns and energetics within the RV apex of rTOF may have effects on remodeling and function. Apical dysfunction has been found to preferentially affect rTOF compared with equally volume-loaded ASD and healthy controls (van der Ven et al. 2019).

In systole, EL did not differ between the groups. This finding was surprising because more energy loss would be expected in rTOF and ASD as the RV stroke volume is increased in these patients compared with controls. The absence of a difference could be attributed to the mostly out-of-plane direction of blood flow in systole when the RV is imaged from the RV4C view. This stems from a well-known and important limitation of 2-D echocardiography in imaging the RV (Haddad et al. 2008).

Contrary to previous studies on flow characteristics and energy loss in children, we could not find a significant correlation between EL and BSA (Hayashi et al. 2015). This explains why EL is expressed as an unindexed measurement in our results. Although systolic EL and diastolic EL did significantly correlate with age in rTOF and CTL, the distribution of EL, especially in older patients, is very wide, and this relationship was not observed in the ASD group. A generalizable conclusion with such data would require more patients.

In addition, the velocity measurements we presented were obtained by blood speckle tracking based on high-frame-rate echocardiography without flow regularization and thus are free of any regularizing assumptions (*e.g.,* without out-of-plane flow). As opposed to techniques such as VFM, wall velocities are not needed to derive any component of the velocity of the blood. The trade-off is dealing with regions of signal dropout as in color Doppler. Two-dimensional energy loss measurements change for physiologic reasons, but also because of variations in the imaging plane and postprocessing settings. As seen from the computer simulation analysis, the wall filter had an overall dampening effect leading to some underestimation of EL, but also changed the curve shape in mid-to-late diastole. The latter could potentially be masking contributing secondary flow patterns and requires further elucidation.

The effect of flow patterns on cardiac morphology and function is complex (Pasipoularides 2012, 2013). Increased fluid shear stress is thought to affect endocardial signaling pathways involved in cardiac remodeling and function (Tseng et al. 1995; Ueba et al. 1997). Disturbances in flow dynamics have been proposed to precede morphologic and functional changes (Pedrizzetti et al. 2015). To study this in the repaired tetralogy of Fallot population, longitudinal changes in flow dynamics and their relationship to RV wall mechanics could be studied. This could provide novel insights into the relationship between flow dynamics and RV remodeling. Energy-based imaging biomarkers are increasingly becoming available based on advancements in MRI and ultrasound technologies (Hirtler et al. 2016; Azarine et al. 2019). Their clinical utility will have to be determined based on longitudinal studies and outcome data. These flow dynamics could reflect RV dysfunction at an earlier, adaptive stage after tetralogy of Fallot repair that would otherwise have been missed using the current imaging biomarkers used. The lack of difference between ASD and rTOF could be related to the small sample size but also reveals the additional value of not only quantitative data of EL and VO, but also qualitative visualization tools allowing differentiation of flow

dynamics between these two groups of volume-loaded RVs. The lack of difference in systolic EL between the groups was a surprising finding. This could again be related to the small sample volume but is more likely explained by the fact the measurements were obtained from a RV4C view, in which systolic flows from the apex to the outlet are largely out of plane. This further indicates the importance of 3-D methods, especially in the setting of complex geometry of the RV.

LIMITATIONS

There were several limitations to this study. The first is the small sample size. The availability of the blood speckle tracking imaging technique only for higher-frequency probes precluded inclusion of older and larger children. This study is to be considered a pilot study hinging on feasibility, validation and potential clinical application of this novel imaging technology.

Acquisition of an RV3C view proved challenging, particularly in healthy controls, in whom the RV is not dilated. However, the RV4C view was more feasible, and we excluded no images in this view. On the basis of results from the validation, we found that it was important to compare images with the same imaging plane to obtain reliable EL and vorticity measurements. Therefore, we chose to exclude 22 of 57 RV3C views with slight differences in angulation. This limitation was compounded by the absence of real-time EL visualization on the modified research scanner used for this study. This meant that quality control was performed offline with no possibility of optimization. As with other Doppler-based techniques of blood flow measurements, multiple acquisitions are analyzed to optimize alignment with the blood flow direction. Similarly, velocities obtained by blood speckle tracking based on high-frame-rate echocardiography will benefit from real-time visualization and analysis.

Another limitation is the 2-D nature of the imaging technique, thus not accounting for through-plane variations. This is highlighted in the systolic EL scatterplots with many values near zero when assessed in the RV4C view (Fig. 2). Because of the crescent shape of the RV, the imaging plane of the RV4C view is nearly perpendicular to the direction of systolic flow toward the outflow tract so that the through-plane component of systolic RV flow is lost.

Calculations of EL are dependent on smoothing parameters. We used the same parameters across our analysis to avoid this potential source of error. However, awareness of this limitation is important for longitudinal studies and for comparison of patient groups in the future.

CONCLUSIONS

Diastolic energy losses in the dilated RVs of patients with ASD and rTOF were similar but significantly higher than in healthy controls, whereas losses were similar in systole. This may support the notion that the dilated RV is less efficient as more energy is lost in diastole (Jeong et al. 2015). In addition, we have found a unique pattern of diastolic energy loss in rTOF within the RV apex, which was not present in the other groups. Colliding jets of pulmonary regurgitation and tricuspid inflow at the RV apex in rTOF are at the origin of this specific pattern. Even though the clinical significance of our findings is not yet clear, the study of disturbances in RV flow and energy loss patterns may provide additional insights into the origin of apical dysfunction seen in the dilated RV of rTOF patients but not ASD. Because no relationship between RV flow dynamics and RV function or mechanics was determined, the link between the two is speculative.

The use of blood speckle tracking for blood flow EL and vorticity quantification proved feasible, with low inter- and intra-observer variability. However, computer simulation validation in this study highlights important aspects related to image acquisition and postprocessing, which can affect the accuracy of the measured blood speckle velocities and EL. Awareness of these limitations is important for future studies and will likely be minimized by the availability of real-time visualization and analysis. High-frame-rate ultrasound and blood speckle tracking are promising new tools in gaining a further understanding of flow dynamics and energetics and their effect on cardiac remodeling and function.

Acknowledgments—We acknowledge the contributions of Guillermo Larios, Wei Hui, Alex Cotoi and Cameron Slorach. We also thank Øyvind Salvesen for advice on the choice of statistical methods.

Conflict of interest disclosure—Exclusive use of a modified GE Vivid E9 was provided by GE during the study period at both institutions. W. M. received funding for this project from the Centre for Innovative Ultrasound Solutions. S.A.N. has funding to this project from the Joint Research Committee between St. Olav's Hospital and the Faculty of Medicine, NTNU, which manages research funding from the Central Norway Regional Health Authority (Reference 2014/23203). Technical development was funded by the Research Council of Norway under RCN 230455 and RCN 237887, the latter through the Centre for Innovative Ultrasound Solutions.

L.L. has a part-time consultancy at GE Vingmed Ultrasound. The other authors have no conflicts of interest to declare.

SUPPLEMENTARY MATERIALS

Supplementary material associated with this article can be found in the online version at doi:10.1016/j.ultrasmedbio.2021.02.004.

REFERENCES

Akiyama K, Maeda S, Matsuyama T, Kainuma A, Ishii M, Naito Y, Kinoshita M, Hamaoka S, Kato H, Nakajima Y, Nakamura N, Itatani K, Sawa T. Vector flow mapping analysis of left ventricular energetic performance in healthy adult volunteers. BMC Cardiovasc Disord 2017;17:21. Erratum: BMC Cardiovasc Disord 2017;17:172.

Azarine A, Garcon P, Stansal A, Canepa N, Angelopoulos G, Silvera S, Sidi D, Marteau V, Zins M. Four-dimensional flow MRI: Principles and cardiovascular applications. Radiographics 2019;39:632–648.

Binter C, Gotschy A, Sündermann SH, Frank M, Tanner FC, Lüscher TF, Manka R, Kozerke S. Turbulent kinetic energy assessed by multipoint 4-dimensional flow magnetic resonance imaging provides additional information relative to echocardiography for the determination of aortic stenosis severity: Clinical perspective. Circ Cardiovasc Imaging 2017;10 e005486.

Dragulescu A, Grosse-Wortmann L, Redington A, Friedberg MK, Mertens L. Differential effect of right ventricular dilatation on myocardial deformation in patients with atrial septal defects and patients after tetralogy of Fallot repair. Int J Cardiol 2013;168:803–810.

Dragulescu A, Friedberg MK, Grosse-Wortmann L, Redington A, Mertens L. Effect of chronic right ventricular volume overload on ventricular interaction in patients after tetralogy of Fallot repair. J Am Soc Echocardiogr 2014;27:896–902.

Fadnes S, Wigen MS, Nyrnes SA, Lovstakken L. In vivo intracardiac vector flow imaging using phased array transducers for pediatric cardiology. IEEE Trans Ultrason Ferroelectr Freq Control 2017;64:1318–1326.

Fogel MA, Sundareswaran KS, De Zelicourt D, Dasi LP, Pawlowski T, Rome J, Yoganathan AP. Power loss and right ventricular efficiency in patients after tetralogy of Fallot repair with pulmonary insufficiency: Clinical implications. J Thorac Cardiovasc Surg 2012;143:1279–1285.

Haddad F, Hunt SA, Rosenthal DN, Murphy DJ. Right ventricular function in cardiovascular disease: Part I. Anatomy, physiology, aging, and functional assessment of the right ventricle. Circulation 2008;117:1436–1448.

Hayashi T, Itatani K, Inuzuka R, Shimizu N, Shindo T, Hirata Y, Miyaji K. Dissipative energy loss within the left ventricle detected by vector flow mapping in children: Normal values and effects of age and heart rate. J Cardiol 2015;66:403–410.

Hirtler D, Garcia J, Barker AJ, Geiger J. Assessment of intracardiac flow and vorticity in the right heart of patients after repair of tetralogy of Fallot by flow-sensitive 4 D MRI. Eur Radiol 2016;26:3598–3607.

Jeong D, Anagnostopoulos PV, Roldan-Alzate A, Srinivasan S, Schiebler ML, Wieben O, François CJ. Ventricular kinetic energy may provide a novel noninvasive way to assess ventricular performance in patients with repaired tetralogy of Fallot. J Thorac Cardiovasc Surg 2015;149:1339–1347.

Nakashima K, Itatani K, Kitamura T, Oka N, Horai T, Miyazaki S, Nie M, Miyaji K. Energy dynamics of the intraventricular vortex after mitral valve surgery. Heart Vessels 2017;32:1123–1129.

Nyrnes SA, Fadnes S, Wigen MS, Mertens L, Lovstakken L. Blood speckle tracking based on high frame rate ultrasound imaging in pediatric cardiology. J Am Soc Echocardiogr 2020;33 493−503.e5.

Pasipoularides A. Diastolic filling vortex forces and cardiac adaptations: Probing the epigenetic nexus. Hell J Cardiol 2012;53:458–469.

Pasipoularides A. Evaluation of right and left ventricular diastolic filling. J Cardiovasc Transl Res 2013;6:623–639.

Pasipoularides A, Shu M, Shah A, Womack MS, Glower DD. Diastolic right ventricular filling vortex in normal and volume overload states. Am J Physiol Heart Circ Physiol 2003;284:H1064–H1072.

Pedrizzetti G, Martiniello AR, Bianchi V, D'Onofrio A, Caso P, Tonti G. Cardiac fluid dynamics anticipates heart adaptation. J Biomech 2015;48:388–391.

Shibata M, Itatani K, Hayashi T, Honda T, Kitagawa A, Miyaji K, Ono M. Flow energy loss as a predictive parameter for right ventricular deterioration caused by pulmonary regurgitation after tetralogy of Fallot repair. Pediatr Cardiol 2018;39:731–742.

Tseng H, Peterson TE, Berk BC. Fluid shear stress stimulates mitogen-activated protein kinase in endothelial cells. Circ Res 1995;77:869–878.

Ueba H, Kawakami M, Yaginuma T. Shear stress as an inhibitor of vascular smooth muscle cell proliferation. Arterioscler Thromb Vasc Biol 1997;17:1512–1516.

Van Cauwenberge J, Lovstakken L, Fadnes S, Rodriguez-Morales A, Vierendeels J, Segers P, Swillens A. Assessing the performance of ultrafast vector flow imaging in the neonatal heart via multiphysics modeling and *in vitro* experiments. IEEE Trans Ultrason Ferroelectr Freq Control 2016;63:1772–1785.

van der Ven JPG, van den Bosch E, Bogers AJCC, Helbing WA. Current outcomes and treatment of tetralogy of Fallot. F1000Research 2019;8:1530.

Wigen MS, Fadnes S, Rodriguez-Molares A, Bjastad T, Eriksen M, Stensæth KH, Støylen A, Lovstakken L. 4-D intracardiac ultrasound vector flow imaging—Feasibility and comparison to phase-contrast MRI. IEEE Trans Med Imaging 2018;37:2619–2629.

Zhong Y, Liu Y, Wu T, Song H, Chen Z, Zhu W, Cai Y, Zhang W, Bai W, Tang H, Rao L. Assessment of left ventricular dissipative energy loss by vector flow mapping in patients with end-stage renal disease. J Ultrasound Med 2016;35:965–973.

PAPER 2

CJC Pediatric and Congenital Heart Disease 1 (2022) 213–218

Original Article

Pulmonary Hypertension in Children is Associated With Abnormal Flow Patterns in the Main Pulmonary Artery as Demonstrated by Blood Speckle Tracking

Wadi Mawad, MD,[a,b,c] Solveig Fadnes, MSc, PhD,[b,d] Lasse Løvstakken, MSc, PhD,[b] Matthew Henry, MD,[a] Luc Mertens, MD, PhD,[a] and Siri Ann Nyrnes, MD, PhD[b,e]

[a] *Division of Cardiology, Department of Paediatric, The Hospital for Sick Children, University of Toronto, Toronto, Ontario, Canada*

[b] *Department of Circulation and Medical Imaging, Norwegian University of Science and Technology (NTNU), Trondheim, Norway*

[c] *Department of Paediatrics, Montreal Children's Hospital, McGill University Health Centre, Montréal, Québec, Canada*

[d] *Moere & Romsdal Hospital Trust, Division of Aalesund Hospital, Department of Pediatrics, Aalesund, Norway*

[e] *Children's Clinic, St. Olavs University Hospital, Trondheim, Norway*

ABSTRACT

Background: Paediatric pulmonary arterial hypertension (PAH) is characterized by increased pulmonary vascular resistance resulting in increased pulmonary artery (PA) and right ventricular pressure (RV). This is associated with disturbed flow dynamics in the PA and RV that are not well characterized. We aimed to compare flow dynamics in children with PAH compared with healthy controls using blood speckle tracking echocardiography.

Methods: Patients <10 years of age with PAH and healthy controls were included. We examined flow dynamics in the main PA (MPA) and right ventricle based on acquisition blood speckle tracking images obtained from the RV and PA. Qualitative and quantitative analyses were performed.

Results: Eighteen subjects were included in each group. A diastolic vortex in the MPA was identified in 16 of the patients with PAH, but not in controls. Significantly higher MPA systolic (4.84 vs 2.42 mW/m; $P = 0.01$) and diastolic (0.69 vs 0.14 mW/m; $P = 0.01$) energy loss, as well as increased vector complexity (systole: 0.21 vs 0.04, $P = 0.003$; diastole: 0.13 vs 0.05, $P = 0.04$) and diastolic vorticity (15.2 vs 4.4 Hz; $P = 0.001$), were noted in PAH compared with controls.

Conclusion: This study demonstrates the presence of abnormal flow patterns in the MPA with diastolic vortex formation in most patients with PAH. This diastolic vortex likely results from reflected waves from the distal pulmonary bed. Our data indicate that the diastolic vortex could potentially be used in the diagnosis of PAH. The clinical significance of the energy loss findings warrants further investigation in a larger cohort of patients with PAH.

RÉSUMÉ

Contexte : L'hypertension artérielle pulmonaire (HTAP) pédiatrique est caractérisée par une résistance vasculaire pulmonaire accrue qui donne lieu à une augmentation de la pression dans l'artère pulmonaire (AP) et dans le ventricule droit (VD). Ce phénomène s'accompagne de perturbations de la dynamique des débits dans l'AP et le VD, qui n'ont pas encore été bien caractérisées. Nous avons cherché à comparer la dynamique des débits chez des enfants atteints d'HTAP avec celle de témoins en bonne santé en utilisant l'échocardiographie de suivi des marqueurs acoustiques du sang.

Méthodologie : Des patients de moins de 10 ans atteints d'HTAP et des témoins en bonne santé ont participé à l'étude. La dynamique des débits du tronc pulmonaire (TP) et du ventricule droit a été examinée à partir d'images de suivi des marqueurs acoustiques du sang de l'AP et du VD. Des analyses qualitatives et quantitatives ont aussi été réalisées.

Résultats : Dix-huit sujets ont été inclus dans chacun des groupes. Un vortex diastolique du TP a été observé chez 16 des patients atteints d'HTAP, mais n'était présent chez aucun des témoins. Une perte d'énergie significativement plus élevée dans le TP a été notée pour la systole (4,84 *vs* 2,42 mW/m; $P = 0,01$) et la diastole (0,69 *vs* 0,14 mW/m; $P = 0,01$) des patients atteints d'HTAP; de plus, une complexité vectorielle accrue (systole : 0,21 *vs* 0,04, $P = 0,003$; diastole : 0,13 *vs* 0,05, $P = 0,04$) et une vorticité diastolique accrue (15,2 *vs* 4,4 Hz; $P = 0,001$) ont été notées chez les patients atteints d'HTAP comparativement aux témoins.

Conclusion : Notre étude fait état d'un profil circulatoire anormal caractérisé par la formation d'un vortex diastolique dans le TP chez la plupart des patients atteints d'HTAP. Ce vortex découle probablement d'ondes réfléchies du lit pulmonaire distal. Les données que nous avons obtenues indiquent que le vortex diastolique pourrait possiblement être utilisé dans le diagnostic de l'HTAP. Par contre, la signification clinique des résultats concernant la perte d'énergie nécessite d'autres études auprès d'une cohorte plus importante de patients atteints d'HTAP.

Received for publication July 3, 2022. Accepted September 1, 2022.

Corresponding author: Dr Wadi Mawad, McGill University Health Centre, B04.2656, 1001 Décarie Boulevard, Montreal, Québec H4A 3J1, Canada. Tel.: +1-514-623-9234; fax: +1-514-412-4273.
E-mail: wadi.mawad@mcgill.ca

https://doi.org/10.1016/j.cjcpc.2022.09.001

Paediatric pulmonary artery hypertension (PAH) is defined by increased pulmonary artery pressure and pulmonary vascular resistance (PVR) resulting in increased right ventricular pressure loading. The impact of PAH on right ventricular (RV) morphologic and functional parameters has been extensively studied, whereas there is limited data available on the changes in flow dynamics associated with PAH.[1-3] Four-dimensional flow magnetic resonance imaging (4D-flow MRI) has been used for qualitative and quantitative flow assessment in PAH. Flow characteristics were shown to differ significantly between patients with PAH and healthy controls (CTL).[4] A decrease in peak systolic vorticity (VO) in the main (MPA) and right pulmonary artery (RPA) was associated with increased PVR and was used in a model to noninvasively predict PVR.[5] Although 3-dimensional assessment of flow is a major advantage of 4D-flow MRI, it comes at the expense of low temporal resolution. This limitation is more significant in children as they have higher heart rates. Blood speckle tracking (BST) echocardiography is a 2-dimensional technique that allows blood flow visualization at high temporal resolution.[6] This allows the study of more short-lived flow events such as early diastolic vortex formation in the MPA. The aim of the current study was to use BST to (1) qualitatively describe MPA flow patterns in patients with PAH compared with healthy CTL and (2) compare quantitative flow parameters including energy loss (EL), VO, and vector complexity (VC) in the MPA and RV between patients with PAH and CTL. The relationship between flow parameters, RV functional parameters, and RPA distensibility (RPA_D) will be evaluated.

Materials and Methods

Between December 2015 and December 2020, we included patients from the Hospital for Sick Children in Toronto, Canada, and St. Olav's Hospital in Trondheim, Norway, who were <10 years of age and who had PAH as defined by an estimated mean pulmonary artery pressure measured by echocardiography exceeding 25 mm Hg as well as healthy CTL matched for age and sex. The study was approved by both institutions' ethics review boards, and informed consent was obtained before enrolment. A Vivid E9 or E95 system (GE Vingmed Ultrasound, Horten, Norway) with research software enabling image acquisitions with a frame rate equal to the pulse repetition frequency, that is, in the kHz range, was combined with the B-mode modality. We acquired a short-axis view of the MPA and RV centred apical views. At least 2 cardiac cycles were recorded with commercially available ultrasound probes including the 6S and 12S phased-array probes (GE Healthcare, Milwaukee, WI). Storage of IQ (in-phase and quadrature) data was done to enable full offline postprocessing and BST analysis. Dedicated in-house software analysis tools were used (PyUSview; NTNU, Trondheim, Norway). Temporal and spatial smoothing parameters were kept identical for all analyses (temporal smoothing = 40 milliseconds, Gaussian spatial smoothing = 5×5 mm^2). The MPA flow field and RV were segmented, and VO, EL, and vector complexity were quantified in the MPA and RV. The calculation of EL and its validation and variability have been previously described by our group.[7,8] The definition of VO as calculated based on BST has been previously published.[7] Vector complexity has been described using other methods.[9] This parameter describes the flow complexity by quantifying the spread of the velocity vectors. It is defined as $1 - r$, where r is the vector concentration as defined by Pedersen et al.[10] The measurements range from 0, where all velocity vectors are in the same direction, to 1, indicating vectors in multiple different directions. It can be thought of as a measure of flow laminarity, with laminar flow having vector complexity approaching 0 and turbulent flow approaching 1. Conventional echocardiographic parameters were obtained based on standard clinical methodology. RPA distensibility was measured as the percentage difference between the maximal and minimal RPA diameters in a parasternal short-axis view (Fig. 1).

Statistical analysis

Comparison between 2 groups was done using the Mann-Whitney *U* test with a *P* value of <0.05, which was

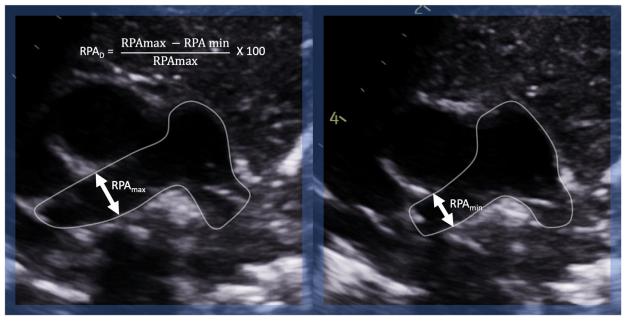

Figure 1. Right pulmonary artery distensibility (RPA_D) index measurement in a parasternal short-axis view of the pulmonary arteries. max, maximal measurement; min, minimum measurement.

Table 1. Demographic and echocardiographic data

	PAH (n = 18)	CTL (n = 18)
Male (%)	50	44
Age (y)	2.8 (0.5-4.2)	3.2 (0.5-4.8)
Height (m)	110 (89-125)	99 (80-122)
Weight (kg)	18.9 (15.4-32.3)	15.8 (10.9-25.6)
BSA (m^2)	0.75 (0.65-0.81)	0.66 (0.50-0.94)
HR (BPM)	86 (75-108)	97 (81-110)
MPA z-score	2.77 (1.62-3.26)	−0.20 (−1.74 to 1.01)*
RPA distensibility (%)	23.9 (12.7-31.7)	24.5 (17.2-30.4)
RV systolic pressure (mm Hg)	82 (42-105)	
RV systolic pressure (% of systemic)	79 (46-104)	
TAPSE z-score	−1.30 (−3.83 to 6.80)	0.02 (−1.18 to 4.71)*
RVFAC (%)	33.5 (30-38)	37 (36-40)*
MPA		
Diastolic MPA vortex	16/18	0/18
MPA diastolic vortex duration (ms)	150 (121-171)	
Avg. VC_S	0.21 (0.08-0.42)	0.04 (0.02-0.06)*
Avg. VC_D	0.13 (0.06-0.30)	0.05 (0.02-0.16)*
Avg. EL_S (mW/m)	4.84 (2.16-11.67)	2.42 (1.11-3.86)*
Avg. EL_D (mW/m)	0.69 (0.28-2.17)	0.14 (0.03-0.39)*
Avg. VO_S (Hz)	17.1 (15.8-21.6)	27.7 (20.6-35.1)
Avg. VO_D (Hz)	15.2 (11.1-20.9)	4.4 (0.2-8.4)*
RV		
Avg. VC_S	0.27 (0.12-0.42)	0.13 (0.09-0.28)*
Avg. VC_D	0.27 (0.15-0.34)	0.12 (0.09-0.16)*
Avg. EL_S (mW/m)	1.54 (0.32-2.67)	0.68 (0.25-1.12)
Avg. EL_D (mW/m)	4.08 (2.19-7.20)	2.87 (1.44-4.86)
Avg. VO_S (Hz)	22.8 (17.9-27.3)	22.1 (18.3-27.5)
Avg. VO_D (Hz)	25.1 (18.5-31.3)	24.2 (17.8-28.2)

BSA, body surface area; BPM, beats per minute; CTL, controls; EL_D, diastolic energy loss; EL_S, systolic energy loss; FAC, fractional area change; HR, heart rate; MPA, main pulmonary artery; PAH, pulmonary arterial hypertension; RPA, right pulmonary artery; RV, right ventricle; RVFAC, right ventricular fractional area change; TAPSE; tricuspid annular plane systolic excursion; VC_D, diastolic vector complexity; VC_S, systolic vector complexity; VO_D, diastolic vorticity; VO_S, systolic vorticity.

* When P value <0.05; values expressed as median, quartiles (Q1-Q3).

considered statistically significant. Correlations were tested using Spearman's rank test. The analyses were conducted using GraphPad Prism 8 (GraphPad Software, La Jolla, CA).

Results

Demographic and hemodynamic characteristics are summarized in Table 1. In total 36 subjects were included, 18 patients with PAH and 18 CTL. All patients with PAH had idiopathic PAH and no history of previous cardiac surgery. The majority (13 of 18) were receiving antipulmonary hypertensive therapy (sildenafil: 4; sildenafil + oxygen: 8; sildenafil + bosentan + macitentan + selexipag: 1). There were no significant differences in baseline characteristics between the groups. The PAH group had a larger MPA size and lower tricuspid annular systolic excursion and right ventricular fractional area change.

Qualitatively, both groups had laminar flow in the MPA in systole. A diastolic vortex in the MPA was observed in 16 of 18 patients with PAH, whereas it was not present in any of the CTL. The diastolic vortex was first observed in the RPA origin in 6 of 16 patients with PAH and in the MPA in 10 of 16 patients. All vortices had a clockwise rotation and dissipated as they migrated from their origin towards the pulmonary valve. In CTL diastolic flow remains laminar without any detectable rotation. Figure 2 shows typical examples from each group illustrating the flow patterns.

Quantitative flow parameters are shown in Figure 3. The rate of EL in the MPA was higher in PAH in systole (4.84 vs 2.42 mW/m) and diastole (0.69 vs 0.14 mW/m). Vector complexity was also higher in systole (0.21 vs 0.04) and diastole (0.13 vs 0.05) in PAH compared with CTL. Vector complexity did not correlate with MPA z-score ($r = 0.37$, $P = 0.15$). Diastolic VO was higher in PAH compared with CTL (15.2 vs 4.4 Hz). In the RV, diastolic VC was higher in PAH compared with CTL, but RV EL and RV VO were not statistically significant between the groups.

The vortex duration did not correlate significantly with RV functional parameters (tricuspid annular systolic excursion: $r = 0.22$, $P = 0.40$; right ventricular fractional area change: $r = -0.45$, $P = 0.11$), with right ventricular systolic pressure ($r = -0.01$, $P = 0.11$) or pulmonary artery dimensions (RPA_D: $r = 0.17$, $P = 0.51$; MPA z-score: $r = -0.21$, $P = 0.41$). MPA EL did not correlate with any RV functional parameters or any RV flow parameters (RV EL, VO, and VC). The quantitative flow parameters in the MPA and RV did not correlate significantly with right ventricular systolic pressure.

When comparing the RPA_D index (Fig. 1), no significant differences were noted between the groups (CTL: 23.9% vs PAH: 24.15%). In patients with PAH, diastolic MPA EL negatively correlated with RPA_D ($r = -0.48$; $P = 0.04$) and positively correlated with MPA z-score ($r = 0.68$; $P = 0.03$) (Fig. 4).

Discussion

Using high-frame-rate BST echocardiography, our data demonstrate important qualitative and quantitative differences in flow dynamics, particularly in the MPA in children with PAH compared with CTL. Interestingly, in the RV, the only difference noted was vector complexity in diastole, with no differences in systole.

The most important finding of our study was the presence of an MPA diastolic vortex in most patients with PAH, which is a distinguishing flow feature in patients with PAH. Abnormal diastolic flow in the MPA and in the pulmonary branches can often be observed using conventional color Doppler and is thought to represent reflection of pulmonary artery flow related to high distal resistance. The advantage of BST technology is that it allows better visualization of the vortices and it allows quantification of flow parameters. In cardiac MRI studies, it was previously suggested that diastolic vortex duration correlated with pulmonary artery pressures,[11] but this could not be demonstrated in our study. A possible explanation is the higher temporal resolution of BST compared with MRI with the echocardiographic data likely to be more physiological. Alternatively, the difference could

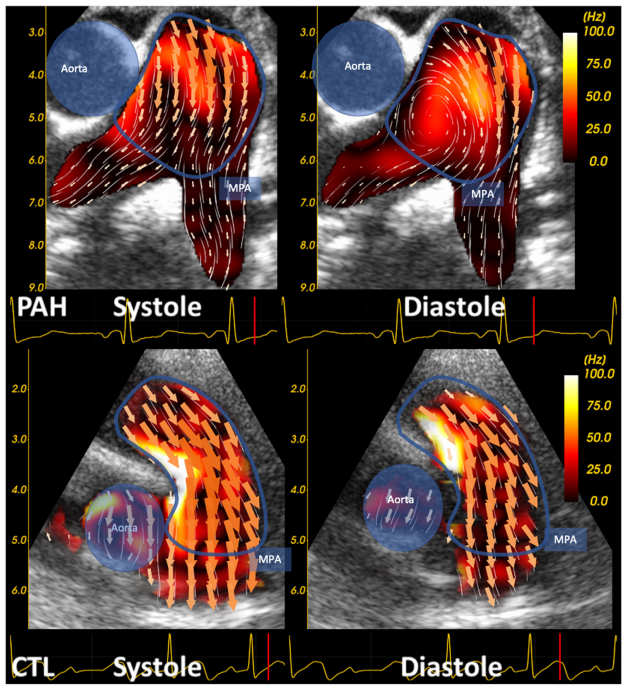

Figure 2. Typical main pulmonary artery (MPA) flow patterns as shown by high-frame-rate ultrasound imaging and blood speckle tracking. The vorticity map is seen in the background. CTL, control; PAH, pulmonary arterial hypertension.

potentially be explained by the 2-dimensional nature of our echocardiographic acquisitions, which may not capture through-plane motion of the vortices, thus leading to an underestimation of their duration compared with a 3-dimensional imaging modality such as MRI. It was interesting to observe that, even in patients' milder PAH with RV systolic pressure less than half-systemic, a diastolic MPA vortex could be observed. Although this study could not validate the value of vortex duration as a noninvasive marker of PAH severity, the use of vortex detection as a diagnostic sign for PAH requires further validation. Some ventricular flow disturbances have been shown to precede geometric remodelling.[12] If this also applies to MPA flow, the value of these novel flow parameters is promising although this study is not geared to demonstrate this.

When quantifying flow parameters, we could find important differences between the groups, especially in the MPA with higher MPA EL and higher VC in patients with PAH vs CTL. The higher EL difference could potentially be explained by a loss of kinetic energy in the blood flow in the form of thermal energy because of friction forces related to the more complex flow patterns in the MPA. Our data demonstrate that the MPA flow was more complex with wider spread of vector directions, suggested by the higher vector complexity. The vortices in the MPA differ from an energetic perspective from the ones observed in the ventricles where they often serve as conservers of kinetic energy from the diastolic to systolic phase. The diastolic vortex observed in most PAH contributes to increased EL contributing to inefficiencies in the pulmonary arterial circulation.

Vector complexity, which is a flow parameter reflecting the spread of the direction of the velocity vector fields,[9] shows significantly higher values in the MPA and RV of the PAH group compared with CTL. This reflects the less laminar flow occurring in PAH both in systole and diastole. Although we did not observe decreased VO in systole as reported previously,[3] VC did show differences between the groups. This is perhaps because the VC parameter is more reflective of the nonlaminarity of flow and less depended on velocities as would EL and VO. This flow metric could also illustrate the

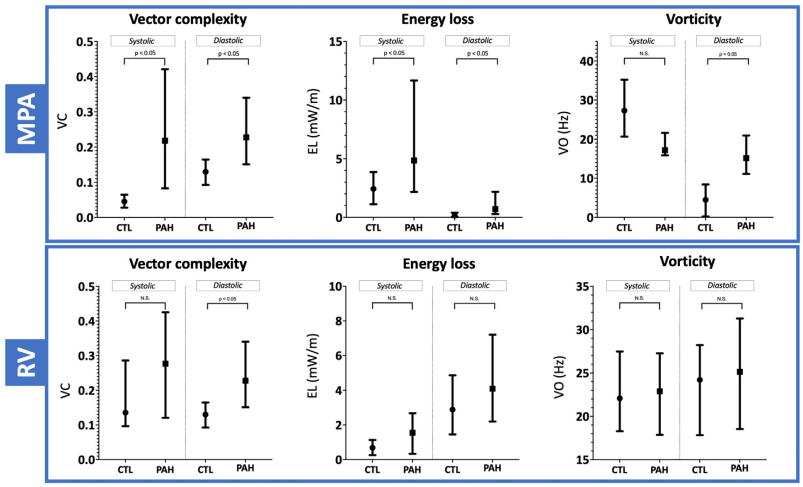

Figure 3. Quantitative flow parameters in the main pulmonary artery (MPA) and right ventricle (RV). Values expressed as median, quartiles (Q1-Q3). CTL, control; EL, energy loss; N.S., not significant; PAH, pulmonary arterial hypertension; VC, vector complexity; VO, vorticity.

systolic-diastolic coupling of flow parameters, where a less laminar, rotating diastolic vortex in the MPA will lead to less laminar flow in systole as well.

In PAH, MPA diastolic EL correlated negatively with RPA_D and positively with MPA z-score, whereas no such correlations were found in CTL. These findings are in favour of increased vascular stiffness as a more dilated and less distensible pulmonary arterial system in PAH provides less elastic recoil to continue propelling blood forward in diastole and predisposes it to circular, more complex flow patterns with higher energy losses. Although the literature is sparse, the role of such a measurement has been shown to be valuable in humans[13-16] and dogs[17,18] with PAH as an additional noninvasive marker of pulmonary arterial stiffness. The combination of blood flow quantification with noninvasive markers of pulmonary arterial stiffness gives more insights into the particularities of the RV-PA unit function in PAH.

Study limitations

There are several limitations to this study. The first is the small sample size. The availability of the BST imaging technique only for higher frequency probes precluded inclusion of older and bigger children, which limited recruitment. The study also suffers from the lack of contemporaneous invasive measurements of PVR, MPA pressures to relate the flow parameters to. In addition, this study is not designed to test clinical uses of qualitative and quantitative flow parameters but rather to use this technology to describe flow disturbances in PAH compared with CTL. This study should be considered a pilot, hypothesis generating and feasibility study using a novel

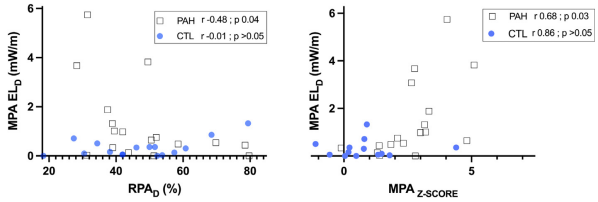

Figure 4. Correlation of main pulmonary artery (MPA) diastolic energy loss (EL_D) with right pulmonary artery distensibility (RPA_D) index and MPA z-score. CTL, controls; PAH, pulmonary arterial hypertension.

imaging technology. Another limitation is the 2-dimensional nature of the imaging technique, thus not accounting for through-plane variations. EL calculations are dependent on smoothing parameters.[8] We used the same parameters across our analysis to avoid this potential source of error.

Conclusion

The use of high-frame-rate ultrasound imaging allows us to demonstrate abnormal flow characteristics in the MPA and RV in patients with pulmonary hypertension compared with CTL. An abnormal MPA diastolic vortex can be identified in most patients with PAH, even in those with milder disease severity compared with CTL. Even as right ventricular EL and VO did not differ significantly, VC was higher in PAH compared with CTL. Higher energy losses and vector complexity in the MPA can result from increased right ventricular afterload due to increased PVR as well as increased MPA stiffness. These novel flow parameters are promising noninvasive markers of disease severity, and further investigation is warranted.

Ethics Statement

The study was approved by the ethics review boards of Hospital for Sick Children in Toronto, Canada, and St. Olav's Hospital in Trondheim, Norway. This study adhered to the ethical guidelines of both institutions.

Funding Sources

Modified GE Vivid E9 and E95 provided by GE were exclusively used during the study period at both institutions. The first author has received funding for this project from Centre for Innovative Ultrasound Solutions. The last author has received funding to this project from the Joint Research Committee between St Olav's Hospital and the Faculty of Medicine, NTNU, which manages research funding from the Central Norway Regional Health Authority (Reference 2018/42794). The technical development was funded by the Research Council of Norway (RCN) 230455 and RCN 237887, the latter reference number through the Centre for Innovative Ultrasound Solutions.

Disclosures

The third author (LL) has a part-time consultancy in GE Vingmed Ultrasound. The other authors have no conflicts of interest to disclose.

References

1. Swift A, Rajaram S, Hurdman J, et al. Noninvasive estimation of PA pressure, flow, and resistance with CMR imaging: derivation and prospective validation study from the ASPIRE registry. *JACC Cardiovasc Imaging*. 2013;6:1036−1047.
2. Foris V, Kovacs G, Tscherner M, Olschewski A, Olschewski H. Biomarkers in pulmonary hypertension: what do we know? *Chest*. 2013;144:274−283.
3. Schäfer M, Barker AJ, Kheyfets V, et al. Helicity and vorticity of pulmonary arterial flow in patients with pulmonary hypertension: quantitative analysis of flow formations. *J Am Heart Assoc*. 2017;6:14−16.
4. Schäfer M, Ivy DD, Abman SH, et al. Apparent aortic stiffness in children with pulmonary arterial hypertension. *Circ Cardiovasc Imaging*. 2017;10:e005817.
5. Kheyfets VO, Schafer M, Podgorski CA, et al. 4D magnetic resonance flow imaging for estimating pulmonary vascular resistance in pulmonary hypertension. *J Magn Reson Imaging*. 2016;44:914−922.
6. Nyrnes SA, Fadnes S, Wigen MS, Mertens L, Lovstakken L. Blood speckle-tracking based on high-frame rate ultrasound imaging in pediatric cardiology. *J Am Soc Echocardiogr*. 2020;33:493−503. e5.
7. Mawad W, Løvstakken L, Fadnes S, et al. Right ventricular flow dynamics in dilated right ventricles: energy loss estimation based on blood speckle tracking echocardiography—a pilot study in children. *Ultrasound Med Biol*. 2021;47:1514−1527.
8. Daae AS, Wigen MS, Fadnes S, Løvstakken L, Støylen A. Intraventricular vector flow imaging with blood speckle tracking in adults: feasibility, normal physiology and mechanisms in healthy volunteers. *Ultrasound Med Biol*. 2021;47:3501−3513.
9. Saris AECM, Hansen HHG, Fekkes S, et al. In vivo blood velocity vector imaging using adaptive velocity compounding in the carotid artery bifurcation. *Ultrasound Med Biol*. 2019;45:1691−1707.
10. Pedersen MM, Pihl MJ, Haugaard P, et al. Novel flow quantification of the carotid bulb and the common carotid artery with vector flow ultrasound. *Ultrasound Med Biol*. 2014;40:2700−2706.
11. Reiter G, Reiter U, Kovacs G, Olschewski H, Fuchsjäger M. Blood flow vortices along the main pulmonary artery measured with MR imaging for diagnosis of pulmonary hypertension. *Radiology*. 2015;275:71−79.
12. Pedrizzetti G, La Canna G, Alfieri O, Tonti G. The vortex—an early predictor of cardiovascular outcome? *Nat Rev Cardiol*. 2014;11:545−553.
13. Rajaram S, Swift AJ, Capener D, et al. Comparison of the diagnostic utility of cardiac magnetic resonance imaging, computed tomography, and echocardiography in assessment of suspected pulmonary arterial hypertension in patients with connective tissue disease. *J Rheumatol*. 2012;39:1265−1274.
14. Vonk-Noordegraaf A, Marcus JT, Holverda S, Roseboom B, Postmus PE. Early changes of cardiac structure and function in COPD patients with mild hypoxemia. *Chest*. 2005;127(6):1898−1903.
15. Ghio S, Schirinzi S, Pica S. Pulmonary arterial compliance: how and why should we measure it? *Glob Cardiol Sci Pract*. 2015;2015:58. https://doi.org/10.5339/gcsp.2015.58.
16. Jardim C, Rochitte CE, Humbert M, et al. Pulmonary artery distensibility in pulmonary arterial hypertension: an MRI pilot study. *Eur Respir J*. 2007;29:476−481.
17. Visser LC, Im MK, Johnson LR, Stern JA. Diagnostic value of right pulmonary artery distensibility index in dogs with pulmonary hypertension: comparison with Doppler echocardiographic estimates of pulmonary arterial pressure. *J Vet Intern Med*. 2016;30:543−552.
18. Venco L, Mihaylova L, Boon JA. Right Pulmonary Artery Distensibility Index (RPAD Index). A field study of an echocardiographic method to detect early development of pulmonary hypertension and its severity even in the absence of regurgitant jets for Doppler evaluation in heartworm-infected dogs. *Vet Parasitol*. 2014;206:60−66.

This paper is submitted for publication and is therefore not included.

PAPER 3 (Submitted)

Intracardiac Flow Dynamics in Children with Functionally Univentricular Hearts using Blood Speckle Tracking

Wadi Mawad[a,b,c], Kristian Sørensen[b,d] , Solveig Fadnes[b,d] , Matthew Henry[a], Lasse Løvstakken[b], Luc Mertens[a], Siri Ann Nyrnes [b,e]

[a] The Hospital for Sick Children, Toronto, Ontario, Canada

[b]Department of Circulation and Medical Imaging, Norwegian University of Science and Technology (NTNU), Trondheim, Norway

[c]Department of Paediatrics, Montreal Children's Hospital, McGill University Health Centre, Montreal, Quebec, Canada

[d] Division of Ålesund Hospital, Department of Pediatrics, Møre and Romsdal Hospital Trust

[e]Children's Clinic, St. Olavs University Hospital, Trondheim, Norway

Word count: 3087

Corresponding author: Wadi Mawad

B04.2718 - 1001 Décarie Boulevard, Montreal, Qc, Canada, H4A3J1.

Email : wadi.mawad@mcgill.ca

Phone : 514 623 9234

Fax : 514 412 4273

ISBN 190 978-82-326-7972-0 (printed ver.)
ISBN 190 978-82-326-7971-3 (electronic ver.)
ISSN 1503-8181 (printed ver.)
ISSN 2703-8084 (online ver.)

NTNU

Norwegian University of
Science and Technology